Role of Fluctuations and Defects in Select Condensed Matter Problems

by

Steve Pressé

B.Sc.(Hon.), McGill University, Montréal (2003)

Submitted to the Department of Chemistry
in partial fulfillment of the requirements for the degree of

Doctor of Philosophy

at the
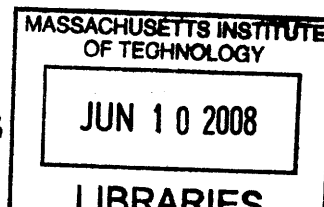
MASSACHUSETTS INSTITUTE OF TECHNOLOGY

June 2008

Author...
Department of Chemistry
May 6, 2008

Certified by ....
U Robert J. Silbey
Class of 1942 Professor of Chemistry
Thesis Supervisor

Accepted by...
Troy Van Voorhis
Chairman, Associate Professor of Chemistry

This doctoral thesis has been examined by a Committee of the Department of Chemistry as follows:

Professor Troy Van Voorhis...............   ....
                                        Chairman, Thesis Committee
                                        Associate Professor of Chemistry

Professor Robert J. Silbey...........:...........//..........\\..........
                                        Thesis Supervisor
                                        Class of 1942 Professor of Chemistry

Professor Jianshu Cao..
                                        Associate Professor of Chemistry

Professor Robert W. Field..   ....
                Chairman, Departmental Committee on Graduate Students

Role of Fluctuations and Defects
in Select Condensed Matter Problems

by
Steve Pressé

Submitted to the Department of Chemistry
on May 6, 2008, in partial fulfillment of the
requirements for the degree of
Doctor of Philosophy

Abstract

Defects and fluctuations dominate both static and dynamical properties of systems in the condensed phase. In this work, we focus on three such examples. Firstly, we model the effect of proton fluctuations on the rate of electron transfer in the condensed phase through an electron donor-acceptor assembly linked via an H-bonding bridge. The model suggests that it is possible for the electron transfer rate through a deuterated H-bonding assembly to exceed the rate through a protonated H-bonding bridge at low temperature, consistent with experimental findings. Next, we consider the convergence properties of Jarzynski's non-equilibrium work relation. This relation expresses the free energy change of a system, onto which finite-time work is done, as an ensemble average over all possible trajectories of the system. We quantify the regime of applicability of this equality by considering the role of rare fluctuations which dominate the work average of entropy generating processes. Lastly, we consider fluorophore lifetime variations arising when single molecules are placed near non-planar metallic surfaces. We compute the exact first order self-fields of vertical dipoles located above locally curved perfectly conducting surfaces by invoking a small slope phase perturbation technique. The results suggest that smooth pertubations lead to deviations from the image theory results extensively used to interpret the experimentally observed single molecule lifetime changes.

Thesis Supervisor: Robert J. Silbey

Title: Class of '42 Professor of Chemistry

3

Acknowledgments

Firstly I would like to thank my advisor, Robert Silbey, who provided me with a constant source of encouragement throughout my stay at M.I.T. I am very grateful for the opportunity of having worked so closely with a scientist of such a high caliber who, above all, is a gentleman. Bob has a remarkable ability to pick out both challenging and interesting problems. While providing me with the guidance necessary to tackle these issues, Bob gave me complete freedom to pursue my own interests as well. His broad interests in a variety of problems have provided me both the enthusiasm and the confidence to seek new challenges.

I would like to thank my thesis committee members as well, Profs. Troy van Voorhis and Jianshu Cao. Their valuable scientific input as well as their thoughtful academic advice throughout my stay at M.I.T is greatly appreciated.

I am very grateful to the many professors from whom I have taken classes. In many respects, they have largely changed the way I look at science. In particular, I am indebted to Profs. Kardar, Bazant and X.G. Wen. Their highly original presentations of both old and new topics alike have completely redefined my M.I.T. experience.

I am indebted to Prof. Nocera's group at M.I.T., in particular J.Hodgkiss, E.Young, N.Damrauer and J. Rosenthal, for their collaboration in the proton-coupled electron transfer project as well as their friendship and support at M.I.T.

I acknowledge Profs. Irwin Oppenheim, Jianshu Cao and David Ronis and Dr. Benoit Palmieri for their insight into the project on the fluctuation theorems and Dr. Hongsheng Chen and Prof. Akbar Salam for their input on my work regarding dipolar radiation near curved surfaces.

It has been a pleasure working as closely I have with my theoretical chemistry seminar colleagues at M.I.T, Harvard, B.C. and B.U. In particular I thank A. Golosov, Y. Tambouret, S. Difley, C.L. Cheng, B. Landry, A. Wasserman, L. Vogt, W. Novak and W. Martin. I also thank Peter Giunta, Li Miao and Gloria Pless, and my advisor, R.J. Silbey, for their role played in this important seminar series.

I also thank my fellow theory and experimental friends and colleagues at M.I.T. who have helped make my Ph.D. experience enjoyable. I will cherish the memory of our (in retrospect mostly unscientific) discussions. In particular, I thank J. Witkoskie, V. Lubchenko, S. Yang, Y.C. Cheng, C.L. Cheng, X.G. Song, E. Young, J. Hodgkiss, X. Xiang, R. Thom, V. Petrovic, M. Artyomov, J. Locasale, E. Zimanyi, J.Y. Sung, M. Kryvohuz, O. Vydrov, Q. Wu, T. Ambjornsson, S. Altunata, I. Rudra, S. Difley, J.S. Evans, L.P. Wang, O. Zhukov, L. Gutman and X. Chen as well as the many others.

Above all, I would like to thank my family, in particular my mother, and siblings, Ken and Cindy, and my girlfriend, Jelena Madic, for their continued support. I dedicate this thesis to them.

Contents

List of Figures

Chapter 1

Introduction

Condensed phase phenomena usually involve the interaction of multiple degrees of freedom at disparate timescales. While simple calculations often provide estimates for average, stationary, macroscopic quantities for systems in the condensed phase, interesting behavior often emerges at the mesoscopic scale from fluctuations and defects[1].

Predicting the effects of fluctuations and defects remains a challenging task. Despite advances in computational techniques, it is still prohibitively difficult to approach condensed phase problems by rigorous computational means; the many interacting length and time scales often limit the applicability of such methods unless important approximations are made.

We tackle condensed phase problems by invoking models which single out features playing an important in the process of interest. By doing so, we retain a simple physical picture while making predictions regarding those effects of the feature within the model. Experiments are therefore crucial in establishing the physical relevance of the simplified model.

As an example, the spin-boson model contains many of the physical attributes needed in describing condensed phase charge transport[2]. This general model describes the competition between coherent quantum mechanical oscillatory behavior and the incoherent hop of the charge from donor to acceptor as we tune the coupling strength of the two-level system, the spin, to the environment, the bosons[3, 2, 4].

In this thesis, we have used the spin-boson model to study the joint isotope and temperature dependence of an electron transfer reaction whose donor and acceptor are linked by two-point H-bonds[5]. In response to questions raised by experiments[6], chapter 2 focuses on the joint temperature-isotope dependence recovered in proton-coupled electron transfer experiments with an emphasis on the experimental motivation for the system under study. We also briefly discuss future experiments underway highlighting the subtleties of the joint temperature-isotope effects observed. The chapter contains a detailed discussion of the model[7] which makes the electron tunneling dynamics susceptible to fluctuations in the position of the proton or deuteron present in the H-bond in what has been experimentally argued to be the reaction bottleneck.

We have also worked on assessing the role of fluctuations on the convergence properties of the nonequilibrium work theorem, often termed the Jarzynski equality[8]. Generally speaking, the Jarzynski equality expresses the average of the exponential of the nonequilibrium work performed on a system, which is sampled from a canonical distribution of initial conditions, to the exponential of the (equilibrium)free energy change. A closely related equality, the Crooks equality, was recently used to determine the free energy difference for unfolding and refolding of RNA three-helix junctions under tension [9].

In chapter 3, we demonstrate how rare configurations, which often asymmetrically broaden work distributions, may contribute highly to free energy estimates for entropy generating processes. Using simple model systems which experience diabatic drops in potential, we show that while rare initial configurations are important in accurately estimating free energy differences, such configurations are often impossible to sample in larger systems[10]. This is because higher order work cumulants contributing to the tails of the work distribution vanish from central limit type arguments.

In chapter 4, we generalize some of the points made in the previous chapter to dynamical systems in the presence of an explicit environment[11]. While large fluctuations lead to poor convergence properties of the Jarzynski equality, in this chapter we note that fluctuations,

responsible for the work distribution breadth, can provide information on parameters of the presumed underlying model beyond free energy changes and profiles in the direction along which the force is applied[12]. From a practical viewpoint, predicting fluctuations is highly relevant in understanding processes in biology which take place in the small number limit[13] as well as operating miniaturized devices[14].

Biology has provided much of the current motivation to study processes at the level of single molecules[15, 16, 17] while improved resolution of spectroscopic techniques has highlighted the effect of microenvironments on properties of single molecules.

Many experiments have exploited radiative rate enhancement effects experienced by single molecules, embedded in a dielectric, near metallic surfaces. For example, it is known that Raman scattering is enhanced by several orders of magnitude for molecular probes neighboring sharp dielectric features[18]. In fluorescence, variations in radiative rate as molecular probes are moved to and from planar surfaces of a differing dielectric are well understood[19, 20, 21]. In addition, strong enhancements in the radiative rate for emitting dipoles in spheres, termed Mie resonances, were even theoretically predicted to survive isotropic averaging[22].

Defects at planar surfaces should lead to observable changes in the radiative properties of single molecule averaged out in ensemble, bulk, experiments. We address a small part of this problem in chapter 5 by considering the effect of surface defects[23], Gaussian bumps or cavities, on fluorescing single molecules located near metallic surfaces and derive deviations of single fluorophore properties predicted from image theory near these locally curved surfaces.

1.1 Bibliography

[1] X.G. Wen. *Quantum Field Theory of Many-Body Systems*. Oxford University Press, 2004.

[2] A.J. Leggett, S. Chakravarty, A.T. Dorsey, Matthew P.A. Fisher, Anupam Garg, and W. Zwerger. *Rev. Mod. Phys.*, 59:1, 1987.

[3] U. Weiss. *Series in modern condensed matter physics: Quantum Dissipative Systems*, volume 10. World Scientific, 1999.

[4] G. Mahan. *Many-Particle Physics*. Kluwer Academic/Plenum Publishers, 2000.

[5] Niels H. Damrauer, Justin M. Hodgkiss, Joel Rosenthal, and Daniel G. Nocera. *J. Phys. Chem. B*, 108:6315, 2004.

[6] Justin M. Hodgkiss, Niels H. Damrauer, S. Pressé, J. Rosenthal, and Daniel G. Nocera. *J. Phys. Chem. B*, 110:18853, 2006.

[7] S. Pressé and R. Silbey. *J. Chem. Phys.*, 5:921, 2006.

[8] C. Jarzynski. *Phys. Rev. Lett.*, 78:2690, 1997.

[9] D. Collin, F. Ritort, C. Jarzynski, S.B. Smith, I. Tinoco Jr, and C. Bustamante. *Nature*, 437:231, 2005.

[10] S. Pressé and R.J. Silbey. *J. Chem. Phys.*, 124:054117, 2006.

[11] S. Pressé and R.J. Silbey. *Phys. Rev. E*, 74:061105, 2006.

[12] G. Hummer and A. Szabo. *PNAS*, 98:3658, 2001.

[13] J.Q. Wu and T.D. Pollard. *Science*, 310:310, 2005.

[14] G.M. Wang, E.M. Sevick, E. Mittag, D.J. Searles, and D.J. Evans. *Phys. Rev. Lett.*, 89:050601, 2002.

[15] G. Popescu, A. Robert, J.R. Howe, and A. Auerbach. *Nat. Lett.*, 430:790, 2004.

[16] G. Bokinsky and X. Zhuang. *Acc. Chem. Res.*, 38:566, 2005.

[17] J.B. Witkoskie and J. Cao. *J. Chem. Phys.*, 121:6361, 2004.

[18] M. Moskovits. *J. Ram. Spec.*, 36:485, 2005.

[19] H. Kuhn. *J. Chem. Phys.*, 53:101, 1970.

[20] R.R. Chance, A. Prock, and R. Silbey. *Adv. Chem. Phys.*, 37:1, 1978.

[21] K.H. Drexhage. *Prog. Opt.*, XII:165, 1974.

[22] H. Chew. *Phys. Rev. A*, 38:3410, 1988.

[23] S. Pressé and R. J. Silbey. *Phys. Rev. A*, 77:043402, 2008.

Chapter 2

Temperature-Isotope Dependence in Proton-Coupled Electron Transfer

2.1 Prologue

The bulk of this chapter, with the exception of a discussion of current experiments underway, is already published in the cited references[1, 2].

Of the material already published, I have clarified a few comments appearing in my joint publication with my advisor which, as I reach the end of my Ph.D., I have found either misleading or unimportant. A few typos present in this publication were also corrected.

Briefly, this work is motivated by the experiments of Hodgkiss *et al.* [1] on electron transfer, ET, through an H-bonding interface. In the current chapter we discuss a new theoretical model for proton-coupled electron transfer, $PCET$, in the condensed phase, that does not involve real proton transfer. These experiments, which directly probe the joint T-isotope effects in coupled charge transfer reactions, show anomalous T-dependence in k_H/k_D, where k_H and k_D are the ET rates through the H-bonding interface with H-bonded protons and deuterons, respectively. We address the anomalous T-dependence of the k_H/k_D in our model by attributing the modulation of the electron tunneling dynamics to bath-induced fluctuations in the proton coordinate, so that the mechanism for coupled charge transfer

might be better termed vibrationally-assisted *ET* rather than *PCET*.

We argue that such a mechanism may be relevant to understanding traditional *PCET* processes, i.e. those in which protons undergo a transfer from donor to acceptor during the course of *ET*, provided there is an appropriate timescale separating both coupled charge transfers. Likewise, it may also be useful in understanding long-range *ET* in proteins, where tunneling pathways between redox cofactors often pass through H-bonded amino acid residues, or other systems with sufficiently decoupled proton and electron donating functionalities.

This chapter is almost exclusively focused on those experimental, physical and mathematical aspects of this problem which I believe to be original contributions to the field by our collaborators as well as my advisor and I.

I have made no attempt at describing, in this already lengthy chapter, the phenomenological justification and mathematical formalism underpinning the spin boson problem. Nor is this chapter meant to serve as an exhaustive account of the growing list of experiments in the field of proton-coupled electron transfer. These points are relegated to the cited literature.

Rather, this chapter builds the case, from the experimental findings to the effective general model posed, in favor of the important role played by of proton fluctuations in *PCET*.

2.2 Introduction

Though the theory of electron transfer, *ET*, in model systems is well understood, the role of the proton in modulating the *ET* dynamics in what is termed proton-coupled electron transfer, *PCET*, has been the focus of recent theoretical and experimental studies.

Early experimental work in *PCET* was performed on simple model systems where both proton and electron transfer collinearly, i.e. along one collinear coordinate [3, 4, 5, 6, 7, 8]. The conclusions reached from these and subsequent *PCET* experiments have had important biological implications[9]. These assessed the effect of the proton bond breaking and reforming process on the dynamics of *ET* and identified this step as playing a crucial role in the overall charge transfer[10, 11, 12, 13, 14, 15].

Two models of *PCET* have been proposed to account for this effect on *ET*[16, 17, 18]. The first, by Cukier and co-workers, uses an adiabatic approximation to find a restricted tunneling path for *PCET* from the starting point of a 2-D *PES* for the transferring particles. The second, by Hammes-Schiffer and co-workers, is a generalization of Marcus theory using a multistate valence bond model for both proton/electron donor/acceptor sites.

With all *T*-dependence made explicit, the Marcus formula for *ET* reads as follows [19]

$$k_{ET} \sim \frac{V^2}{\sqrt{T}} e^{-E/T} \tag{2.1}$$

where V is the electron tunneling frequency and the exponential is a Boltzmann weighting factor with activation energy E. This latter quantity depends on system-specific re-organizational energies and free energy differences for donor and acceptor electronic states.

Both theoretical formulations of *PCET* make use of the Fermi golden rule to compute the *PCET* rate. The form of the rate expression obtained in this manner resembles the Marcus result for single *ET*. Differences include adjusting the activation energy to take into consideration re-organization and free energy differences associated to the transferring

proton(deuteron) and summing over contributions to the $PCET$ rate from all vibrationally excited proton(deuteron) donor states. In addition a sum is performed over Franck-Condon overlaps involving all possible acceptor proton(deuteron) vibrational state and each proton(deuteron) donor vibrational state. The vibration referred to here is that of the 2-atom bond involving the proton(deuteron) which is broken in proton transfer.

Strictly speaking, for a proton(deuteron) tunneling from its ground donor state to an acceptor state, the entirety of the isotopic dependence in the $PCET$ rate expression is recovered in the term corresponding to the electron tunneling frequency, V, of the Marcus expression for single ET. In dealing with $PCET$ processes, we relabel this term V_{eff} because it is renormalized by bath-system interactions and includes Franck-Condon overlaps from the transferring proton(deuteron). More specifically from Eq.(2.1), using k_H to label the $PCET$ rate in the presence of a tunneling proton and k_D for the corresponding rate expression in the presence of a tunneling deuteron, the ratio of k_H/k_D simplifies to a ratio of effective tunneling frequencies, i.e. $k_H/k_D = V_{H,eff}^2/V_{D,eff}^2$.

Hammes-Schiffer and co-workers have attributed the system-specific nature of the isotopic dependence in V_{eff} to factors such as proton-donor acceptor distance, endothermicity of the reaction and solvent polarity[20]. From this we conclude that Marcus theory for single ET, equivalent to the case where a proton(deuteron) tunnels from its ground donor state to an acceptor state, predicts an isotope effect which is either normal, $k_H/k_D > 1$, or reverse, $k_H/k_D < 1$, depending on the specificities of the system[21, 20].

By contrast, recent experiments in 2-methylTHF involving a photoinduced forwards ET process, from a singlet excited state in Zn-porphyrin electron donor to a diimide electron acceptor, have shown that a T-dependent reverse isotope effect, $k_H/k_D < 1$, steadily reverted to a normal isotope effect, $k_H/k_D > 1$, at an approximate crossover T of $160K$[1]. The forwards process is immediately followed by a reverse ET process where the electron hops back to the donor ground singlet state of the Zn-porphyrin.

In order for the ratio of k_H/k_D to exhibit the T-dependence observed in experiments, we may either consider a strong isotope-dependence in the re-organizational energy component of a Marcus-type model or alternatively consider an excited state contribution with a ratio of zeroth to first order terms of $\sim \mathcal{O}(0.1)$. With regards to the first point, Decornez *et al.* have already noted that a possible, though insignificant, difference on the solvent re-organizational energies upon isotope substitution could arise, the magnitude of which is restricted by time-scale separation arguments in *PCET* processes[20].

Furthermore, it is clear that if the total rate expression is written as a sum over many independent rates, e.g. rates originating from multiple channels available for *PCET* as a function of increasing T, then non-trivial T-dependence in k_H/k_D could emerge though the increase of k_H/k_D with T is not immediately obvious. More importantly, in the current experiments under investigation, it is unlikely that a proton(deuteron) transfers in the relevant timescale separating forwards and reverse ET[1]. The experiments are briefly discussed in 2.3.

A reasonable analytic model of vibrationally-assisted ET, involving no proton transfer, is proposed in section 2.4. This model makes the electron tunneling barrier susceptible to fluctuations in the local equilibrium coordinates of an H-bonded proton(deuteron). We demonstrate that considering fluctuations in a single mode localized in the H-bond is sufficient to account for the T-dependence of k_H/k_D recovered in experiments. This treatment is consequently a natural progression of earlier work on the role of local intramolecular H-bond vibrations on proton transfer rates [22, 23]. For completeness, we note that the effect on the ET rate induced by correlated fluctuations in both H-bonded protons is ignored.

The remainder of the article is partitioned as follows: section 2.5 includes the evaluation of the rate expression in the appropriate limits and section 2.6 involves a short discussion of the parameter dependence of the rate with illustrations of important trends exhibited by this model. We conclude in section 2.7.

2.3 Experiments

2.3.1 Motivation for Experiments Across Amidinium-Carboxylate Functionalities

This section is taken from a joint publication written with my collaborators[1].

To date, most experiments have indirectly inferred the role of the proton in $PCET$ from ET experiments while little is known of $PCET$ reactions in which the proton is incompletely transferred. We wish to start by motivating the choice of electron donor-acceptor moieties in experiment.

In proteins, ET often occurs through pathways with H-bonded contacts[24, 25]. The stabilizing guanidinium-carboxylate salt-bridges, obtained from arginine-aspartane interactions as shown in Fig.(2.1), are found in a number of natural systems including RNA stem loops, zinc finger/DNA complexes, the active sites of dihydrofolate reductase, cytochrome c oxidase and siroheme sulfite reductase (SiRHP) [26, 27, 28, 29, 30, 31, 32, 33, 34]. Experiments on ET with donor and acceptor functionalities coupled via a guanidinium-carboxylate bridges are often complicated by complex equilibria between the various binding modes of this H-bonding interface, also shown in Fig.(2.1). This motivates the current ET experiments across the amidinium-carboxylate salt-bridge which, while preserving the H-bonding interactions present in guanidinium-carboxylate, has only one binding mode along which both electron and proton-transfer coordinates are collinear[4, 35, 36].

The model system (1-H:2), shown in Fig.(2.2), is comprised of a Zn(II) porphyrin photoreductant, labeled 1-H, and a naphthalene diimide electron acceptor, labeled 2, linked via an amidinium-carboxylate salt-bridge. NMR spectroscopy shows that electron acceptor-donor assemblies are linked by 2 point H-bonds and do not stack upon one another[37].

The forward rate constant in the presence of the H-bonding bridge is slowed by almost two orders of magnitude as compared to nearly identical donor and acceptor groups positioned in a similar geometry but connected via covalent bonds[38]. While both driving force and

re-organization energies are similar in both systems, the differing rates imply that the H-bond reduces the donor and acceptor elecronic coupling, in other words it plays the role of a reaction bottleneck. This system is therefore used to probe the mechanism of *PCET* via nonradical, non X-H bond breaking, pathways.

2.3.2 Experimental Results Across Amidinium-Carboxylate Functionalities

The $PCET$ proceeds from the S_1 states of the 1-H(D) excited by using 560-nm laser pulse excitation.

For this reason, the S_1 states of the 1-H(D) and ZnTMP, Zn(II) tetramesitylyporphyrin, which is the Zn porphyrin without the amidinium functionality, are initially characterized in the absence of a quencher. Both exhibited minimal fluorescence spectral shifts over 120-300K. The solvent used, 2-Methyltetrahydrofuran abbreviated as 2-MeTHF, is not only optically transparent from 120-300K, a range well above its liquid to glass transition of 86K, it also does not disrupt the two-point H-bond in the molecular assemblies and axially binds to the Zn(II), preventing formation of amidine-zinc linkages between different molecules of species 1-H(D)[37, 39]. In the absence of a quencher, there is a non-radiative decay path, via inter-system crossing, to the excited triplet, T_1, state.

Fig.(2.3) shows the temperature dependent fluorescence lifetime of the 1-H(D) and ZnTMP porphyrins versus temperature. The fluorescence lifetimes, obtained by integrating portions of the appropriately chosen fluorescence peaks and fitting to mono-exponential functions. decrease with increasing T. This is consistent with previous experimental findings of Zn porphyrins in the same solvent[40]. In addition, this implies that the inter system crossing to the triplet state is a thermally activated process. In contrast to the ZnTMP porphyrins, the smaller fluorescence lifetimes of the porphyrin 1-H(D) over the entire T-range reflects the electronic perturbations induced by the amidinium functionality which presumably accelerate inter system crossing. Furthermore, the isotopic effect recovered from the fluorescence lifetime 1-H(D) curves is modest though statistically significant, at about 3%.

Now that we have established that the T_1 state is likely thermally activated, we probe the reference rate for the S_1 state deactivation by considering perturbations to the inter system

crossing dynamics in the presence of stable 2 point H-bonds. This was done by analyzing the fluorescence emission spectra of 1-H:benzoate and 1-D:benzoate which, while forming stable two point H-bonds, are incapable of quenching the S_1 state via electron, energy or proton transfer. From Fig.(2.4) we see modest lifetime increases in the presence of benzoate, consistent with previous work [37]. This effect is ascribed to the reduced motion of the amidinium protons when participating in H-bonding interactions.

Within uncertainty, the slopes of Figs.(3)-(4) are identical implying that the benzoate does not appreciably alter the the activation barrier for inter system crossing. Furthermore, no significant spectral shift in either emission or absorption is observed attesting to the weak electronic coupling between the porphyrin and the amidinium functionality rotated out of plane with respect to the conjugated porphyrin π system on account of the steric repulsion between the external amidinium hydrogens and the mesityl group at the adjacent meso position of the porphyrin ring.

In addition, transient absorption spectroscopy had previously been used to show that *ET* accounts for the quenching of the S_1 state of 1-H upon association with 2[37].

The *PCET* experiments carried in 2-MethylTHF contain both bound and unbound 1-H(D):2 species, at about 85% bound at 298K in THF. The presence of both species resulted in a clear biexponential fluorescence lifetime decay over the entire T-range since the fluorescence lifetime of 1-H(D):2 is shorter than that of unbound 1-H(D) while the ratio of short and long lifetime components is related to the association constant. Furthermore, the short to long fluorescence lifetime ratio increases with decreasing T highlighting the temperature dependence of the association constant. For the shorter lifetime components, the rate of *PCET*, k, is measured as the difference in rates between that bound to 2 and that bound to benzoate for each temperature in order to account for the electronic perturbation on the S_1 state induced by the presence of the H-bond.

The resulting $PCET$ rates in the presence of protonated and deuterated H-bond, denoted k_H and k_D respectively, are plotted versus T with experimental uncertainty in Fig.(2.10). We note the surprising outcome; at 300K the ratio of k_H/k_D is 1.2 while that at 120K is 0.9.

2.3.3   Brief Note on Current Experiments Across Different Bridges

The previous section introduces in relative detail the experiments on $PCET$ transfer across the non-ionized amidine carboxylic acid 2-point H-bond for which we have developed an effective model presented in the next section.

In this section, we wish to describe in qualitative terms current unpublished results obtained by collaborators, principally E.R. Young, on the effect of solvent and bridge modification on the $PCET$ rate. We refer the interested reader to the manuscript, once published, for all obvious omissions including raw data[41].

As an extension to the previous experiments, current experimental work contrasts the $PCET$ rate across the amidine carboxylic acid 2-point H-bond and the ionized amidinium-sulfonate 2-point H-bond. We use the notation of the upcoming publication and denote these donor-acceptor assemblies, appearing in Fig. (2.5), as 1-H(D):2 and 1-H(D):3, respectively.

Experiments across this acceptor-donor assembly are carried out in both 2-MeTHF as well as the slightly more polar THF over a temperature range similar to that of the previous section.

The protonated state of the amidine functionality is ascertained from the distinctive shifts present in the absorption spectrum while the driving force for electron transfer between donor and acceptor groups varies negligibly little from 1-H(D):2 to 1-H(D):3.

The experimental outcomes illustrate a critical point; these highlight how subtle structural changes in the bottleneck region for the $PCET$ reaction qualitatively alter the temperature-isotope rate dependencies. Specifically, the ionized interface is more strongly coupled to the solvent exhibiting considerably more pronounced solvent rate dependence than its non-ionized counter-part. Furthermore, while no crossover is observed except for 1-H(D):2 in 2-MeTHF, the $PCET$ rates do in general exhibit weak non-constant k_H/k_D ratios over the experimental T-range conferring upon the H-bond protons and deuterons some role in electron transfer which merits attention.

2.4 General Model

The spin-boson formalism is used to describe the dissipative ET tunneling dynamics in the presence of a bath modeled as a set of N harmonic oscillators and a proton(deuteron) from the H-bonding interface involved in a normal mode vibration of the system, labeled the $N + 1^{th}$ mode.

Prior to writing down our model Hamiltonian for the system, we address in relative detail both the form of the electron tunneling frequency and the nature of the $N + 1^{th}$ mode.

Without loss of generality, the electron tunneling matrix element is reexpressed as $V_{ij} \propto e^{-g(\mathcal{Q})}$ where $g(\mathcal{Q})$ is some function of the proton(deuteron) coordinate, $\mathcal{Q}$, in some convenient coordinate system with the electron donor center defining the origin. The coordinate $\mathcal{Q}$ is subsequently expanded in the normal mode coordinates of the system $\mathcal{Q} = \sum_\mu \chi_\mu q_\mu$.

Presumably $g(\{q_\mu\})$ is well-behaved in the limit that the electron and proton(deuteron) are separated by a wide energetic barrier, as is expected for reasonable ET rate, and that $g(\{q_\mu\})$ has some local maximum for each eigenmode, $\{q_{\mu,M}\}$, not too far from its equilibrium coordinate, $q_{\mu,eq}$. The latter provision stems from our interpretation for the proton(deuteron) effect on the ET rate. Expanding $\{q_\mu\}$ around $\{q_{\mu,M}\}$ returns $V_{ij} \propto e^{-g(\{q\})} = e^{-g(\{q_{\mu,M}\})-\sum_\mu \gamma_\mu(q_\mu-q_{\mu,M})^2+\cdots}$, hence $\gamma_\mu \geq 0$. We note that the displacements, $\{q_{\mu,M}\}$, need not coincide with a physically realizable molecular re-arrangement induced by local thermal bath fluctuations, only displacements that would maximize the electron tunneling matrix element.

Since the displacement $\{q_{\mu,M}\}$, and consequently the energy in re-centering the harmonic oscillator, show no isotope dependence within the Born-Oppenheimer approximation, we tentatively write the electron tunneling frequency as $V_{ij} = \prod_\mu C_\mu e^{-\gamma_\mu(q_\mu-q_{\mu,M})^2}$.

While fluctuations in multiple modes may provide a better microscopic description of the ET dynamics, i.e. fluctuations in each particular mode of interest may play a role over some T-range, our discussion is restricted to a fluctuation in a single mode. This mode will be referred to as the $N + 1^{th}$ mode with coordinate re-labeled as $q_{N+1} = Q$. The numerics

of section 2.6 demonstrate that this approximation directs us to that mode which is both closest to the timescale of the experimental *ET* rate and which is reasonably well-localized to the H-bonding network. For interpretive reasons, we state that the quantity Q_M is now associated to a shift from equilibrium of a reasonably well-localized mode, i.e. with a reduced mass roughly comparable to that of its lightest atom. This displacement can be interchanged with a shift of the actual proton(deuteron) coordinate up to a small change in γ_{N+1} and C_{N+1}.

The effective microscopic Hamiltonian for the tunneling electron linearly coupled to $N+1$ bath modes is therefore

$$
\mathcal{H} = \Delta_o \sigma_z + 1/2 \sum_{j=1}^{N+1} (p_j^2 + \omega_j^2 q_j^2) + \sum_{j=1}^{N+1} f_j q_j \sigma_z
$$
$$
+ C e^{-\gamma(Q-Q_M)^2} \sigma_x + \sum_{j=1}^{N+1} \frac{f_j^2}{2\omega_j^2} \tag{2.2}
$$

where all the symbols take on their usual meaning and units are rescaled so that $m = \hbar = 1$.

Also, the following abbreviations were introduced for convenience $Q = q_{N+1}, C = C_{N+1}, \gamma = \gamma_{N+1}$ and the following contractions will be used in the remainder of our discussion $\omega = \omega_{N+1}, f = f_{N+1}, p = p_{N+1}$.

The remainder of this work will largely be focused on the features, both physical and mathematical, of the the essential new aspect of this model, namely the gaussian splitting, as applied to this problem. The rest of the material, covering the multi-faceted features of the spin boson problem, is covered in many standard and specialized texts[42, 43, 44] as well as being dispersed in the literature. Their careful exposition is relegated to the references cited where appropriate.

For this reason, we only incidentally highlight that since we will be interested in cases where the tunneling matrix element is small and where the system bath coupling may be strong, a better zeroth order Hamiltonian, with eigenstates as localized states, may be more adequately described by the tunneling dynamics of an electron "self-trapped" by its envi-

ronment. In this case, we partially diagonalize our Hamiltonian using the small polaron transformation $U = e^{i\sum_{j=1}^{j=N+1} \frac{f_j p_j}{\omega_j^2}\sigma_z}$ [42, 23]. While this transformation is unitary, the transformed Hamiltonian remains Hermitian and reads as follows

$$\mathcal{H}_{\text{transf}} = \Delta_o \sigma_z + 1/2 \sum_{j=1}^{N+1} \left(p_j^2 + \omega_j^2 q_j^2\right) + V\sigma_x \tag{2.3}$$

where, for future convenience, we write the transformed tunneling matrix elements read as follows

$$V = Ce^{-\gamma(Q-\frac{f}{\omega^2}\sigma_z)^2 + 2\gamma Q_M(Q-\frac{f}{\omega^2}\sigma_z) - \gamma Q_M^2}$$
$$\times e^{-2i\sum_{j=1}^{j=N+1} \frac{f_j p_j}{\omega_j^2}\sigma_z} \tag{2.4}$$

2.5 Rate Evaluation

For the case of sufficiently weak electronic coupling, we cite the result for the rate of transition from localized states 1 to 2, given by the Fermi Golden Rule expression averaged over bath donor states, [45, 23, 46]

$$k = \int_{-\infty}^{\infty} dt e^{-2i\Delta_o t} \langle V_{12}(t)V_{21}\rangle \qquad (2.5)$$

In integral is assured to converge in the high temperature bath limit since, in that case, the tunneling matrix element time correlation function decays as a Gaussian in time.

Thermal averages of expressions such as those of Eq.(2.4), involving exponentials of terms quadratic and linear in Q and p, can be performed by reducing the above trace operation to a harmonic oscillator path integral calculation as follows

$\langle \mathcal{O}_1...\mathcal{O}_n\rangle = \int ... \int \prod_i dx_i \langle x_1|\mathcal{O}_1|x_2\rangle \langle x_2|...\mathcal{O}_n|x_1\rangle$. This method is particularly useful in evaluating the thermal average of Eq.(2.4) over the $N+1^{th}$ mode as it readily reduces the problem to a generalized Gaussian integral.

Evaluation of the thermal average $\langle V_{12}(t)V_{21}\rangle$, carried out using this method initially yields

$$\langle V_{12}(t)V_{21}\rangle =$$

$$C\int dx_1 dx_2 dx_3 \langle x_1|e^{-\beta\mathcal{H}_{HO}}|x_2\rangle$$

$$\times \langle x_2|e^{i\mathcal{H}_{HO}t}|x_3\rangle$$

$$\times e^{-\gamma(x_3-\frac{f}{\omega^2})^2+2\gamma Q_M(x_3-\frac{f}{\omega^2})-\gamma Q_M^2}$$

$$\times \langle x_3-\frac{2f}{\omega^2}|e^{-i\mathcal{H}_{HO}t}|x_1-\frac{2f}{\omega^2}\rangle$$

$$\times e^{-\gamma(x_1-\frac{f}{\omega^2})^2+2\gamma Q_M(x_1-\frac{f}{\omega^2})-\gamma Q_M^2}$$

$$\times \langle e^{-2i\sum_{j=1}^{j=N}\frac{f_j p_j(t)}{\omega_j^2}}e^{2i\sum_{j=1}^{j=N}\frac{f_j p_j}{\omega_j^2}}\rangle_N \qquad (2.6)$$

where the subscript on the last average indicates a thermal trace over the bath oscillators. The average over the first N bath modes is straightforwardly taken by setting γ of the $N+1^{th}$ mode thermal average to 0 once the latter is computed. Re-writing the first two averages in the integral of Eq.(2.6) as simple harmonic oscillator path integrals in both real and imaginary time with harmonic oscillator Hamiltonian $\mathcal{H}_{HO}$ reduces the average over the $N+1^{th}$ mode to a two-dimensional Gaussian integral. The rate is then

$$k = 2C^2\omega\sinh\frac{\beta\omega}{2}\int_{-\infty}^{\infty}dt e^{-2i\Delta_o t}\frac{e^{-2\gamma Q_M^2-\frac{4\gamma Q_M f}{\omega^2}-\frac{2\gamma f^2}{\omega^4}+\frac{4if^2}{\omega^3}\frac{\cos\omega t-1}{\sin\omega t}}}{\sqrt{\sin\omega t\,\sinh((\beta-it)\omega)}}$$

$$\times \frac{e^{\frac{(\frac{2\gamma f}{\omega^2}+2\gamma Q_M+\frac{2if}{\omega}\frac{1-\cos\omega t}{\sin\omega t})^2}{2\gamma+\omega\frac{\cosh((\beta-it)\omega)-1}{\sinh((\beta-it)\omega)}+i\omega\frac{1-\cos\omega t}{\sin\omega t}}}}{\sqrt{4\gamma^2+2\omega^2+4\gamma\omega(\frac{1}{\tanh((\beta-it)\omega)}-\frac{i}{\tan\omega t})+2i\omega^2\frac{1-\cos\omega t\cosh((\beta-it)\omega)}{\sin\omega t\,\sinh((\beta-it)\omega)}}}$$

$$\times e^{-\sum_{j=1}^{j=N}\frac{2f_j^2}{\omega_j^3}\coth(\frac{\beta\omega_j}{2})+\sum_{j=1}^{j=N}\frac{2f_j^2}{\omega_j^3}(\coth(\frac{\beta\omega_j}{2})\cos\omega_j t-i\sin\omega_j t)}$$

$$\qquad (2.7)$$

While the above expression looks complicated, there exists at least one alternative method which may be employed to verify the validity of Eq.(2.7). This method is considerably more

involved and a brief derivation is sketched in appendix 1.

We now specify a form for the bath spectral function, $J(\omega) \equiv \sum_{j=1}^{j=N} \frac{f_j^2}{\omega_j} \delta(\omega - \omega_j)$,

$$J(\omega) = \frac{\eta \omega^s}{\omega_c^2} e^{-\frac{\omega}{\omega_c}} \tag{2.8}$$

where ω_c is the ultraviolet cutoff for the bath and η is the system-bath coupling for which the strong damping limit implies, η is appreciably larger than unity. We will chose $s = 3$ and briefly note under which conditions our result is qualitatively independent of s. Provided we use the spectral function given in the main body to rewrite the bath contribution appearing for arbitrary s, in the $\beta \omega_j \ll 1$ limit we obtain, $-\sum_{j=1}^{j=N} \frac{2f_j^2}{\omega_j^3} \coth(\frac{\beta \omega_j}{2}) + \sum_{j=1}^{j=N} \frac{2f_j^2}{\omega_j^3}(\coth(\frac{\beta \omega_j}{2}) \cos \omega_j t - i \sin \omega_j t) \sim \frac{-4\eta}{\beta} \omega_c^{s-2} \Gamma(s-2) + \frac{-4\eta}{\beta} \omega_c^{s-2}(1 + t^2 \omega_c^2)^{1-\frac{s}{2}} \cos[2(\frac{s}{2} - 1) \arctan(t\omega_c)]\Gamma(s-2)$. Our theory does not diverge in the infrared selecting $s \geq 3$.

Before doing so, however, we note that it is in the high T-limit for the solvent, $\beta \omega_c << 1$, that the convergence of Eq.(2.7) can be assured. This is done by selecting a rectangular integration contour upon subsituting t for $\tau - i\frac{\beta}{2}$ [47]. For this integral, it is easy to show that the region of integration $[\pm\infty, \pm\infty + \frac{i\beta}{2}]$ vanishes asymptotically.

We refer the reader to appendix 2 for a short discussion on $s < 3$.

Given a set of parameter values, a numerical expression for the rate may be evaluated by expanding the argument of the exponential and the τ-dependent prefactor around the approximate saddle point at $\tau = 0$ to high order in τ.

With the intent of highlighting important qualitative features in the next section, we expand to leading order in $x \equiv e^{-\frac{\beta \omega}{2}}$, i.e. the quantum limit for the $N + 1^{th}$ mode assisting the ET, and perform a saddle point integration. To leading order in x the expansion yields

$$k \sim \frac{C^2 \omega}{2(\gamma + \omega)} \sqrt{\frac{\pi \beta}{\omega_c \eta}} e^{-\frac{2Q_M^2 \gamma \omega}{(\gamma + \omega)} - \frac{2f^2}{\omega^3} - \beta \frac{(2\Delta_0 + 4\eta\omega_c)^2}{16\eta\omega_c}} [1 + e^{-\frac{\beta \omega}{2}} \mathscr{F}(\beta) + \mathcal{O}(e^{-\beta \omega})] \tag{2.9}$$

where

$$\mathscr{F}(\beta) \equiv \frac{1}{8(\omega_c\eta)^2\omega^3(\gamma+\omega)^2}((32(\eta\omega_c)^2 + \beta^2\Delta_o^2\omega^2 - 2(\eta\omega_c)\beta\omega^2)(Q_M^2\gamma^2\omega^4 +$$

$$f^2(\gamma+\omega)^2) + 16(\eta\omega_c)\beta\omega^3 Q_M\gamma\Delta_o f(\gamma+\omega))$$

$$(2.10)$$

To zeroth order in x, Eq.(2.9) maps directly onto the Marcus result with $4\eta\omega_c$ readily identified as the Marcus re-organizational energy, λ.

This zeroth order term is insufficient to account for the T-dependence of k_H/k_D. This is the limiting trait of the Marcus result emerging from all other $PCET$ models. Despite the apparent complexity of higher order contributions to Eq.(2.9), we show that their behavior is easily interpretable by recalling the features of the underlying model.

2.6 Discussion of Parameters and Numerical Examples

We address the emergent T-dependence of k_H/k_D in the context of Eq.(2.9), with a study of higher order terms. We then illustrate our arguments using numerical examples.

In order to do so, we first consider the renormalized tunneling frequency of the zeroth order term in the x-expansion, $\frac{C^2\omega}{2(\gamma+\omega)}e^{-\frac{2Q_M^2\gamma\omega}{(\gamma+\omega)}-\frac{2f^2}{\omega^3}}$, whose isotopic dependence is recovered in two parameters. The first parameter, $e^{-\frac{2f^2}{\omega^3}}$, roughly serves as a unitless measure of the coupling between the localized mode of the proton(deuteron) and the electron. Once dimensionalized, this parameter is larger for the lighter isotope since the degree of coupling to the electron ψ-function measures the degree of its delocalization.

The second parameter, $\frac{\omega}{\gamma+\omega}$, is a unitless quantum factor obtained through thermal averaging. It renormalizes both the bare γ and tunneling frequency, C. It is smaller for the lighter isotope in dimensional units.

To zeroth order in x in Eq.(2.9), where $\beta\omega \gg 1$ holds, we obtain a consistent and predictive low-T theory for the fluctuating mode. The important emergent feature for large Q_M is the normal isotope effect, $k_H/k_D > 1$. This is reasonable since in the absence of fluctuations, or alternatively when the proton(deuteron) cannot sample the region neighboring Q_M, the tails of the more diffuse ψ-function, in this case the proton, better sample the region closest to Q_M. The opposite holds for small Q_M where a reverse isotope effect is recovered from the zeroth order of Eq.(2.9) provided the coupling, f, between the proton(deuteron) and electron is sufficiently weak.

So far we have only considered the case where the $N+1^{th}$ mode is in its ground state. In the high-T regime, excited vibrational states must be considered. The population of excited states leads to a shift in the probability density away from its equilibrium coordinate. In the case that $\beta\omega \ll 1$, the contribution from many excited states is considered, for large Q_M the normal isotope effect is recovered while the opposite holds true for smaller Q_M.

Aspects of the simple physical picture just described are depicted in Fig. (2.6).

While the extreme cases are simple to understand, the intermediate-T regime, with $\beta\omega \sim \mathcal{O}(1)$, involving few low-lying vibrational states requires a quantitative analysis. Before we move onto discussing the effect of higher order terms in Eq.(2.9), we note that there is a simple physical picture from which crossover emerges in the model when a low frequency bridge mode with large Q_M couples to the electron transfer. In the low to intermediate T-regime of the fluctuating mode, the reverse isotope effect is due to a difference in zero-point energies of the proton versus deuteron; in the high-T regime fluctuations become the dominating feature resulting in the recovery of the normal isotope effect.

Within this framework, we briefly discuss the qualitative change in T-dependence arising from the leading order corrections in x to Eq.(2.9) introduced by the low-lying vibrationally excited states. The key observation is the following: although a maximum in the ET rate is reached at $T = T_M$, in accordance with our zeroth order Marcus theory, T_M acquires an isotopic shift from higher orders in x. The shift in the peak, dominated by the values assigned to ω and Q_M, determine the physics at high T, e.g. whether fluctuations eventually cause a shift from reverse to normal isotope effect if a reverse isotope effect exists for some low T. In anticipation of this result, we relabel the shifted peaks T_M^H and T_M^D for now and turn to numerics.

We perform a saddle-point integration of Eq.(2.7) where we expand higher orders in t outside the exponential, keeping all orders in x for an accurate determination of the rate. Perhaps not so surprisingly, all qualitative features discussed earlier hold even when all orders in x are retained for all reasonable sets of parameters.

We illustrate our argument by plotting Eq.(2.9) to zeroth, first and all order in x for proton-assisted ET. As a sidenote we point out that since $x = e^{-\frac{\beta\omega}{2}}$ *two* higher order corrections in x account for the correction to the ET rate of a *single* excited vibrational state. We readily identify the shift in T_M in moving from zeroth to first order in x in Fig.(2.7) for a given set of parameter values.

We wish to take a moment to discuss the parameter values assigned in the plot. For an

electron transferring through an H-bond, the f selected is reasonable since it falls $\sim \mathcal{O}(10^3)$ below what would be expected for a bare Coulomb interaction per typical H-bond length, $\sim \frac{e^2}{4\pi\varepsilon(3\mathring{A})^2}$, C $<<$ Δ_o and a Q_M of $0.80\mathring{A}$ is purposefully exaggerated.

As for vibrations in H-bonds, the ω selected in Fig.(2.7) corresponds to a localized three bond ν_σ, e.g. $N - H \cdots O$ vibrations in amidinium-carboxylate H-bonding networks [1, 48, 49, 50, 51]. For H-bond vibrations which are sufficiently localized, the change in reduced mass upon deuteration may be non-negligible. For example, 3-atom H-bond vibrations are localized in amidinium-carboxylate functionalities which are reasonably unhindered by the surrounding molecular framework while, for example, it is difficult to find localized low frequency vibrations in H-bonding phenols, which have a rigid framework. This issue is adressed in much greater depth in the cited references[49, 48].

In order to investigate the isotope effect on the rate, we replot the curve in Fig.(2.7), for ET assisted by the proton, to all orders in x and superpose onto this curve the corresponding curve for the deuteron for a reasonably large value of Q_M in Fig.(2.8).

From Fig.(2.8). the mechanism for crossover in the rates becomes apparent. It is the result of fluctuations in the high-T limit that are amplified by using large Q_M. This feature results in a change in slope for both curves which eventually leads to T-crossover.

Though the coefficients of the higher order terms of Eq.(2.9) depend non-trivially on all parameters of the theory, their effect is fortuitously simple to interpret if we recall both the physical picture which motivated the form for the electron tunneling matrix element of section 2.4 and the physical significance we associated to Q_M. The ratio of k_H/k_D varies with the thermally induced probability density of the proton(deuteron) ψ-funtion across the point Q_M. Provided $\beta\omega$ is low enough and that, as a result of this, roughly equal numbers of excited proton and deuteron states are populated, then the proton better samples the region near Q_M than does the deuteron. This effect is exacerbated by increasing Q_M and γ. For large $\beta\omega$, excited vibrational states play a lesser role and the effect of the isotope on ET is that predicted for lower T.

The above is illustrated in Fig.(2.9) by replotting the data of Fig.(2.8) for smaller Q_M where the rates, compared to Fig.(2.8), are faster as expected for small Q_M and $k_H/k_D < 1$ over the entire T-range.

As a check, reasonable parameter values appearing in the model were selected in order to fit the rough experimental trend. In Fig.(2.10) we superpose the experimental and predicted theoretical curves. The experimental curves extend slightly beyond the T-range plotted.

Note that the theoretical Δ_o selected is close to the experimental value[1], $\beta\omega_c \ll 1$ holds over the entire T-range, $\Delta_o{}^2 \gg C^2$ and that the ω selected is in the range of what is expected for a low-frequency 3-atom H-bond vibration, say in $N - H \cdots O$.

We note that the curves crossover again in the low-T on the theoretical curve. From the model this behavior is simply accounted for because, for reasonably large Q_M, the isotope effect at very low T must be normal when absolutely no vibrational states are excited. It is only when there is a thermally induced shift in probability density for the deuteron that the isotope effect inverts. Given the parameter values selected this happens in according to the model when $T \sim 150K$.

This second low-T crossover is not observable from the experimental data. While we have proven that the crossover at higher T only requires fluctuations in a single mode, it is likely that more than a single mode involving the proton couple to ET at any given T, their effect being manifest at low T.

While we have only considered fluctutations in the mode compressing and decompressing the H-bonded bridge, fit to the experiment may be improved by considering other relevant fluctuations of the H-bonded bridge.

2.7 Conclusion

We have derived a *PCET* model for the condensed phase motivated by the experiments of Hodgkiss *et al.* in which the *ET* rate is measured across an H-bond[1].

To our knowledge, the experiments of Hodgkiss *et al.* constitute the first joint T-isotope dependence experiments in what would typically be regarded as *PCET* experiment. It is interesting to see that the naive T-dependence of the rates predicted by the Marcus model may be inadequate for certain parameter ranges, as shown here.

The model is suitable to the description of an event for which either no proton formally transfers or for which there exists a sufficient timescale separation between transfer of proton and electron. For this reason, it might be better termed vibrationally assisted *ET*.

The model was developed by considering the proton-dependence of the electron tunneling matrix element by expanding the proton coordinate in the system eigenmodes around some value which extremizes the electron tunneling matrix element. One single mode, labeled the $N + 1^{th}$ mode, was retained in the ensuing analysis. The idealized model presented is thus a simplified description of a complex chemical process for which the relevant vibrational degrees of freedom involved in modulating the *ET* over any given T-range may presumably outnumber the single relevant fluctuating mode considered in this treatment. In the appropriate limit, the model reduces to Marcus theory.

By considering thermal fluctuations in the mode corresponding to compression-decompression of the H-bond, the model simply accounted for the experiments in which it was shown that a T-dependent reverse isotope effect, $k_H/k_D < 1$, steadily reverted to a normal isotope effect, $k_H/k_D > 1$, with increasing T. Clearly, better fit to the experimental data can be achieved by considering other relevant fluctuations in the H-bridge.

As demonstrated by the model, the above crossover behavior is not a universal feature of vibrationally-asisted *ET*. Rather, it is the emergent T-dependence of k_H/k_D which is characteristic of this type of charge transfer. Conclusions regarding the specific class of problems involving strongly coupled charge transfer, i.e. those systems where it can verified

that both charge transfer happen "simultaneously" and inter-dependently, cannot be drawn from this study. The model of *ET* developed here possibly bears instead on the issue of charge transport in biology where tunneling pathways between redox cofactors often pass through H-bonded amino acid residues[24, 25, 9]. While more experiments are needed to study the mechanism of transfer of coupled charges, it would be interesting to consider the role of vibrationally assisted *ET* in long-range *ET* in proteins or other systems with sufficiently decoupled proton and electron donating functionalities.

2.8 Appendix 1

Another method of evaluating the thermal average in Eq.(2.4) involves re-writing the above as an average over exponentials of linear and quadratic creation and annihilation operators. By doing so, we immediately recover the expected result $\langle V_{12} \rangle = \langle V_{21} \rangle$. The average is then computed by breaking up the exponentials of quadratic operators as

$e^{-\Gamma\{2(b^\dagger b+1)+b^\dagger b^\dagger +bb\}} = e^{p_o(\Gamma)2(b^\dagger b+1)} e^{p_+(\Gamma)b^\dagger b^\dagger} e^{p_-(\Gamma)bb}$ provided the initial conditions $p_-(0) = p_+(0) = p_o(0) = 0$ are satisfied[52]. This separation procedure, similar to a demonstration of the Baker-Hausdorff lemma, reduces the problem to an easily solvable Ricatti differential equation. Normal ordering of the operators such as $e^{p_-(\Gamma)bb} e^{\zeta_+ b^\dagger} e^{\zeta_- b}$, where ζ_+ and ζ_- are c-numbers, is then performed in a similar fashion resulting in simple first order differential equations. After the average is re-written in the form $\langle \mathcal{O}(b)\mathcal{O}(b^\dagger) \rangle$ where $\mathcal{O}$ is an operator, a coherent state identity is inserted following the method introduced by Kassner et al. [53]. The thermal average is then easily completed as a generalized Gaussian integral. We note that the most tedious step, namely the normal ordering, is crucial since it circumvents the difficulty of having to perform multiple restricted sums over coherent state identities.

2.9 Appendix 2

In this appendix we address the infrared divergences associated to bath spectral functions, $J(\omega) = \frac{\eta \omega^s}{\omega_c^2} e^{-\frac{\omega}{\omega_c}}$, with $s < 3$.

We recall the thermal average of Eq.(2.4) with respect to the $N+1$ modes

$$\langle V \rangle = \tilde{C} \langle e^{-2i \sum_{j=1}^{j=N} \frac{f_j p_j}{\omega_j^2} \sigma_z} \rangle_N \tag{2.11}$$

where $\tilde{C}$ incorporates all other factors. Relabelling $\langle V \rangle \equiv \tilde{V}$ then

$$\tilde{V} = \tilde{C} e^{-\sum_{j=1}^{j=N} \frac{f_j}{\omega_j^3} \coth(\beta \omega_j / 2)} \tag{2.12}$$

The ensuing discussion closely follows an argument laid out by Silbey et $al.$[54]. We transform our Hamiltonian in Eq.(2.2) using $\mathrm{U} = e^{i \sum_{j=1}^{j=N+1} \frac{g_j p_j}{\omega_j^2} \sigma_z}$ where g_j is a variational parameter. After adding and subtracting $\tilde{V}$ to the transformed Hamiltonian, we recover

$$
\begin{aligned}
\mathcal{H}_{\mathrm{transf}} &= \mathcal{H}_{\mathrm{transf,o}} + \mathcal{H}'_{\mathrm{transf}} \\
&= \Delta_o \sigma_z + \tilde{V} \mathbb{1} + \mathcal{H}_{boson} + \sum_{j=1}^{N+1} (g_j^2 - 2 f_j g_j) \omega_j^{-1} \\
&\quad + coupling\ terms\ with\ 0\ thermal\ average
\end{aligned}
\tag{2.13}
$$

with $\mathcal{H}_{\mathrm{transf,o}} = \Delta_o \sigma_z + \tilde{V} \mathbb{1} + \mathcal{H}_{boson} + \sum_{j=1}^{N+1} (g_j^2 - 2 f_j g_j) \omega_j^{-1}$. From the above construction, the thermal average of the perturbation vanishes. We write down the Peierls-Bogoliubov bound on the spin-boson free energy from basic first order perturbation theory and convexity conditions on the free energy

44

$$F_B = F_{boson} - \beta^{-1} \ln[2\cosh(\beta\tilde{V})] + \sum_{j=1}^{N+1} (g_j^2 - 2f_j g_j)\omega_j^{-1} \tag{2.14}$$

We minimize the free energy with respect to g_j and find

$$g_j = f_j \left(1 + \frac{2\tilde{V}\coth(\beta\omega_j/2)\tanh(\beta\sqrt{\Delta_o^2 + \tilde{V}^2})}{\omega_j\sqrt{\Delta_o^2 + \tilde{V}^2}} \right)^{-1} \tag{2.15}$$

By combining Eq.(2.12) and Eq.(2.15) we obtain a self-consistent equation for $\tilde{V}$. In the limit $\Delta_o \gg \tilde{V}$ and $\beta\Delta_o \gg 1$, the self-consistent equation trivially reduces to

$$\tilde{V} \sim \tilde{C} e^{\int_0^\infty d\omega \frac{J(\omega)\coth(\beta\omega/2)}{\omega^2}} \tag{2.16}$$

where, for $s < 3$, there are no tunneling dynamics, i.e. the system remains localized to a single well for all time (and T). Since we wish to describe damped tunneling dynamics, we restrict our discussion in the main body to $s \geq 3$.

2.10 Bibliography

[1] Justin M. Hodgkiss, Niels H. Damrauer, S. Pressé, J. Rosenthal, and Daniel G. Nocera. *J. Phys. Chem. B*, 110:18853, 2006.

[2] S. Pressé and R. Silbey. *J. Chem. Phys.*, 5:921, 2006.

[3] C. Turró, C.K. Chang, G.E. Leroi, R.I. Cukier, and D.G. Nocera. *J. Am. Chem. Soc.*, 114:4013, 1992.

[4] J.A. Roberts, J.P. Kirby, and D.G. Nocera. *J. Am. Chem. Soc.*, 117:8051, 1995.

[5] A. Harriman, Y. Kubo, and J.L. Sessler. *J. Am. Chem. Soc.*, 114:388, 1992.

[6] J.L. Sessler, B. Wang, and A. Harriman. *J. Am. Chem. Soc.*, 115:10418, 1993.

[7] P.J.F. deRege, S.A. Williams, and M.J. Therien. *Science*, 269:1409, 1995.

[8] V.Y. Shafirovich, S.H. Courtney, N. Ya, and N.E. Geactinov. *J. Am. Chem. Soc.*, 117:4920, 1995.

[9] J. Stubbe, D.G. Nocera, C.S. Yee, and M.C.Y. Chang. *Chem. Rev.*, 103:2167, 2003.

[10] James M. Mayer. *Ann. Rev. Phys. Chem.*, 55:363, 2004.

[11] My Hang V. Huynh and Thomas J. Meyer. *Chem. Rev.*, 107:5004, 2007.

[12] L. Biczók, N. Gupta, and H. Linschitz. *J. Am. Chem. Soc.*, 119:12601, 1997.

[13] M. Sjödin, S. Styring, B. Åkermark, L. Sun, and L. Hammarström. *J. Am. Chem. Soc.*, 122:3932, 2000.

[14] C. Carra, N. Iordanova, and S. Hammes-Schiffer. *J. Am. Chem. Soc.*, 125:10429, 2003.

[15] D. Shukla, R.H. Young, and S. Farid. *J. Phys. Chem. A*, 108:10386, 2004.

[16] R.I. Cukier. *J. Phys. Chem.*, 99:16101, 1995.

[17] R.I. Cukier. *J. Phys. Chem. B*, 106:1746, 2002.

[18] Alexander Soudackov and Sharon Hammes-Schiffer. *J. Chem. Phys.*, 111:4672, 1999.

[19] R.A. Marcus. *J. Chem. Phys.*, 24:966, 1956.

[20] Hélène Decornez and Sharon Hammes-Schiffer. *J. Phys. Chem. A*, 104:9370, 2000.

[21] Ivan Rostov and Sharon Hammes-Schiffer. *J. Chem. Phys.*, 115:285, 2001.

[22] Daniel C. Borgis, Sangyoub Lee, and James T. Hynes. *Chem. Phys. Lett.*, 162:19, 1989.

[23] A. Suárez and R. Silbey. *J. Chem. Phys*, 94:4809, 1991.

[24] D.N. Beratan, J.N. Onuchic, and J.J. Hopfield. *J. Chem. Phys.*, 86:4488, 1987.

[25] D.N. Beratan, J.N. Onuchic, J.N. Winkler, and H.B. Gray. *Science*, 258:1740, 1992.

[26] S. Kumar and R. Nussinov. *Chem. Bio. Chem.*, 3:604, 2002.

[27] H.R. Bosshard, D.N. Marti, and I. Jelesarov. *J. Mol. Recognit.*, 17:1, 2004.

[28] J.D. Puglisi, L. Chen., A.D. Frankel, and J. R. Williamson. *Proc. Natl. Acad. Sci. U.S.A.*, 90:3680, 1993.

[29] N.P. Pavletich and C.O. Pabo. *Science*, 252:809, 1991.

[30] J. M. Berg. *Acc. Chem. Res.*, 28:14, 1995.

[31] E.H. Howell, J.E. Villafranca, M.S. Warren, S.J. Oatley, and J. Kraut. *Science*, 231:1123, 1986.

[32] B.E. Ramirez, B.G. Malmström, J.R. Winkler, and H.B. Gray. *Proc. Natl. Acad. Sci. U.S.A.*, 92:11949, 1995.

[33] P. Brzezinksi. *Biochemistry*, 35:5611, 1996.

[34] B.R. Crane, L.M. Siegel, and E.D. Getzoff. *Science*, 270:59, 1995.

[35] J.P. Kirby, J.A. Roberts, and D.G. Nocera. *J. Am. Chem. Soc.*, 119:9320, 1997.

[36] J.A. Roberts, J.P. Kirby, S.T. Wall, and D.G. Nocera. *Inorg. Chim. Acta*, 263:395, 1997.

[37] Niels H. Damrauer, Justin M. Hodgkiss, Joel Rosenthal, and Daniel G. Nocera. *J. Phys. Chem. B*, 108:6315, 2004.

[38] A. Osuka, R. Yoneshima, H. Shiratori, S. Okada, S. Taniguchi, and N. Mataga. *Chem. Comm.*, page 1567, 1998.

[39] J. Otsuki, K. Iwasaki, Y. Nakano, M. Itou, Y. Araki, and O. Ito. *O. Chem. Eur. J.*, 10:3461, 2004.

[40] M.U. Winters, K. Pettersson, J. Martensson, and B. Albinsson. *Chem. Eur. J.*, 11:562, 2005.

[41] E.R. Young, J. Rosenthal, J.M. Hodgkiss, and D.G. Nocera. To be submitted.

[42] G. Mahan. *Many-Particle Physics*. Kluwer Academic/Plenum Publishers, 2000.

[43] A.J. Leggett, S. Chakravarty, A.T. Dorsey, Matthew P.A. Fisher, Anupam Garg, and W. Zwerger. *Rev. Mod. Phys.*, 59:1, 1987.

[44] U. Weiss. *Series in modern condensed matter physics: Quantum Dissipative Systems*, volume 10. World Scientific, 1999.

[45] R. Wertheimer and R. Silbey. *Chem. Phys. Lett.*, 75:243, 1980.

[46] J.J. Sakurai. *Modern Quantum Mechanics*. Addison Wesley Pub. Co., 1994.

[47] Sighart Fischer. *J. Chem. Phys.*, 53:3198, 1970.

[48] G.C. Pimentel and A.L. McClellan. *Annu. Rev. Phys. Chem.*, page 347, 1971.

[49] D.Hadži and S.Bratos. *The hydrogen bond-recent developments in theory and experiments*, pages 567–611. North-Holland Publ. Co., 1976.

[50] W.A.Herrebout, K.Clou, and H.O. Desseyn. *J. Phys. Chem. A*, 105:4865, 2001.

[51] Koichi Itoh and Takehiko Shimanouchi. *Biopolymers*, 5:921, 1967.

[52] D. Rodney Truax. *Phys. Rev. D*, 31:1988, 1985.

[53] K. Kassner and R. Silbey. *J. Phys. A: Math. Gen.*, 20:4355, 1987.

[54] Robert J. Silbey and Robert A. Harris. *J. Chem. Phys*, 80:2615, 1984.
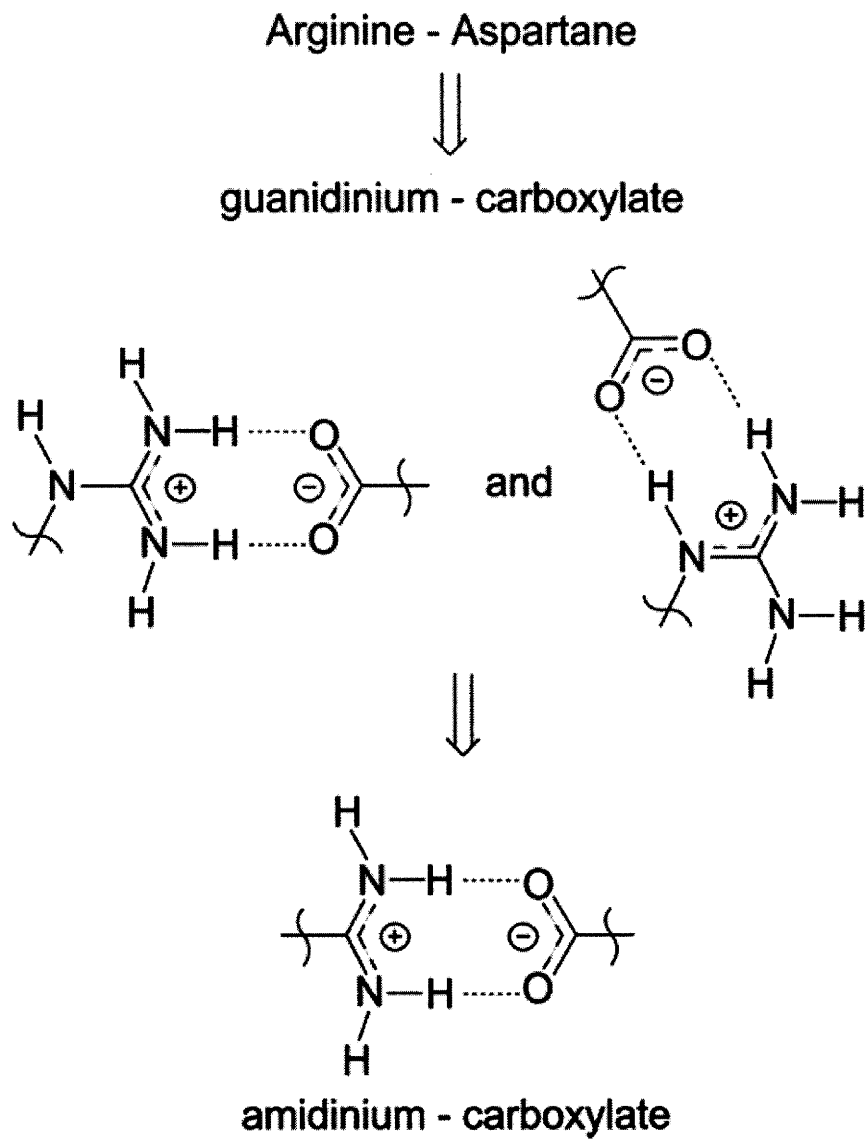
Figure 2.1: This figure, taken from Hodgkiss *et al.*[1] depicts the two binding modes of the guanidinium-carboxylate H-bond which arises in arginine and aspartane complexes. Also depicted is the single binding mode of the amidinium-carboxylate H-bond.
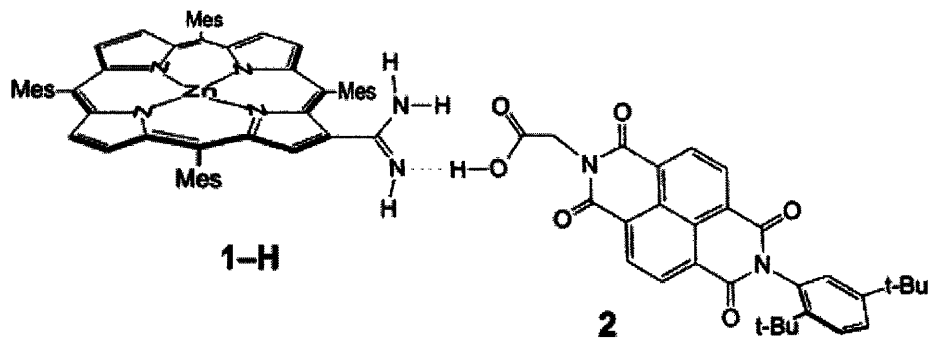
Figure 2.2: This figure, taken from Hodgkiss *et al.*[1], depicts the *PCET* donor acceptor assembly discussed in the main body, 1-H:2.
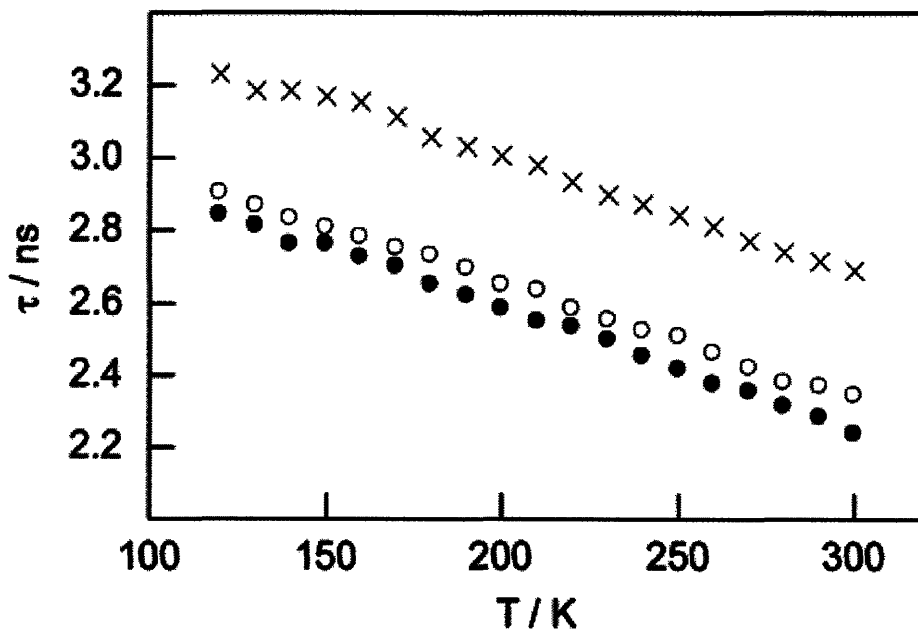
Figure 2.3: Fluorescence lifetimes, τ, versus temperature for 1-H (dark circles), 1-D (open circles), and ZnTMP (crosses) in 2-MeTHF[1].
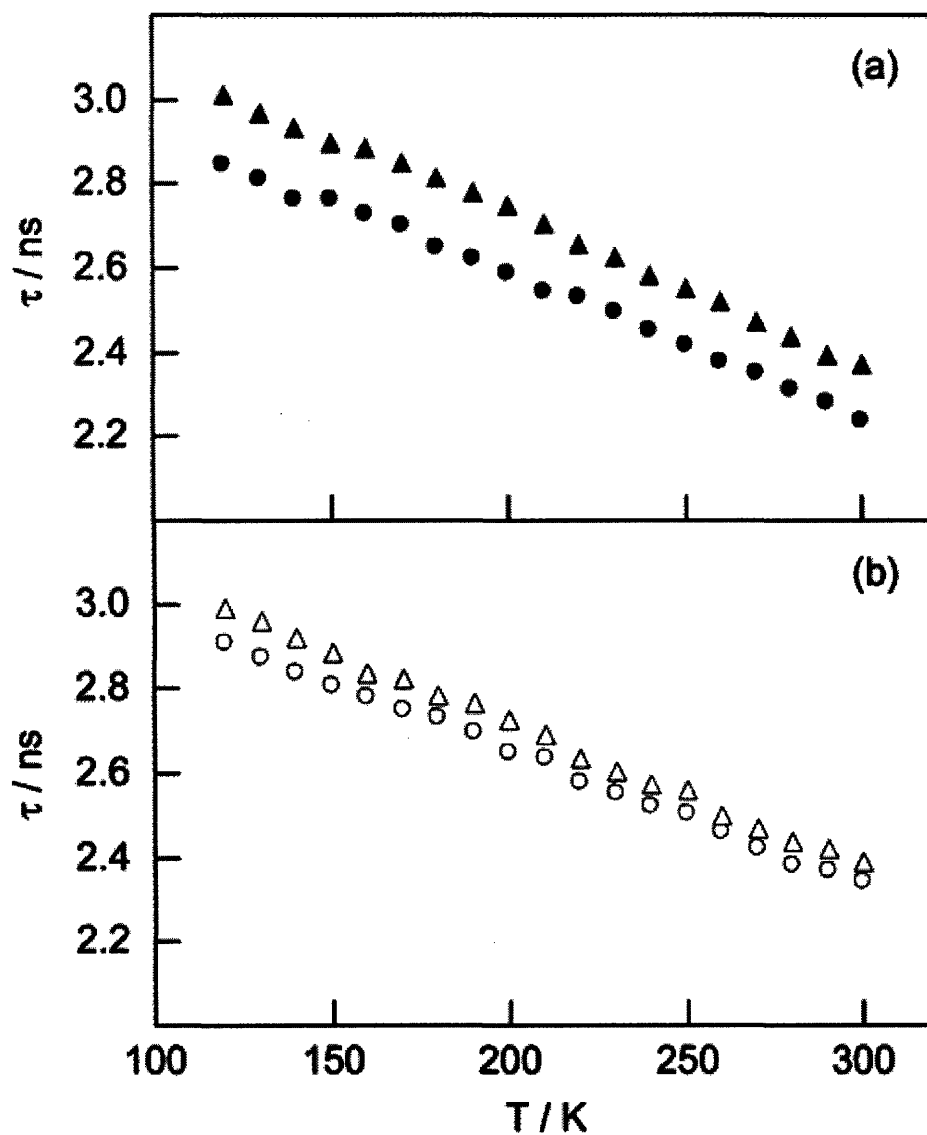
Figure 2.4: Top figure: fluorescence lifetimes, τ, versus T for 1-H (dark circles) and 1-H:benzoate (dark triangles) in 2-MeTHF. Bottom figure: Same as above but for 1-D (open circles) and 1-D:benzoate (open triangles) in 2-MeTHF[1].

1

2 : CO₂H – NI
3 : SO₃ – NI
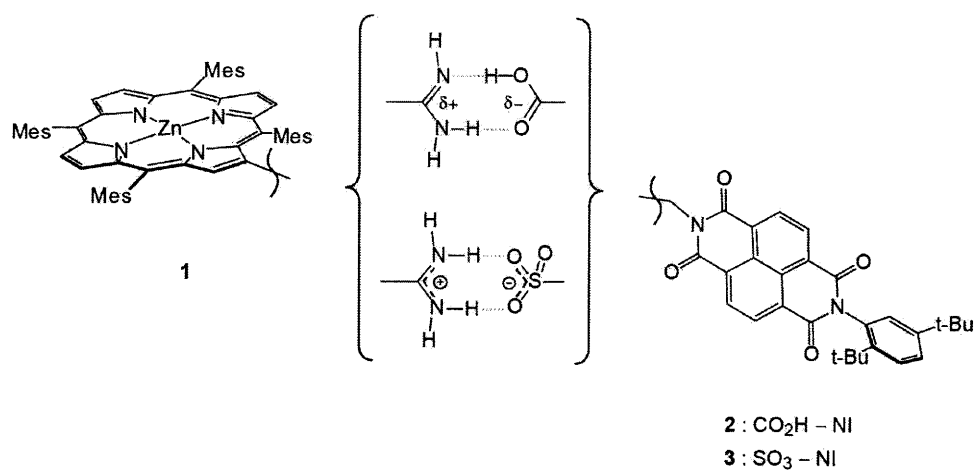
Figure 2.5: This figure, taken from the cited reference[41], depicts the *PCET* donor acceptor assembly, 1-H:2 and 1-H:3, discussed in the main body.
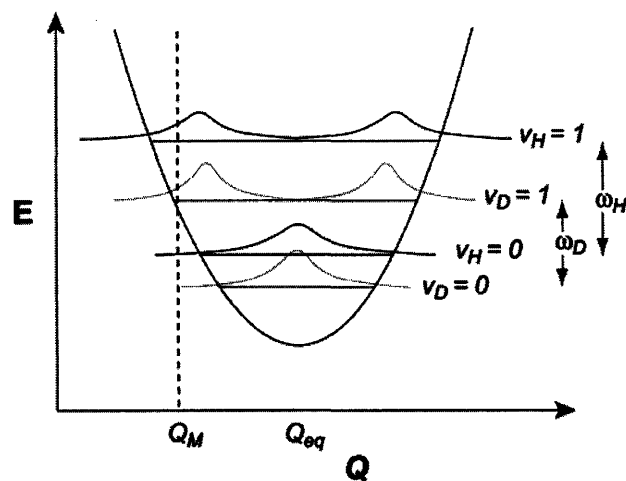
Figure 2.6: This figure, taken from Hodgkiss et al.[1], depicts the underlying microscopic features of the model. In this figure, the probability densities for each of the energy levels of the $N + 1^{th}$ mode are plotted versus the vibrational coordinate Q for the mode. The energy levels are labeled by successive ν, for both deuterated, ν_D, and non-deuterated, ν_H, cases. In the model, the electron tunneling matrix element is maximized at the point Q_M labeled by the dashed line. This rough sketch is meant to capture the high T as well as low T features of the model; at high T and larger Q_M, the electron transfer rate is maximized in the presence of protonated mode while for small Q_M and low T, the opposite holds. The other two cases, high T small Q_M and low T large Q_M, immediately follow from this discussion.

54
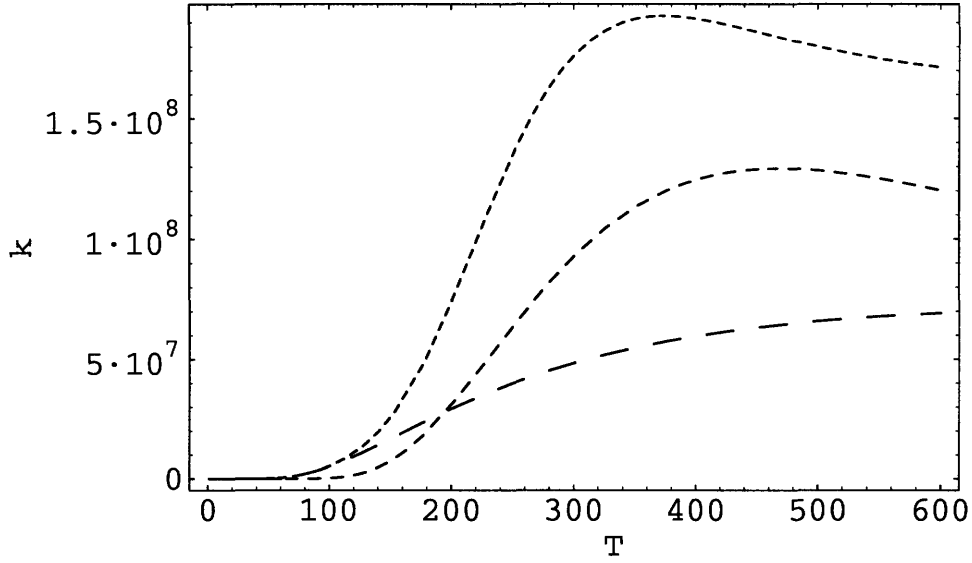
Figure 2.7: Theoretical curves of the rate k in s^{-1} versus T in K for the zeroth order term of Eq.(2.9)(long dashing), the zeroth plus first order term of Eq.(2.9)(intermediate dashing) and the sum of all orders(short dashings). The following parameter values were used: m=mass of proton, $\Delta_o = -220\text{meV}$, $C = \frac{-\Delta_o}{139}$, $Q_M = 0.80\text{Å}$, $\nu = 127\text{cm}^{-1}$, $\gamma = \frac{1.20}{Q_M{}^2}$, $4\eta\omega_c = 25.3meV$, $f = 1.38 \times 10^{-10} J/m$.
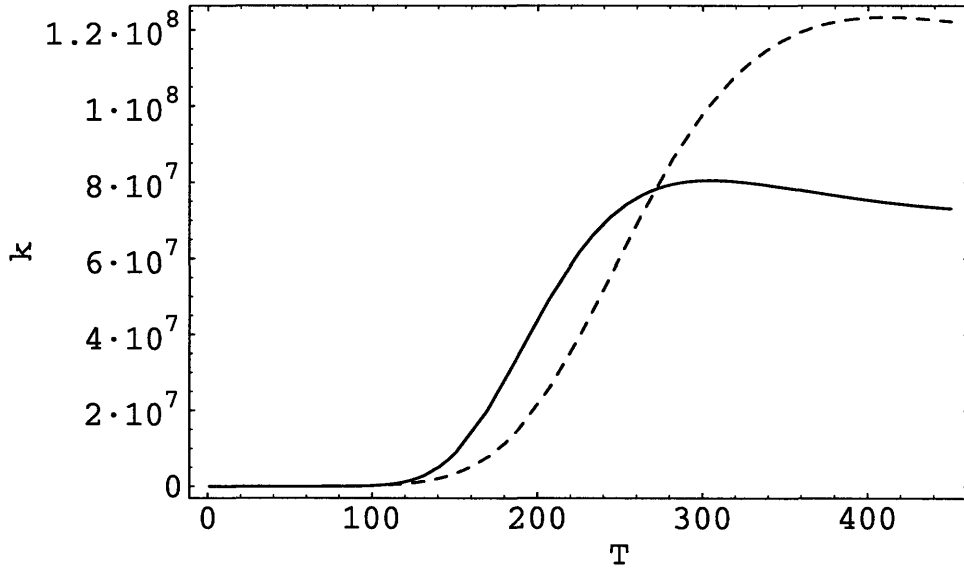
Figure 2.8: Theoretical curves depicting T-isotope dependence for ET rates with protons, dashed line, and deuterons, solid line, along the H-bonding interface. The axes are the same as in Fig.(2.7). The following parameter values were used: isotope effect used is the usual ~ 1.414, m=mass of proton, $\Delta_o = -220\text{meV}$, $C = \frac{-\Delta_o}{139}$, $Q_M = 0.80\text{Å}$, $\nu = 127\text{cm}^{-1}$, $\gamma = \frac{1.20}{Q_M{}^2}$, $4\eta\omega_c = 25.3meV$, $f = 1.38 \times 10^{-10} J/m$.
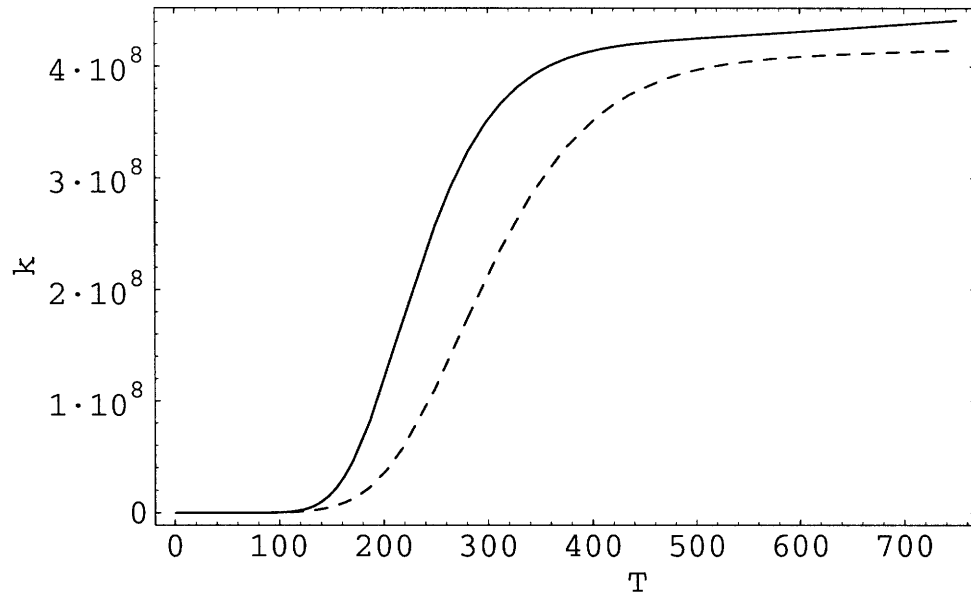
Figure 2.9: Theoretical curves depicting T-isotope dependence for ET rates with protons, dashed line, and deuterons, solid line, along the H-bonding interface. The axes are the same as in Fig.(2.7). The following parameter values were used: isotope effect used is the usual ~ 1.414, m=mass of proton, $\Delta_o = -220$meV, $C = \frac{-\Delta_o}{139}$, $Q_M = 0.10\overset{\circ}{A}$, $\nu = 127$cm^{-1}, $\gamma = \frac{1.20}{Q_M^2}$, $4\eta\omega_c = 25.3meV$, $f = 1.38 \times 10^{-10} J/m$.
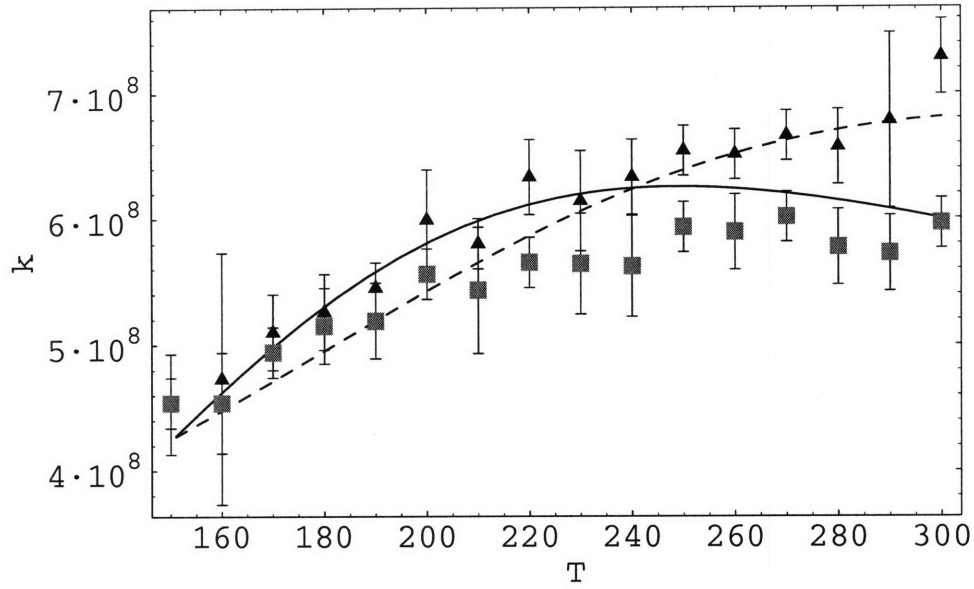
Figure 2.10: Theoretical and experimental curves(with error bars) depicting T-isotope dependence for ET assisted by protons, dashed line and triangles, respectively, and deuterons, solid line and squares, respectively. The axes are the same as in Fig.(2.7). The following parameter values were used: isotope effect used is the usual ~ 1.414, m=mass of proton, $\Delta_o = -260$meV, $C = \frac{-\Delta_o}{104}$, $Q_M = 0.93\mathring{A}$, $\nu = 143$cm^{-1}, $\gamma = \frac{1.35}{Q_M{}^2}$, $4\eta\omega_c = 38.9 meV, f = 1.38 \times 10^{-10} J/m$

Chapter 3

Ordering of Limits in the Jarzynski Equality

3.1 Prologue

The contents of this chapter have already been published in the cited reference[1]. Minor typos appearing in the original publication were corrected.

The rising number of citations of Jarzynski's original publication[2], in which his work relation first appears, are a clear demonstration of the growing enthusiasm in nonequilibrium fluctuation theorems.

Much like in the previous chapter, we have refrained from giving any background literature review beyond what is necessary to understand this work.

In this chapter we consider the sampling problems encountered in computing free energy differences using Jarzynski's non-equilibrium work relation [2]. This relation expresses the free energy change of a system, on which finite-time work is done, as an average over all possible trajectories of the system. This average can then be expressed as a cumulant expansion of the work. We study the scaling of these cumulants with an appropriately defined measure of phase space accessibility, ε, and particle number, N, for two simple changes in state. We find that the cumulant expansion is slowly convergent for predominantly entropic

processes, those where ε is considerably altered during the course of the process. An accurate determination of the free energy change requires some knowledge of the behavior of the tails of the work distribution associated with this process. Jarzynski's irreversible work relation is only valid with the correct ordering of the infinite limits of N and ε, clarifying the regime of its applicability.

3.2 Introduction

The Jarzynski equality, JE, is one of the few known general expressions in non-equilibrium statistical mechanics[2]. Provided certain conditions are satisfied, this relation expresses an equilibrium free energy change for a classical system, subject to an exterior force, as a cumulant expansion in the work.

Since the first derivation of this expression, some of the conditions used to derive the JE have been relaxed while other more general non-equilibrium fluctuation theorems have been proposed[3, 4, 5, 6, 7, 8, 9, 10, 11, 12, 13]. In addition, Hummer and Szabo observed that the JE could be used to compute a free energy profile as a function of some predefined axis along which the work is performed[14, 15]. From then on, the JE has been used in both simulations and experiments[16, 17].

Although formally correct, Jarzynski's relation works best for microscopic systems and experiments performed slowly compared to the system's characteristic relaxation times. This is because for short experimental times, work distributions are centered at values large compared to the free energy difference, and important features of the work distribution are difficult to extract for experiments with large numbers of particles, especially for non-Gaussian distributions of work[18, 2, 19]. However, simple model systems interacting via harmonic potentials or governed by linear stochastic equations of motion, for example, are guaranteed to have Gaussian work distributions[20].

Purely entropic processes have received little attention in the discussions of the JE. This is because an accurate free energy determination would rely on sampling of rare events. Although extracting the free energy change for entropically driven processes may be of little practical use, the convergence properties of the work cumulants exhibited in this regime are of interest. The remainder of this chapter is organized as follows. In section 3.3 we review important features of the JE and introduce some of the scaling parameters used to test convergence properties of the work cumulant expansion. In section 3.4 and 3.5 we consider two examples of entropically driven changes in state: the expansion of an ideal gas

and the expansion of a Gaussian polymer chain from one container to another. Because these examples are exactly solvable, we are able to make strong statements about limits and convergence that would not be possible in more complex, and realistic, examples. In section 3.6 we discuss the thermodynamic limit and conclusions are given in section 3.7.

3.3 Jarzynski's Non-Equilibrium Work Relation

We begin by imagining an apparatus performing work, W, via a generalized force on a system coupled to its bath. The definition of bath employed here is utilitarian: the bath consists of those degrees of freedom whose free energy change is not explicitly calculated. The system plus bath are presumed ergodic, by virtue of having been brought into canonical equilibrium by a supersystem of finite temperature β^{-1}. We set Boltzmann's constant to unity throughout. In addition, by generalized force we mean one that may not be derivable from a potential in the limit considered for the process[21].

Jarzynski defines the work to be equal to the change in total system plus bath energy. Incidentally, this is the only definition from which the JE may be derived [2, 22]. This definition is equivalent to the *charging energy* ubiquitously appearing in the theory of the statistical mechanics of the liquid state [23]. It is not the Newtonian work in general, although both the total Hamiltonian change and the Newtonian work are simply related provided there exists a Hamiltonian describing the process.

We assume that the particle number, N, and the total phase space volume Ω, obtained by integrating the Liouville measure over all of phase space, are conserved quantities so that the corresponding Liouville measure represents a complete set of trajectories, i.e. metrically indecomposable[24].

In the Hamiltonian formulation of the JE it is then sufficient to use the properties discussed above in conjunction with the usual statistical mechanical definition of free energy, F, in order to show that[2, 22]

$$e^{-\Delta F} = \langle e^{-W} \rangle \tag{3.1}$$

where the average on the RHS corresponds to a canonical average over all classical trajectories. Also, β has been absorbed into both the work term and free energy definition.

For a system with partition function Z, we explicitly re-write the average of Eq.(3.1) as follows

$$e^{-\Delta F} = e^{\sum_{n=1} \frac{\partial_k^n \log[\tilde{Z}(k=0)]}{i^n n!}}$$

(3.2)

where $\tilde{Z}(k) = \int \mathscr{D}[x] e^{-\mathscr{H}(x) - ikW(x)}$ is the characteristic function of Z with x as a phase point, and $\mathscr{H}(x)$ is the system plus bath Hamiltonian rescaled by β. The logarithm of $\tilde{Z}(k)$ is the corresponding cumulant generating function.

The Hamiltonian can be made explicitly dependent on a measure of phase space accessibility, labeled ε. In our treatment, ε is equal to some applied potential, over a region of phase space, which suddenly changes at time $t = 0$. We are thereby considering a special case of the JE, namely the free energy perturbation method [25]. The degree to which the entropic contributions dominate the total free energy change is related to the variation in phase space accessibility at $t = 0$.

However, provided certain conditions are satisfied, in the thermodynamic limit, $N \to \infty$, the work distribution sharpens from central limit theorem type arguments. In other words, unique initial and final configurations may survive the limiting procedure. When this happens, typical values of W measured are those associated to the trajectories linking the remaining initial and final configurations.

The above highlights the heart of the problem; in the strict $N \to \infty$ limit, entropic contributions may incorrectly vanish. Work cumulants are thus sensitive to how the limits of N and ε are taken. This is illustrated below for the examples of the ideal gas and Gaussian chain. In addition, these examples show that it is generally incorrect to assume monotonic convergence of the work cumulant expansion, for sensible parameter values, and that even purely entropic processes show model-dependent N-scaling for the cumulants of the work.

3.4 Ideal Gas

We begin by considering a simple ideal gas in equilibrium at temperature β^{-1}. We partition the coordinate phase space into two regions of equal volume, labeled I and II, where region II is disfavored by a small biasing potential ε relative to region I. In this example, the system serves as its own bath. For the remainder of this discussion, we conveniently set ε to zero in region I.

In the usual case taught in elementary thermodynamics courses, $\varepsilon = \infty$ in region II; i.e. there is a hard constraint that is removed at $t = 0$ in order to allow the gas to expand into region II. This process does not conserve the phase space of the system. Instead of that, we consider the case of non-infinite ε so as to conserve phase space.

We let m be the number of particles that are located in region II for a possible discrete configuration of the system. For simplicity we assume regions I and II are of equal volume. We then tentatively write an absolute free energy for the configuration of the system in which m particles are in II and $N - m$ are in I as $f_m = E_m - \log P_m$ where P_m is the normalized equilibrium probability for that configuration and β is again absorbed into the energy term, E_m. This is entirely analogous to the loaded dice problem or the statistical mechanics of the two-level system[26]. More explicitly, we recover for this example

$$f_m = -\log \binom{N}{m} \frac{e^{-m\varepsilon}}{2^N} \tag{3.3}$$

The total absolute free energy, $F_N(\varepsilon)$, therefore follows by considering all configurations

$$F_N(\varepsilon) = -\log \sum_{m=0}^{N} \binom{N}{m} \frac{e^{-m\varepsilon}}{2^N} \tag{3.4}$$

Defining $\Delta F_N = F(\varepsilon = 0) - F_N(\varepsilon)$, where $F(\varepsilon = 0) = 0$, we write

$$e^{+\Delta F_N} = \frac{(1 + e^{-\varepsilon})^N}{2^N} \tag{3.5}$$

where ΔF_N corresponds to the following change in state: expansion from region I to the combined volume of regions I and II as the potential in region II is lowered from $\varepsilon > 0$ to zero at $t = 0$.

We rewrite $e^{-\Delta F_N}$ as

$$e^{-\Delta F_N} = \sum_{m=0}^{N} \binom{N}{m} \frac{e^{-m\varepsilon} e^{+m\varepsilon}}{(1 + e^{-\varepsilon})^N} \tag{3.6}$$

Physically associating the probability of a particle being in I with $P_I = \frac{1}{1+e^{-\varepsilon}}$ and the probability of being in II with $P_{II} = \frac{e^{-\varepsilon}}{1+e^{-\varepsilon}}$ we verify the JE

$$e^{-\Delta F_N} = \sum_{m=0}^{N} \binom{N}{m} P_I^{N-m} P_{II}^m e^{m\varepsilon} = \langle e^{-W} \rangle \tag{3.7}$$

where $n\varepsilon \equiv -W$ is the total change in the Hamiltonian. As a check, we note that the limit $\varepsilon \to \infty$, leads to the correct free energy change while satisfying the constraint imposed on phase volume.

The above discussion summarizes the statistical mechanics of the expansion of an ideal gas within the context of the JE.

For this example, since each particle is independent, all work cumulants trivially scale as N. We now consider convergence properties of the sum over work cumulants when the potential of region II, ε, is set to 0, at $t = 0$. The two cases considered are those when ε is either initially $\varepsilon \ll 1$ or $\varepsilon \gg 1$ in region II.

In the first case, all of coordinate phase space is initially thermally accessible. Since phase space density is negligibly redistributed in dropping the potential of region II to zero, the free energy change is purely energetic up to order ε^2. From Eq.(3.2) we obtain

$$e^{-\Delta F} = e^{N \sum_{n=1} \frac{\partial_k^n \log[1+e^{\varepsilon(ik-1)}]|_{k=0}}{i^n n!}}$$

$$\sim 1 + \frac{N\varepsilon}{2} + \mathcal{O}(\varepsilon^2) \tag{3.8}$$

where the argument of the logarithm is the characteristic function of the partition function. The normalization factor of the latter quantity, having no k-dependence, is ignored. We can identify the free energy, $\Delta F = -\frac{N\varepsilon}{2}$, as that performed by the single configuration with N/2 particles in I and N/2 particles in II. Thus, when phase space is negligibly redistributed, a single configuration dominates the free energy change. The results remain unchanged as $N \to \infty$.

In the second case, region II initially has a potential $\varepsilon \gg 1$. We may calculate the nth work cumulant using $\frac{\partial_k^n \log[1+e^{\varepsilon(ik-1)}]|_{k=0}}{i^n}$. For this case, we find $\langle W^n \rangle_c \sim N\varepsilon^n e^{-\varepsilon}$. As opposed to the small ε limit, a reasonable estimate of the free energy change requires sampling increasingly rare configurations as $\varepsilon \to \infty$. Then $N \to \infty$ must follow $\varepsilon \to \infty$ because the large N limit supresses rare configurations which contribute to the free energy change. This is verified for $\varepsilon = 0$ by using Stirling's formula for the factorials in order to re-write Eq.(3.3) as

$$e^{-f_m} = \frac{\sqrt{N}}{\sqrt{2\pi m(N-m)}} e^{-N(\frac{m}{N} \log \frac{m}{N} + \frac{N-m}{N} \log \frac{N-m}{N} + \log 2)} \tag{3.9}$$

This discussion is trivially generalizable to any set of non-interacting particles by discretizing the corresponding phase space. Consider discretizing coordinate phase space into many regions, I, II, III,..., with potentials, 0, ε_1, ε_2,...ε_d. Then the free energy for a single configuration with m_1 particles in region I, m_2 in region II ... and $m_d = N - \sum_{i=1}^{i=N-1} m_i$ in

the last region follows from the normalized multinomial distribution $f_{m_1 \ldots m_d} = m_1 \varepsilon_1 + \ldots +$ $m_d \varepsilon_d + \log \left(\frac{N!}{m_1! m_2! \ldots (m_d - m_1 - \ldots m_{d-1})!} \frac{1}{d^N} \right)$. As each $\varepsilon_i \to 0$ then $\langle W \rangle = \frac{N(\varepsilon_1 + \ldots + \varepsilon_d)}{d-1}$. Likewise, as $\varepsilon_i \to \infty$, for $\frac{\varepsilon_i}{\varepsilon_j} = finite \ number$, then $\langle W^n \rangle_c \sim N(\varepsilon_1^n e^{-\varepsilon_1} + \ldots + \varepsilon_d^n e^{-\varepsilon_d})$.

To summarize, the ideal gas example illustrates the subtlety of the limiting process: the conservation of phase space volume requires that ε be non-infinite from the onset. Furthermore, $N \to \infty$ must follow $\varepsilon \to \infty$ since a single configuration is only sufficient in the trivial case that all of phase space is thermally equally accessible.

We conclude that free energy changes for entropy-generating processes are extractable from Jarzynski's formalism by extrapolating the result of microscopic systems where cumulants of the work distribution are *a priori* not supressed. The scaling of the work cumulants with N for the selected parameter values however is unknown in general, i.e. is model-dependent.

3.5 Expansion of the Gaussian Chain

We briefly consider another example below, that of the expansion of a Gaussian chain of N Kuhn steps, each of length l, initially located in a spherical vessel of radius R_1, into a second vessel of radius R_2. The model follows Muthukumar's paper on the dynamics and thermodynamics of the escape of a polymer chain[27].

There are two features of the expanding polymer's free energy profile versus the number of subunits in the second vessel that deserve attention. Firstly, there is an entropic barrier in the free energy profile of the expanding model polymer as it funnels through, one subunit at a time, from the first to the second vessel. Secondly, there are two minima in the free energy profile corresponding to the polymer entirely located in one or another of the two vessels. We will refer to the configurations corresponding to the polymer entirely located in either of the two vessels as endpoint configurations. Provided there is no charging potential required to place a polymer subunit into the second vessel, the most stable configuration is the one in which the polymer is located in the larger of the two vessels.

We are interested in determining the scaling properties of the work cumulants as the polymer expands into the second vessel; therefore we begin by setting the charging potential associated to placing one polymer subunit into the second vessel to ε. We then diabatically set the charging potential of the second vessel to zero at time $t = 0$. Given reasonable parameter values, with $R_2 > R_1$, ε must be large enough so that the polymer will expand into the second vessel, otherwise the larger configurational entropy of the subunits gained by placing these in the second vessel outweighs the energetic cost of translocation.

In the subsequent calculation, we will exclude from consideration the endpoint configurations since these only change the initial and final equilibrium state of the polymer. The most stable configuration is now the one where all of the subunits, except one, are located in the larger of the two vessel. In a way, the sampling problem is worsened for the Gaussian chain as compared to the ideal gas example; intermediate configurations are largely supressed by the entropic barrier for modest N values.

For $m = [1, N - 1]$, the probability of finding $N - m$ Gaussian subunits in the first vessel and m in the other is[27]

$$P_1(N - m, R_1)P_2(m, R_2) = \frac{4a^2}{R_1 R_2} \sum_{p,j=1}^{\infty} e^{-\frac{p^2 l^2 \pi^2 (N-m)}{6R_1^2} - \frac{j^2 l^2 \pi^2 m}{6R_2^2}} \qquad (3.10)$$

to second order in a/R_i, for $i = 1, 2$, where the mth subunit is separated by a distance a from the opening separating both vessels.

Using the probability distribution from Eq.(3.10), we illustrate in Fig.(3.1) the supression of rare configurations with increasing values of N for $m = [1, N - 1]$.

We compute the work cumulants from the characteristic function of the partition function using Eq.(3.10)

$$\frac{(-)^n \langle W^n \rangle_c}{n!} = \frac{\partial_k^n}{n! i^n} \log[\sum_{m=1}^{N-1} P_1(N - m, R_1)P_2(m, R_2)e^{-m\varepsilon(ik+1)}]|_{k=0} \qquad (3.11)$$

In constrast to the ideal gas example, we have a degeneracy factor of unity.

Interchanging the order of summations in Eq.(3.11), we can immediately perform the summation over m, yielding

$$\frac{(-)^n \langle W^n \rangle_c}{n!} = \frac{\partial_k^n}{n! i^n} \times$$

$$\log[\sum_{p,j=1}^{\infty} e^{-\frac{p^2 l^2 \pi^2 N}{6R_1^2}} \frac{[e^{\frac{p^2 l^2 \pi^2}{6R_1^2} + \varepsilon(ik+1)} - e^{\frac{j^2 l^2 \pi^2}{6R_2^2}} (e^{\frac{p^2 l^2 \pi^2 N}{6R_1^2} - \frac{j^2 l^2 \pi^2 N}{6R_2^2} + N\varepsilon(ik+1)})]}{e^{\frac{j^2 l^2 \pi^2}{6R_2^2}} - e^{\frac{p^2 l^2 \pi^2}{6R_1^2} + \varepsilon(ik+1)}}]|_{k=0} \qquad (3.12)$$

To complete this example, we illustrate in Fig.(3.2) and Fig.(3.3) 3D plots of the value of the nth cumulant contribution versus increasing ε and n for small and large ε. We conclude this section by briefly outlining the similarity between this example and that of the ideal gas

for small and large ε.

From Fig.(3.2), for small ε, we note by inspection that as ε is raised, more cumulants are needed to compute free energy changes to some desired percent accuracy. This is numerically verified for the first 12 terms in the cumulant expansion, *e.g.* the ratio of the third to first order terms in the cumulant expansion monotonically increases from 0.02% to 0.2% as ε is raised from 0.005 to 0.01625.

In Fig.(3.3) we see that for large ε, each successive $|\frac{\langle W^n \rangle_c}{n!}|$ grows with n. This is also verified for the first 12 cumulants. Eventually, as in the case of the ideal gas, convergence of the cumulant expansion is assured for any physical system. For intermediate ε values, the behavior is more complicated. The successive terms show neither a clearly increasing nor decreasing trend for apparently sensible parameter values.

3.6 Thermodynamic Limit

From sections 3.4 and 3.5 we have quantitatively addressed the issue of sharpening of the work distribution for large N. In this section we reformulate our problem but using a new variable, the exponential of $-W$ and ask about the resulting distribution in the thermodynamic, $N \to \infty$, limit. We find this presentation conceptually clearer than one on the distribution of W in the thermodynamic limit since it gives a direct measure of how well the mean of this distribution, i.e. the exponential of the free energy, is sampled in varying $\langle e^{-W} \rangle / \sqrt{\langle e^{-2W} \rangle_c}$.

We begin by considering a discrete system for which we let $\log \mathscr{X} = \frac{\sum_i \log \chi_i}{N}$ where $\chi_i = e^{-\varepsilon_i}$ and ε_i is the work performed by the ith particle in a given configuration. From this it follows that $N \log \mathscr{X}$ is the negative of the total work associated to a single configuration.

Provided $\sum_{i_1, i_2 \ldots, i_n} \langle \log \chi_{i_1} \log \chi_{i_2} \ldots \log \chi_{i_n} \rangle_c \ll \mathscr{O}(N^{n-1})$, which trivially holds for systems of independent particles, then the distribution of configurations is log normally distributed in the thermodynamic limit

$$P(\mathscr{X}) = \frac{\sqrt{N}}{\sqrt{2\pi \langle \log \mathscr{X}^2 \rangle_c} \mathscr{X}} e^{-N \frac{(\log \mathscr{X} - \langle \log \mathscr{X} \rangle)^2}{2 \langle \log \mathscr{X}^2 \rangle_c}} \tag{3.13}$$

The first and second cumulants of the above distribution are easily calculated yielding $\langle \mathscr{X} \rangle = e^{\langle \log \mathscr{X} \rangle + \frac{\langle \log \mathscr{X}^2 \rangle_c}{2}}$ and $\langle \mathscr{X}^2 \rangle_c \propto (e^{\langle \log \mathscr{X}^2 \rangle_c} - 1)$.

For small $\langle \log \mathscr{X}^2 \rangle_c$, as is the case for energetic processes, $\langle e^{-W} \rangle / \sqrt{\langle e^{-2W} \rangle_c}$ grows and the mean of the distribution, which relates to the free energy change through the JE, is easily determined.

We are therefore faced with the problem of how small N must be taken in order to sample the relevant configurations in experiments. This can only be resolved on a case by case basis for various model Hamiltonians because there exists no general work cumulant scaling form for entropic processes.

A note on the apparent paradox of the ideal gas within the context of the JE is now in order. We explain the paradox as follows: no work is performed by releasing a hard wall constraint allowing a gas to expand against a vacuum. This incorrectly leads to the conclusion, when applying the JE, that the free energy change associated to the expansion of a gas is zero. As noted earlier however, ε cannot strictly be infinite since phase space volume would no longer be a conserved quantity. Instead we need to consider, as we had done before, quasi-hard wall constraints with rare configurations sampling the region of high potential to which a non-zero charging energy is associated. Taking the $N \rightarrow \infty$ from the very beginning however would lead to the conclusion that the only probable configuration is the one with all particles originally located in the region of lower potential for which the charging energy is clearly zero.

3.7 Conclusion

We have studied the convergence properties of the work cumulant expansion of the JE for processes in which the entropic contribution to the free energy change is large. This is done by adjusting the degree of phase space accessibility of regions in phase space while holding the total phase volume fixed.

We conclude that in the absence of important phase space density redistribution during the course of a process, the work cumulant expansion rapidly converges. The scaling of the work cumulant expansion with phase space accessibility is however model-dependent. In addition, it does not matter when the large N limit is taken for energetic processes since the most likely configuration is the one which dominates the free energy change.

In sharp contrast to energetic processes, entropic processes require sampling over rare configurations. Since the exponential of the sum of the microscopic work terms is log normally distributed in the large N limit, provided the usual conditions are satisfied, fluctuations needed to calculate an accurate entropic contribution to the free energy change incorrectly vanish for large enough N. This follows from the formulation of the JE: free energy differences are computed from the mean of a random variable which corresponds to the exponential of work. For this reason, it is difficult to assess *a priori* the accuracy of an experiment on larger, more flexible molecules.

As a note, broadening of the distribution in the work for entropy generating processes is generic and therefore applies to complicated interacting systems which are fundamentally two-state problems. Examples of this include the protein folding problem or the RNA hairpin and 3-helix junction stretching experiments. In particular, it has recently been shown that the distribution in the work for unfolding the RNA 3-helix junction is broader than that of refolding it[28].

Exactly soluble problems generating linear equations of motion lead to simple work distributions. For stretching experiments performed on complicated molecules with an arbitrary number of subunits, mapping the problem onto one with a Gaussian work distribution from

the onset is not justifiable. In the absence of a model for the system of interest, scaling properties of the work cumulants with N can be inferred by analyzing subunits of the system, if possible, and rescaling with the system size. Only then can it be verified that the system is not being probed in the regime where the central limit theorem supresses important entropic contributions to the free energy.
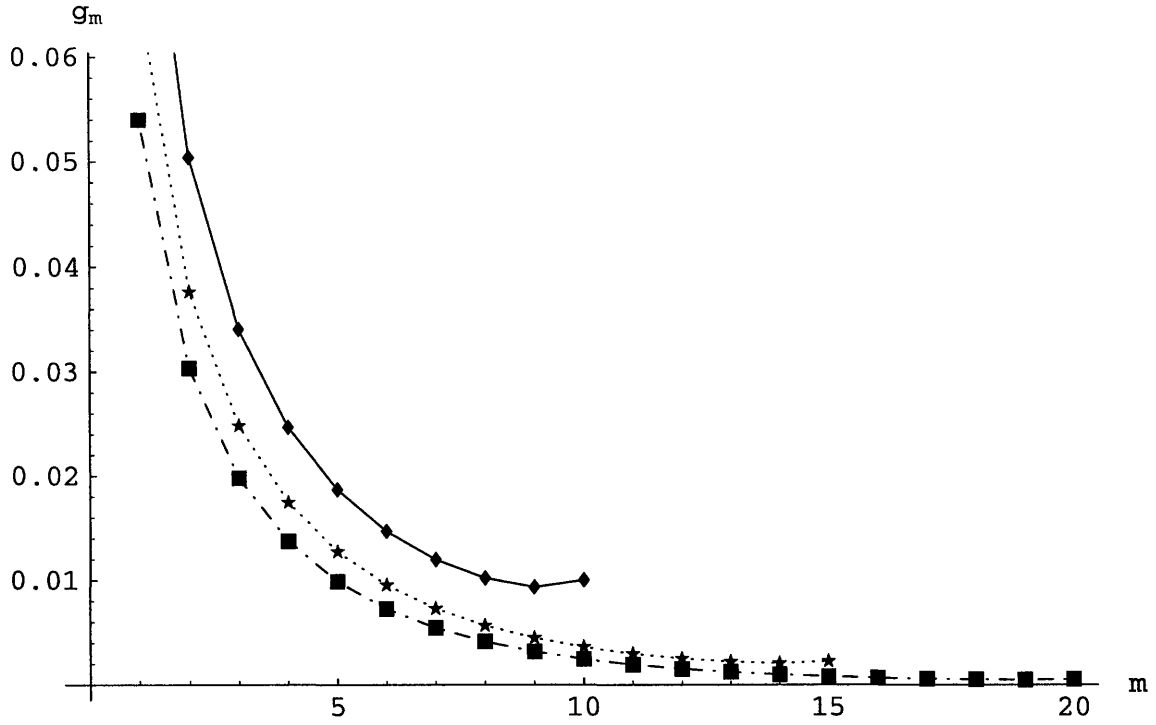
Figure 3.1: $g_m = e^{-f_m}$, where f_m is defined in a fashion analogous to Eq.(3.3) for the Gaussian chain, versus m for $m = [1, N-1]$. We use N=11(diamonds), 16(stars), 21(squares), $R_1 = 10$, $R_2 = 18$, $l = 1$, $a = 1/2$ and $\varepsilon = 0.25$. The free energy minimum, maximum in g_m, corresponding to all particles located in the second vessel(large m) becomes apparent in a plot of e^{-f_m} versus m for Gaussian chains with fewer subunits.
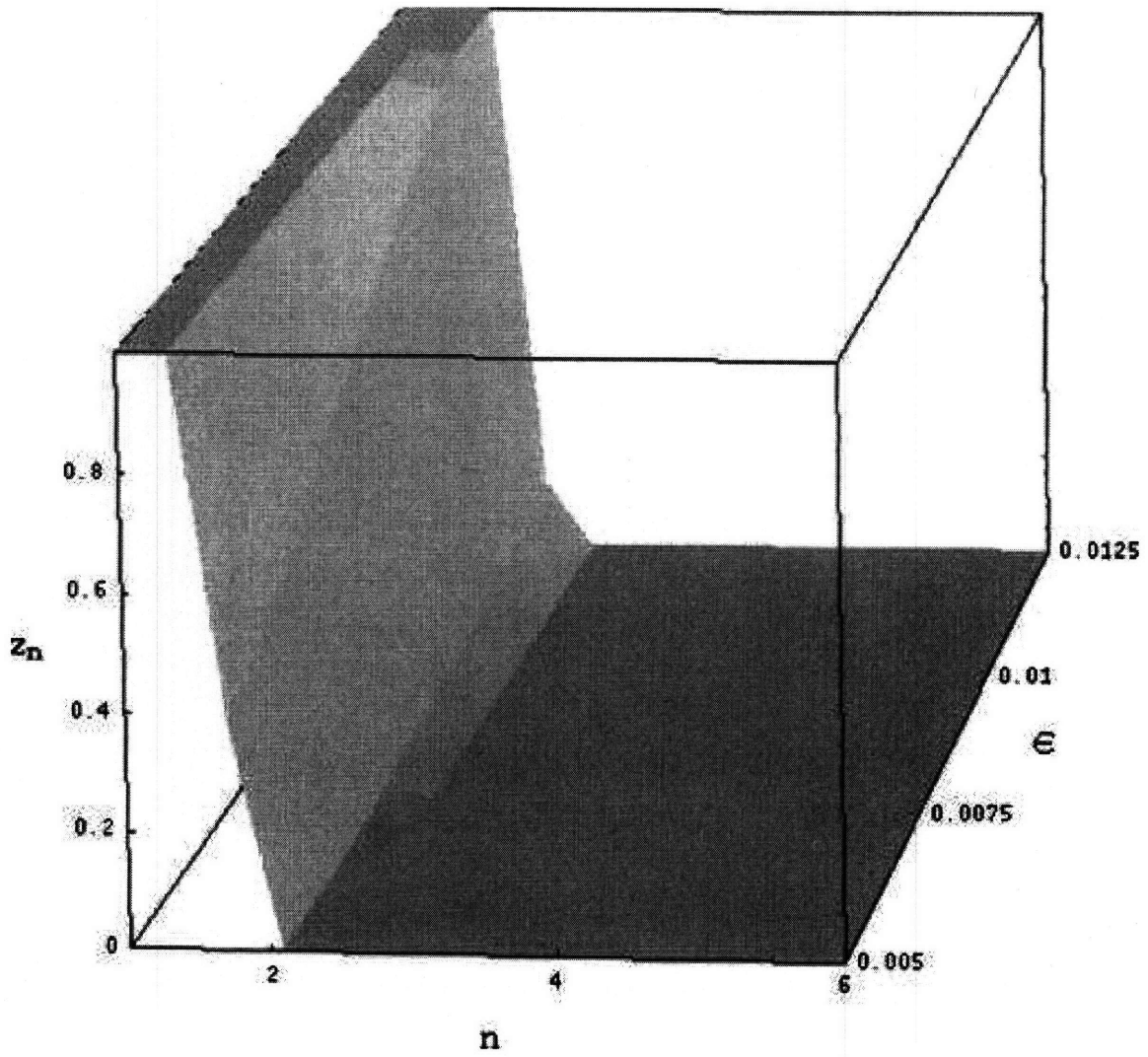
Figure 3.2: $z_n = |\frac{\langle W^n \rangle_c}{n!}|$(z-axis) versus cumulant number(horizontal axis), n, for small values of ε. We use $R_1 = 10$, $R_2 = 12$, $l = 1$, $a = 1/2$ and $N = 10$.
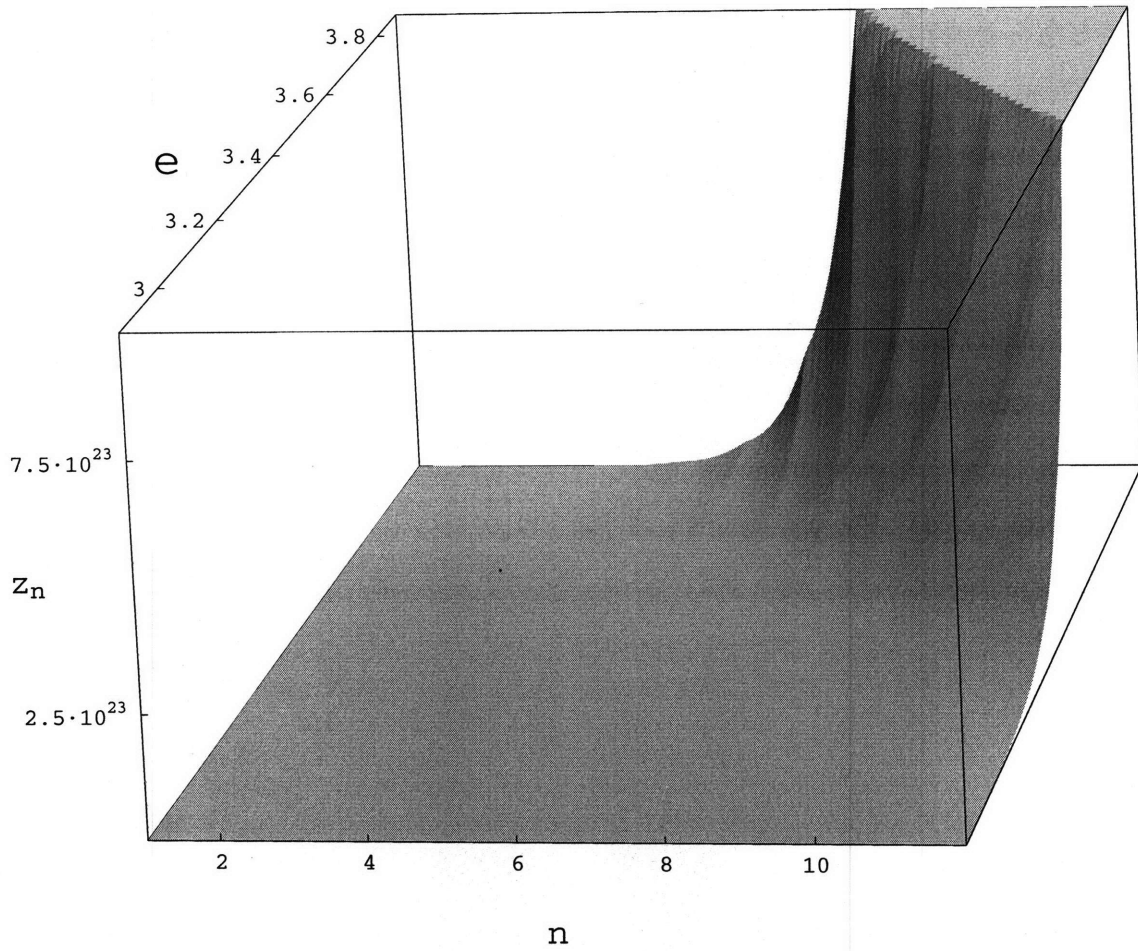
Figure 3.3: $z_n = |\frac{\langle W^n \rangle_c}{n!}|$(z-axis) versus cumulant number(horizontal axis), n, for large values of ε. We use the same values for R_1, R_2, l, a and N as in Fig.(3.2).

3.8 Bibliography

[1] S. Pressé and R.J. Silbey. *J. Chem. Phys.*, 124:054117, 2006.

[2] C. Jarzynski. *Phys. Rev. Lett.*, 78:2690, 1997.

[3] R. van Zon and E.G.D. Cohen. *Phy. Rev. Lett.*, 91:110601, 2003.

[4] O. Narayan and A. Dhar. *J. Phys. A: Math. Gen.*, 37:63, 2003.

[5] C. Jarzynski. *Phys. Rev. E*, 56:5018, 1997.

[6] U. Seifert. *Phys. Rev. Lett.*, 95:040602, 2005.

[7] G.E. Crooks. *Phys. Rev. E*, 61:2361, 2000.

[8] C. Jarzynski. *Dynamics of Dissipation*, pages 63–82. Springer, 2002.

[9] T. Hatano. *Phys. Rev. E*, 60:R5017, 1999.

[10] W. De Roeck and C. Maes. *Phys. Rev. E*, 69:026115, 2004.

[11] V. Chernyak, M. Chertkov, and C. Jarzynski. *Phys. Rev. E*, 71:025102, 2005.

[12] S. Mukamel. *Phys. Rev. Lett.*, 90:170604, 2003.

[13] T. Hatano and S. Sasa. *Phys. Rev. Lett.*, 86:3463, 2001.

[14] G. Hummer and A. Szabo. *PNAS*, 98:3658, 2001.

[15] G. Hummer and A. Szabo. *Acc. Chem. Res.*, 38:504, 2005.

[16] J. Liphardt, S. Dumont, S.B. Smith, I. Tinoco, and C. Bustamente. *Science*, 296:1832, 2002.

[17] S. Park, F. Khalili-Araghi, E. Tajkhorshid, and K. Schulten. *J. Chem. Phys.*, 119:3559, 2003.

[18] A. Dhar. *Phys. Rev. E*, 71:036126, 2005.

[19] H. Oberhofer, C. Dellago, and P.L. Geissler. *J. Phys. Chem. B*, 109:6902, 2005.

[20] O. Mazonka and C. Jarzynski. *cond-mat/9912121*, 1999.

[21] R.C. Lua and A.Y. Grosberg. *J. Phys. Chem. B*, 109:6805, 2005.

[22] C. Jarzynski. *J. Stat. Mech.*, page P09005, 2004.

[23] T.L. Hill. *Statistical Mechanics: Principles and Selected Applications*, pages 191–194. McGraw-Hill Book Co., 1956.

[24] A. Muenster. *Statistical Thermodynamics*, volume I, pages 28–30. Springer-Verlag, 1969.

[25] R.W. Zwanzig. *J. Chem. Phys.*, 22:1420, 1954.

[26] S.R.S. Varadhan. *Entropy*, pages 199–214. Princeton University Press, 2003.

[27] M. Muthukumar. *J. Chem. Phys.*, 118:5174, 2003.

[28] D. Collin, F. Ritort, C. Jarzynski, S.B. Smith, I. Tinoco Jr, and C. Bustamante. *Nature*, 437:231, 2005.

Chapter 4

Memory Effects in the Jarzynski Equality

4.1 Prologue

Most parts of this chapter are contained in the cited reference[1]. This chapter should be regarded as an extension of the last chapter.

In the present chapter, we consider solvable model systems onto which finite-time, rather than diabatic, work is done. For the systems and changes in state considered, there is no entropic change and the ensuing work distributions are Gaussian.

We focus on the fluctuations in the work, W, for such systems, arising from system-bath interactions and finite system recurrences, and study the resulting effect of dynamical broadening on the corresponding distribution $P(e^{-\beta_o W})$ with β_o as the inverse temperature.

This allows us to describe the dependence of $P(e^{-\beta_o W})$ on time and system-bath interactions. From the long-time behavior of the work fluctuations and $P(e^{-\beta_o W})$, we clarify both i) when a stochastic treatment of the dynamics may be legitimately invoked and ii) how information on the system-bath interaction for stochastic, near-equilibrium, systems may be extracted for such processes where a final temperature is well-defined.

4.2 Introduction

It was first shown by Jarzynski that, under certain circumstances, a change in free energy for a system, ΔF, induced by applying a force over some time τ may be computed by summing over all work cumulants for a system and bath initially equilibrated to temperature β_o^{-1} by a supersystem. More explicitly the Jarzynski equality, JE, reads[2, 3]

$$e^{-\Delta F} = \langle e^{-W} \rangle_o = e^{\sum_{n=1}^{\infty} \frac{(-)^n \langle W^n \rangle_{o,c}}{n!}} \tag{4.1}$$

where Jarzynski's *work* $W = W(\tau)$ is $W(\tau) = \int_0^\tau dt \partial_t \mathscr{H}$ and the subscript c above denotes cumulants. The average, $\langle \cdots \rangle_o$, is performed with respect to the (canonical) distribution of the system plus bath initial conditions. For convenience, all quantities with units of energy are rescaled by the inverse of temperature, β_o, throughout and Boltzmann's constant, k_B, is set to 1.

Since the derivation of Eq.(4.1), experiments and simulations have verified the equality and related fluctuation theorems with varying success [4, 5, 6, 7, 8, 9] while, from the theoretical standpoint, some of the conditions used to derive the JE have been relaxed and notable points have been clarified[10, 11, 12, 13, 14, 15, 16, 17, 18, 19, 20, 21, 22, 23, 24, 25, 26]. Alternate fluctuation theorems have also been proposed[27, 28, 29, 30, 31, 32, 33, 34, 35, 36].

In previous work, we studied the effect of large phase space density redistribution of the system on the convergence properties of the work cumulant expansion of Eq.(4.1) in the limit of a temporally diabatic process where the system served as its own bath [37].

Since the change in potential was diabatic, time did not explicitly enter into our analysis. Instead, we dealt with the expansion of the ideal gas and the Gaussian chain both of which are exactly solvable. We were thereby able to address the subtle issue of the thermodynamic limit on sampling of higher-order work cumulants for the case that the free energy change is

primarily entropic and for which an accurate determination of the free energy change relies on the tails of the work distribution.

However, the strength of Jarzynski's formalism lies in characterizing thermodynamic quantities for finite-time experiments on systems coupled to their environment and attention has thus been drawn to the convergence of the work cumulant expansion in time[26, 15, 38, 39].

There is another fundamental issue regarding the inherent time-dependence in the formulation of the JE which has received less attention in the literature. Consider the crucial step in the derivation of the JE which involves disconnecting a finite number of canonically distributed degrees of freedom, labeled as system plus bath at initial temperature β_o^{-1}, and allowing these to evolve under the action of a force from time 0 to τ. The question arises whether the final system plus bath Boltzmann weights, used in computing free energy differences according to Eq.(4.1), can be related to the true Boltzmann weights in the absence of disconnection from the microcanonical supersystem[40, 3, 41]. In general, this is not true because the temperature of a supersystem (and thus the temperature of any finite number of degree of freedom contained within the microcanonical ensemble) changes for an arbitrary variation in the total energy content.

In a related context, previous work by I. Oppenheim has demonstrated how the temperature of a microcanonical supersystem is renormalized by the application of an external force using nonlinear response theory[42, 43]. This was shown for the case of an adiabatic change by an expansion in N^{-1}, where N is the number of degrees of freedom contained in the microcanonical supersystem.

For the case when the applied force only recenters the work distribution of the system, the above difficulties do not arise. The same holds for a system with strongly dissipative dynamics where the system may be near-equilibrium at every step of the way and the temperature is instead defined through a fluctuation-dissipation theorem[44].

In this chapter, we consider model systems with Gaussian $P(W)$ onto which finite-time

work is done and for which the change in free energy is attributed solely to an energy change.

In section 4.3 we consider the case of stretching a one dimensional harmonic chain. We study the fluctuations in the work for this model when the stretching dynamics are both deterministic and dissipative, i.e. Rouse chain. In section 4.4 the study is extended to the multiply-bonded system, i.e. the Zwanzig problem[44].

With the results derived in sections 4.3 and 4.4 at hand, we turn in section 4.5 to an analysis of the distribution $P(e^{-W})$. While the mean of $P(e^{-W})$, $e^{-\Delta F}$, is related to the thermodynamic changes undergone by the system for the models studied, the width of $P(e^{-W})$ depends on parameters including bath-system coupling. In section 4.5 we discuss when stochastic dynamics may be legitimately invoked to model the breadth of the distribution $P(e^{-W})$ and indicate how information on the system-bath interaction may be extracted from $P(e^{-W})$. We conclude in section 4.6 and include a brief, unpublished, comment in the appendix on pulling of chains in which the change of state is purely entropic.

4.3 Memory effects for the harmonic chain

4.3.1 Deterministic case

We first consider the example of a classical harmonic chain with N subunits and coupling matrix K in real space with cyclic boundary conditions and further add that the Nth subunit is *linearly* coupled to an external force $f(t)$ which is non-zero from $[0, \tau]$. We emphasize that the total phase volume is conserved throughout. Under certain circumstances, we may exactly diagonalize K and compute the partition function, Z, after having applied a force for any given time, τ, such that $ln\,(Z(\tau)/Z(0)) \propto f(\tau)^T K^{-1} f(\tau)$ where $f(\tau)^T = (0, 0, ..., f(\tau))$. The proportionality constant is τ-independent. The 0-eigenvalue mode, which arises for the case of cylic boundary conditions, can be avoided by subtracting the kinetic energy associated to the center of motion from the Hamiltonian.

The purpose of this short introduction is simply to highlight that, given $ln\,(Z(\tau)/Z(0))$, it is easily verified that the free energy difference arises from changes to the internal energy exclusively. Thus, all such models are special in the sense that no entropy is generated. On the other hand, these models can be used to single out dynamical broadening effects in the work distribution arising from system-bath interaction and finite system recurrence time. The remainder of our discussion will be restricted to such models.

For now, we calculate the free energy using Jarzynski's formalism by explicitly computing all non-zero work cumulants for the case of tridiagonal K with Hamiltonian

$$\mathscr{H} = \sum_{m=1}^{N} \left(\frac{1}{2} p_m^2 + \frac{1}{2} K \left(x_m - x_{m-1} \right)^2 - f(t) x_m \delta_{Nm} \right) \tag{4.2}$$

where the mass of each subunit is set to 1. We use the Fourier representation for the set of coordinates x_m in real space in mass rescaled units, $x_m = \frac{1}{\sqrt{N}} \sum_{k=1}^{N} e^{\frac{2\pi i m k}{N}} x_k$ appropriate for the case where cyclic boundary conditions are employed, such that

$$\mathscr{H} = \sum_{k=1}^{N} \left(\frac{1}{2} p_k p_{-k} + \frac{1}{2} \omega_k^2 x_k x_{-k} - \frac{f(t)}{2\sqrt{N}} (x_k + x_{-k}) \right) \tag{4.3}$$

where $\{p_k\}$ are the k-space momenta, $\{\omega_k^2 \equiv 4K \sin^2 \left(\frac{\pi k}{N} \right)\}$ are the successive eigenvalues of the coupling matrix and the last term has been re-written in symmetric form.

It follows from the definition of $W(\tau)$ that $W(\tau) = -\int_0^\tau dt \dot{f}(t) x_N(t) = -\sum_{k=1}^{N} \int_0^\tau dt \frac{\dot{f}(t)}{\sqrt{N}} x_k(t)$. The average work may be simplified to

$$\langle W(\tau) \rangle = -\sum_{k=1}^{N} \int_0^\tau dt \frac{\dot{f}(t)}{\sqrt{N}} \langle x_k^p(t) \rangle \tag{4.4}$$

where the superscript p labels the particular solutions of the full $\{x_k(t)\}$, since the mean for the set $\{x_k(0), p_k(0)\}$ is 0. Furthermore, it follows from the fact that members of the set $\{x_k(0), p_k(0)\}$ are Gaussian random variables that all work cumulants above the second are identically zero so that

$$\Delta F(\tau) = \langle W(\tau) \rangle - 1/2 \langle W(\tau)^2 \rangle_c \tag{4.5}$$

We may evaluate $\langle W(\tau) \rangle$ by formally inserting the particular solution of the equation of motion, EOM, for every k-mode, obtained from the Hamiltonian of Eq.(4.2), into Eq.(4.4) yielding for the deterministic, subscripted det, case

$$\langle W(\tau) \rangle_{det} = -\sum_{k=1}^{N-1} \frac{1}{N} \int_0^\tau dt \int_0^t ds \dot{f}(t) G^{det}(t-s) f(s) \tag{4.6}$$

where $G^{det}(t) \equiv \sin \omega_k t / \omega_k$. The summation excludes the $k = N$ mode so that $G^{det}(t)$ be

well defined for all k. Integrating by parts, and using $f(0) \equiv 0$, we obtain

$$\langle W(\tau) \rangle_{det} = - \sum_{k=1}^{N-1} \frac{f(\tau)^2}{2N\omega_k^2} + \sum_{k=1}^{N-1} \int_0^\tau dt \int_0^t ds \dot{f}(t) \frac{\cos(\omega_k(t-s))}{N\omega_k^2} \dot{f}(s) \qquad (4.7)$$

By direct calculation from Eq.(4.2), the change in free energy is $\Delta F = -\sum_{k=1}^{N-1} \frac{f(\tau)^2}{2N\omega_k^2}$. From this change in free energy and Eq.(4.5) the fluctuations in the work are

$$\langle W(\tau)^2 \rangle_{det,c} \rightarrow 2 \sum_{k=1}^{N-1} \int_0^\tau dt \int_0^t ds \dot{f}(s) \frac{\cos(\omega_k(t-s))}{N\omega_k^2} \dot{f}(t) \qquad (4.8)$$

Alternatively, we may have explicitly calculated the second work cumulant and verified the JE.

4.3.2   Rouse dynamics and comparison to A.

The above methodology is particularly useful for the Gaussian set $\{x_k(0), p_k(0)\}$, introduced in the Hamiltonian of Eq.(4.3), with zero mean and may be readily adapted to treat Rouse dynamics of the harmonic chain, labeled R, by modifying the above treatment at the level of the particular EOM. The EOM for the case of Rouse dynamics is simply

$$\boldsymbol{x}(t) = e^{-\gamma^{-1}\boldsymbol{K}t}\boldsymbol{x}(0) + \int_0^t ds e^{\gamma^{-1}\boldsymbol{K}(s-t)} \left(\gamma^{-1}\boldsymbol{f}(s) + \gamma^{-1}\boldsymbol{\eta}(s) \right) \qquad (4.9)$$

where $\boldsymbol{\eta}(t)$ is the random noise term with zero mean and variance $\langle \eta_m(t)\eta_n(t') \rangle = 2\delta_{mn}\delta(t-t')$ and γ is the dissipation strength.

The average work then follows

87

$$\langle W(\tau)\rangle_R \quad = \gamma^{-1} \int_0^\tau dt \int_0^t ds \dot{\boldsymbol{f}}(t)^T e^{\gamma^{-1} \boldsymbol{K}(s-t)} \boldsymbol{f}(t)$$

$$= \gamma^{-1} \int_0^\tau dt \int_0^t ds \dot{f}(t) \left(e^{\gamma^{-1}\boldsymbol{K}(s-t)}\right)_{NN} f(t) \tag{4.10}$$

Since K has earlier been diagonalized, the second equality of Eq.(4.10) above is easily evaluated. Integrating by parts we obtain

$$\langle W(\tau)\rangle_R = -\sum_{k=1}^{N-1} \frac{f(\tau)^2}{2N\omega_k^2} + \sum_{k=1}^{N-1} \int_0^\tau dt \int_0^t ds \dot{f}(t) \frac{e^{\gamma^{-1}\omega_k^2(s-t)}}{N\omega_k^2} \dot{f}(s) \tag{4.11}$$

The work fluctuations follow from the above and Eq.(4.5)

$$\langle W(\tau)^2\rangle_{R,c} = 2\sum_{k=1}^{N-1} \int_0^\tau dt \int_0^t ds \dot{f}(s) \frac{e^{\gamma^{-1}\omega_k^2(s-t)}}{N\omega_k^2} \dot{f}(t) \tag{4.12}$$

The results of Eqs.(4.11)-(4.12) are consistent with the results of the insightful work of Dhar [39]. As before, it is simple to verify the JE by explicitly computing Eq.(4.12).

We wish to compare the results for the work for both deterministic and Rouse dynamics, Eq.(4.7) and Eq.(4.11) respectively, for a general applied force of the form αt^n where α is a t-independent proportionality constant, n is greater than or equal to 1 and the applied force is linearly coupled to a system coordinate. It is straightforward to do so by adopting the following convenient notation for the general form for the average work applicable to both deterministic and Rouse dynamics

$$\langle W(\tau)\rangle = -\sum_{k=1}^{N-1} \frac{1}{N} \int_0^\tau dt \int_0^t ds \dot{f}(t) G(t-s) f(s) \tag{4.13}$$

where $\int_0^t ds G(t-s) f(s)$ is identified with $[\partial_t^2 + \omega_k^2]^{-1} f(t)$ for the deterministic chain and $[\gamma \partial_t + \omega_k^2]^{-1} f(t)$ for the Rouse chain. As a note, the inverse of the operator is guaranteed to exist because the summation over k excludes $k = N$.

It is now possible to rescale time such that $t \to \tilde{t}\tau$, where $\tilde{t}$ is a dimensionless time, and rewrite the average work of Eq.(4.13) as follows

$$\langle W(\tau) \rangle_{det} = -\sum_{k=1}^{N-1} \int_0^1 d\tilde{t} \frac{\dot{\tilde{f}}(\tilde{t})}{2N\omega_k^2} \left(1 - \frac{\partial_{\tilde{t}}^2}{\tau^2 \omega_k^2} + \mathscr{O}(\tau^{-4}) \right) f(\tilde{t}) \tag{4.14}$$

$$\langle W(\tau) \rangle_R = -\sum_{k=1}^{N-1} \int_0^1 d\tilde{t} \frac{\dot{\tilde{f}}(\tilde{t})}{2N\omega_k^2} \left(1 - \frac{\partial_{\tilde{t}}}{\gamma^{-1}\tau \omega_k^2} + \mathscr{O}(\tau^{-2}) \right) f(\tilde{t}) \tag{4.15}$$

where $\dot{\tilde{f}}(\tilde{t}) \equiv \partial_{\tilde{t}} f(\tilde{t})$ and we have expanded the general $G(t)$ as a geometric series. Memory effects are unimportant when τ exceeds the relaxation time of the most sluggish of the k-modes, i.e. $\tau \gg \frac{\gamma}{\omega_k^2}$ and it is thus possible to approximate the exact $P(W)$ beyond the first few recurrence times of the system by some dissipative approximation.

Also, it is surprising to see that even as the force grows in time, the effect of fluctuations in the work become negligible for long time implying that the distribution in W or e^{-W} eventually peaks around its thermodynamic value. As a sidenote, fluctuations are not subdominant when the force is applied on resonance. This scenario however is not considered because assuming a closed set of trajectories for the system and bath is merely an idealization.

As an additional sidenote, we may reconsider the Hamiltonian from Eq.(4.2) with the summation index, m, running from 1 to $N + 1$ with open chain boundary conditions, i.e. $x_0 = x_{N+1} = 0$. The coupling matrix is easily diagonalized by the discrete sine transform, $x_m(t) = \sqrt{\frac{2}{N+1}} \sum_{k=0}^N \sin\left(\frac{\pi m k}{N+1}\right) x_k(t)$ which satisfies the specified boundary conditions. It is important to note that the work, when applied to a single bead, is a boundary effect. As an example, if the work is applied to the last bead the analogue of Eq.(4.3) follows with some

89

differences, namely $\omega_k = 2\sqrt{K}\sin\left(\frac{\pi k}{2(N+1)}\right)$ and $f(t)x_N = f(t)\sum_{k=1}^{N}\sqrt{\frac{2}{N+1}}\sin\left(\frac{\pi N k}{N+1}\right)$. The free energy for open ends is then

$$\Delta F = -\sum_{k=1}^{N}\frac{f(\tau)^2}{N+1}\left(\frac{\sin^2\left(\frac{\pi N k}{N+1}\right)}{4K\sin^2\left(\frac{\pi k}{2(N+1)}\right)}\right)$$

$$= -\frac{f(\tau)^2}{N+1}\left(\frac{N}{2K}+\frac{1}{2K}\cos\left(\frac{N\pi}{2(N+1)}\right)\csc\left(\frac{\pi}{2(N+1)}\right)\right) \sim -\frac{f(\tau)^2}{2K}+\mathcal{O}(N^{-1}).$$

On the other hand it is possible to compute a free energy change with open chain boundary conditions when the force is applied to a bead in the middle of the open-ended chain. In this case both τ-dependence and N-scaling of the free energy change are identical to the free energy change computed using cyclic boundary conditions for the chain.

4.4 Memory effects for a system with explicit bath

We extend the analysis to an explicit bath model, the multiply-bonded system, MBS, in which a known potential energy surface is coupled to N bath modes[44]. We show how the dependence of the work fluctuations on realistic bath parameters simplifies beyond the first few recurrence times of the system.

We begin by defining the Hamiltonian

$$\mathscr{H} = \frac{1}{2}p^2 - f(t)x + \frac{K}{2}x^2 + \sum_{j=1}^{N}\left(\frac{1}{2}p_j^2 + \frac{1}{2}\omega_j^2\left(q_j - \frac{\gamma_j}{\omega_j^2}x\right)^2\right) \tag{4.16}$$

with index j denoting the bath and where γ_j is a measure of the bath-system coupling strength. In order to compute both average work and fluctuations we first write coupled EOM for system and bath and eliminate bath variables to obtain an EOM depending exclusively on system variables. The resulting system EOM is often written as $\ddot{x}(t) = \sum_j F_j(t) - \int_0^t ds \sum_j M_j(t-s)\dot{x}(s) - f(t) - Kx(t)$ where the memory kernel $\sum_j M_j(t) = \sum_j \frac{\gamma_j^2}{\omega_j^2}\cos(\omega_j t)$ and the random noise term $F_j(t) = \gamma_j\left(q_j(0) - \frac{\gamma_j}{\omega_j^2}x(0)\right)\cos(\omega_j t) + \frac{\gamma_j}{\omega_j}p_j(0)\sin(\omega_j t)$. In the continuum limit, $\sum_j M_j(t)$ smoothly goes over to $\int_0^\infty d\omega g(\omega)\gamma(\omega)^2\cos(\omega t)/\omega^2$ where $g(\omega)$ is a bath density of states.

It is natural to solve the resulting system EOM in Laplace space. Since both system and bath degrees of freedom are initially Gaussian random variables with zero mean, the average work is simply

$$\langle W(\tau)\rangle_{MBS} = -\int_0^\tau dt \int_0^t ds \dot{f}(t)G^{MBS}(t-s)f(s) \tag{4.17}$$

where

$$\int_0^t dsG^{MBS}(t-s)f(s) = \mathscr{L}^{-1}\left([K + z^2 + \sum_j z\hat{M}_j(z)]^{-1}\hat{f}(z)\right)$$

$$= \mathscr{L}^{-1}\left(\hat{a}(z)\hat{f}(z)\right) \qquad (4.18)$$

with $\mathscr{L}^{-1}$ denoting the inverse Laplace transform operation and $\hat{a}(z)$ is defined through the expression above. We note however that by the (inverse) Laplace convolution theorem, $\mathscr{L}^{-1}\left(\hat{f}(z)\hat{a}(z)\right) = \int_0^t dsf(s)a(t-s)$. It is now straightforward to integrate Eq.(4.18) by parts

$$\langle W(\tau) \rangle_{det} = -\frac{f(\tau)^2}{2K} + \int_0^\tau dt \int_0^t ds\dot{f}(t)v(t-s)\dot{f}(s) \qquad (4.19)$$

where $v(t)$ is implicitly defined through Eqs.(4.18)-(4.19) and depends on the pole structure of $\hat{a}(z)$. The average work is entirely analogous to the form of Eq.(4.7) and Eq.(4.11). As expected, we verify that the bath does not contribute to the system free energy change $-\frac{f(\tau)^2}{2K}$.

By selecting, for simplicity, identically distributed $\{\gamma_j, \omega_j\}$, i.e. $g(\omega) = N\delta(\omega - \omega_o)$ with $\gamma(\omega) = \gamma$, then for arbitrary $f(t)$ we recover a closed form expression for the average work

$$\int_0^t dsv(t-s)\dot{f}(s) = \mathscr{L}^{-1}\left(z\hat{f}(z)\frac{r_1 r_2 + (r_1 + r_2 - z^2)\omega^2}{r_1 r_2 (r_1 - z^2)(r_2 - z^2)}\right) \qquad (4.20)$$

where $r_{1,2} = \dfrac{-\left(\omega^2 + \frac{\gamma^2 N}{\omega^2} + K\right) \pm \sqrt{\left(\omega^2 + \frac{\gamma^2 N}{\omega^2} + K\right)^2 - 4K\omega^2}}{2}$. Though we will come back to this point in the context of a discussion on a more general spectral function, it suffices to indicate for now that for sufficiently large τ the work fluctuations, expressed in Eqs.(4.19)-(4.20), considerably simplify and eventually vanish for large enough τ. As a check, we expand

Eq.(4.19) with $v(t)$ specified by Eq.(4.20) in the weak coupling limit $\lim_{\gamma \to 0} \langle W(\tau) \rangle_{det} =$ $-\frac{f(\tau)^2}{2K} + \int_0^\tau dt \int_0^t ds \dot{f}(t) \frac{\cos\left(\sqrt{K}(t-s)\right)}{K} \dot{f}(s) + \mathcal{O}(\gamma^2)$ which is the correct analog of Eq.(4.7).

While identically distributed bath couplings and frequencies lead to closed expressions for work averages and fluctuations, Eq.(4.20), it is straightforward to extend the analysis to more realistic bath models. By doing so, we make explicit the dependence of the work fluctuations on parameters of interest including system-bath coupling strength and as an aside obtain the expected result that the average work is indeed independent of the choice of bath spectral function for long times.

As an illustration, we select a Lorentzian density of states $g(\omega) = \frac{2}{\pi} \frac{\omega_c}{\omega_c^2 + \omega^2}$ with ohmic coupling, $\gamma(\omega) = c\omega$. We identify ω_c as the bath cutoff frequency and c as a measure system-bath coupling strength with units of inverse time. Given the above, the Laplace transform of the term containing the memory kernel in Eq.(4.18) takes the form

$$z \sum_j \hat{M}_j(z) = z \int_0^\infty d\omega \frac{2c^2}{\pi} \frac{\omega_c}{\omega_c^2 + \omega^2} \frac{z}{z^2 + \omega^2} \tag{4.21}$$

By repeating the arguments that lead to Eqs.(4.14)-(4.15), we first expand the denominator on the RHS of Eq.(4.18) as a geometric series

$$[K + z^2 + \sum_j z\hat{M}_j(z)]^{-1} = \frac{1}{K}\left(1 - \left(\frac{z^2}{K} + \frac{z \sum_j \hat{M}_j(z)}{K}\right) + ...\right) \tag{4.22}$$

where by rescaling $t = \tilde{t}\tau$ such that $z = \tilde{z}\tau^{-1}$ (and $\mathcal{L}^{-1} = \tilde{\mathcal{L}}^{-1}\tau^{-1}$) terms not explicitly written are at least $\mathcal{O}(\tau^{-2})$. Since z is the Laplace variable integrated along a vertical line in the complex z-plane to the right of the real part of all singularities we take $Re(z) > \omega_c$

and expand the integral for large τ

$$(z/K)\sum_j \hat{M}_j(z) = \frac{\tilde{z}c^2}{\tau K\omega_c}\left(1 - \frac{\tilde{z}}{\tau\omega_c} + \mathcal{O}(\tau^{-2})\right) \qquad (4.23)$$

Inserting Eq.(4.23) back into Eq.(4.22) we recover

$$[K + z^2 + \sum_j z\hat{M}_j(z)]^{-1}$$
$$= \frac{1}{K}\left(1 - \frac{\tilde{z}c^2}{\tau K\omega_c}\left(1 - \frac{\tilde{z}}{\tau\omega_c} + \mathcal{O}(\tau^{-2})\right) + \mathcal{O}(\tau^{-2})\right) \qquad (4.24)$$

In analogy to Eqs.(4.14)-(4.15), we recover a single condition to leading order which must be satisfied in order for work fluctuations to have small effect for long τ; $\tau \gg \sum_j \hat{M}_j(\tilde{z} \to 0)/K$. This condition, roughly interpreted, leads to the conclusion that for stretching times exceeding the typical system relaxation time, work fluctuations are subdominant. Thus, $P(W)$ and correspondingly $P(e^{-W})$ are sharply peaked around their thermodynamic mean and there is some flexibility as to how the bath system-interaction may be modeled.

Additional conditions, appearing at higher order in τ^{-1}, simply arise because we have not set the inertial term of the system EOM to zero, i.e. assumed overdamped dynamics as was the case for the Rouse model presented earlier. The dependence of the width of the work distribution with the cutoff frequency and bath system coupling follows from Eq.(4.24).

4.5 Bath-dependence and long-time behavior of $P(e^{-W})$

The work distribution is defined as the expectation value of $\delta\left(W - W(\{q_i(0), p_i(0)\}, \tau)\right)$ over an initial distribution of phase points $\varrho(\{q_i(0), p_i(0)\})$ as follows

$$P(W) \equiv \int \mathscr{D}[\{q_i(0), p_i(0)\}]\varrho(\{q_i(0), p_i(0)\})$$
$$\times \delta\left(W - W(\{q_i(0), p_i(0)\}, \tau)\right) \tag{4.25}$$

with all other factors absorbed into the above defined measure. By decomposing the δ-function in its Fourier representation, $\delta(x) = \int_{-\infty}^{\infty} dm e^{imx}$, with m as the dummy Fourier index, it is possible to show that for all examples considered, the work distribution, $P(W, \{\alpha_i\})$, is Gaussian where $\{\alpha_i\}$ is the set of system and bath parameters. Assuming the order of integration of the variables $\{q_i(0), p_i(0)\}$ and m is interchangeable, we recover an integrand with respect to m which is commonly referred to as the characteristic funtion of $P(W, \{\alpha_i\})$. In general, the dependence of first and second work cumulants on $\{\alpha_i\}$ is complicated.

From the approach we have taken to compute the fluctuations in the work for various models, we concluded that $\langle W^2 \rangle_c$ is subdominant in τ for $f(\tau)$ varying as any power of τ, in the case of linear coupling to the external force.

The long-time limit is obtained by subsequently integrating over m thus reducing $P(W, \{\alpha_i\})$ to the following

$$\lim_{\tau \to \infty} P(W) = \delta\left(W - \langle W\left(\{q_i(0), p_i(0)\}, \tau\right)\rangle\right) \tag{4.26}$$

which is a reasonable result.

We are however interested in the properties of the distribution of $P(x \equiv e^{-W}, \{\alpha_i\})$ whose width measures the degree of accuracy of a free energy measurement using Jarzynski's

prescription. Moreover, for Gaussian $P(W, \{\alpha_i\})$, $P(x, \{\alpha_i\})$ is log-normal with

$$P(x, \{\alpha_i\}) = x^{-1}/\sqrt{2\pi \langle W^2 \rangle_c} e^{-\frac{(\ln x + \langle W \rangle)^2}{2\langle W^2 \rangle_c}} \tag{4.27}$$

The long-time behavior of $P(x, \{\alpha_i\})$ then follows

$$\lim_{\tau \to \infty} P(e^{-W}, \{\alpha_i\}) = e^{\langle W \rangle} \delta \left(W - \langle W \left(\{q_i(0), p_i(0)\}, \tau \right) \rangle \right) \tag{4.28}$$

Given the results derived from section 4.3 and 4.4, it is possible to quantify whether certain regimes of bath parameters lead to efficient sampling of $P(x, \{\alpha_i\})$ and how these may be extracted from work distribution widths. We will show this for particular α_i appearing in the models considered earlier for the special case where $f(t)$ is linear in t.

The first such parameter considered is γ defined in part B of section 4.3, Eq.(4.9), as the measure of dissipation in the Rouse model. We assume for now that all parameters, aside from γ, are specified and held fixed so that $P_R(x, \{\alpha_i\})$, determined from Eqs.(4.11)-(4.12) and Eq.(4.27), is simply re-written as $P_R(x, \gamma)$. This distribution plotted in Fig.(4.1) has a mean $e^{-\Delta F} = 2.29$ which is independent of γ. Clear sharpening of the distribution around its thermodynamic mean is apparent for increasing dissipation. Note that in Eq.(4.9), *decreasing* γ implies stronger dissipation in this model[33].

The joint γ-τ dependence can also be probed by reconsidering an equivalent distribution to that of Fig.(4.1) for longer τ. The mean of $P_R(x, \gamma)$ is higher in Fig.(4.2) for the set of parameters selected, $e^{-\Delta F} = 27.8$, though all other features of interest remain unchanged. Incidentally, by comparing Eq.(4.7) and Eq.(4.11) it is easy to verify that the approximate $P_R(x, \gamma)$ becomes indistinguishable from the deterministic $P_{det}(x, \{\alpha_i\})$ when both τ and γ^{-1} are large since this is precisely the regime where the dynamical broadening effects become negligible. Extracting γ from the standard deviation of the work distribution is then possible in certain limits provided the system under study can be mapped onto one with Rouse dynamics.

Figure 4.1: Effect of dissipation on the sharpening of the distribution $P_R(x, \gamma)$ with $\{N, K, \alpha, \tau\} = \{20, 1, 1, 1\}$ in the appropriate units.

Many of the above arguments carry over directly to the MBS though a few remarks are in order. we first consider the distribution of $P_{MBS}(x, \gamma)$, constructed using Eqs.(4.19)-(4.20) and Eq.(4.27), in the strong coupling limit to the bath, large γ. In this limit, memory effects induced by coupling of the system to the medium are important, the resulting distribution is broad and the corresponding mean of $P_{MBS}(x, \gamma)$ difficult to sample. The opposite holds true for weak coupling to the bath though for long enough τ, memory effects become subdominant as shown in Eq.(4.24) for the case of a more general bath spectral function. The effect of coupling to the environment on the distribution of $P_{MBS}(x, \gamma)$ is reproduced in Fig.(4.3) for a specified set of parameters with mean $e^{-\Delta F} = 8.27$.

As before, while the ease of extracting thermodynamic information is determined by the shape of $P_{MBS}(x, \gamma)$, bath parameters of interest can be reliably extracted from the breadth of the work distribution provided the system can be mapped to the Zwanzig model.
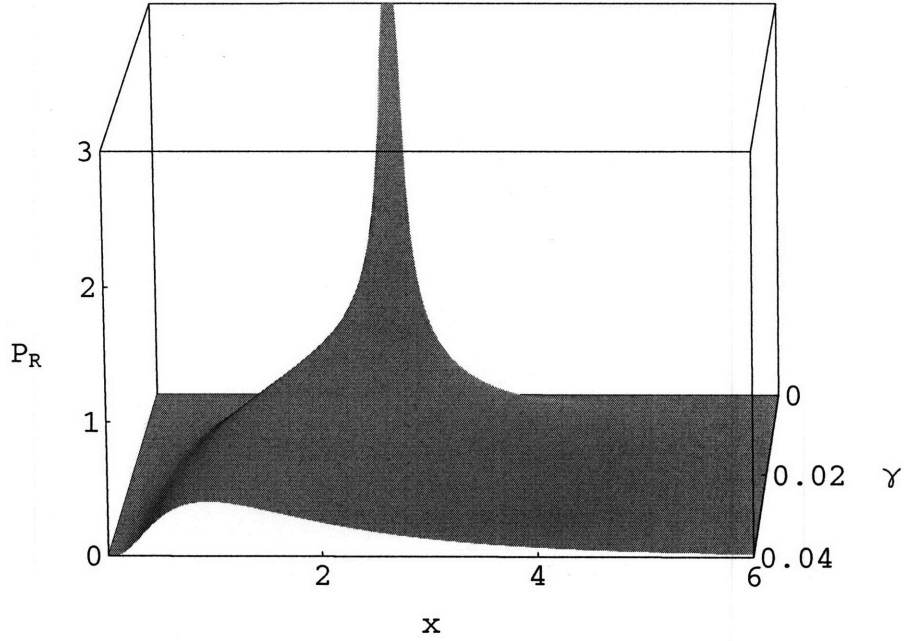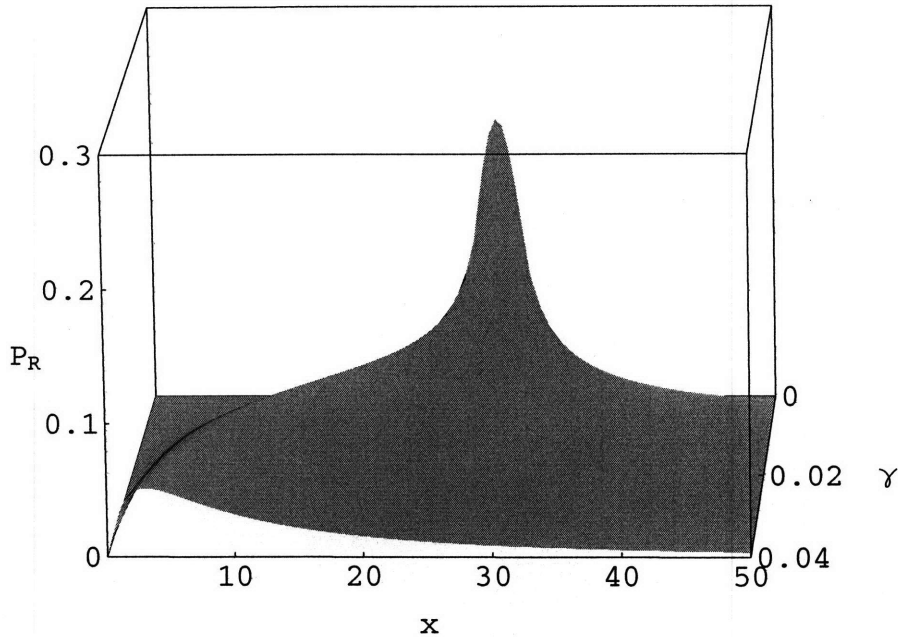
Figure 4.2: Effect of dissipation on the sharpening of the distribution $P_R(x, \gamma)$ using $\{N, K, \alpha, \tau\} = \{20, 1, 1, 2\}$ in the appropriate units.

4.6 Conclusion

This chapter is meant to serve a threefold purpose. We first note that the difficulty of having to deal with the notion of a general non-equilibrium temperature appropriate to the description of the final system plus bath Boltzmann weights is circumvented by dealing with systems of a special type. More specifically, our analysis is limited to stretching of a harmonic system through linear coupling to an external force, for which there is only an energy change. By extension, the case of Rouse dynamics or other strongly dissipative systems is also special by virtue of having well defined Boltzmann weights while work is applied onto the system.

Secondly, we extend our previous work on convergence properties of the JE by eliminating all sources of broadening in $P(W)$ except those arising from dynamical origins[37]. This is done by explicitly calculating work fluctuations for various harmonic models containing the essence of the more-general non-linear problem. We relate this discussion back to how various
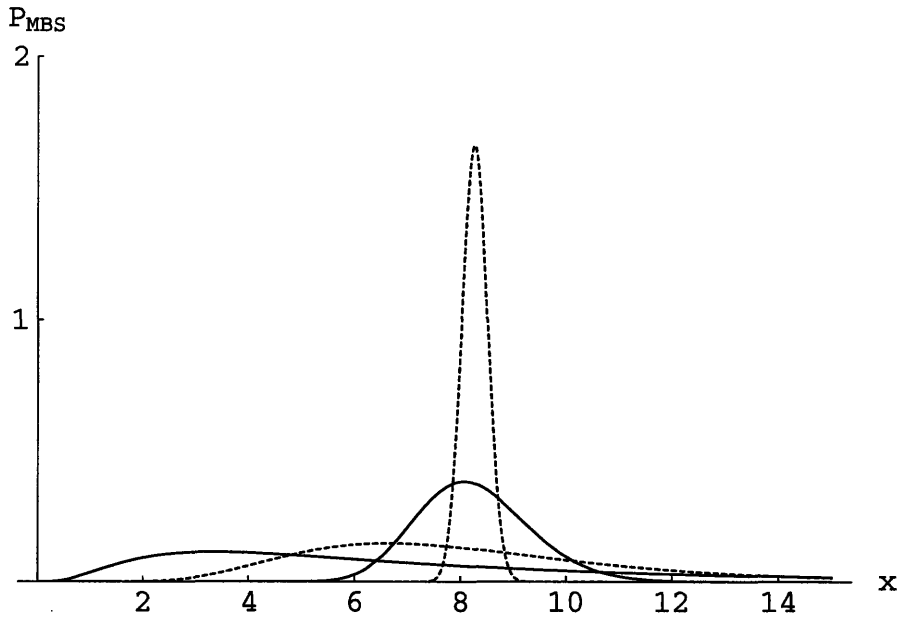
Figure 4.3: Effect of coupling to the environment on the sharpening of the distribution $P_{MBS}(x, \gamma)$ using $\{N, K, \alpha, \tau, \omega\} = \{10, 10, 0.65, 10, 1.5\}$ in the appropriate units. Increasing values of γ, $\{5, 4, 0.5, 0.1\}$, are depicted by successive dashed and solid lines respectively.

non-equilibrium parameters of the model affect the breadth of the distribution $P(e^{-W})$ and thus how simply the mean($e^{-\Delta F}$) is selected for various parameter regimes.

Thirdly, from the behavior of $P(W)$, alternatively $P(e^{-W})$, it is shown how important parameters relating to the bath-system interaction may be simply extracted.

For weak nonlinear coupling to the external force, it is possible to imagine changing the force constant of the harmonic system in time which, following arguments identical to those at the beginning of section 4.3, leads to generation of entropy. From these arguments, the dynamics of systems with slightly anharmonic potentials are equally good candidates for the study of dynamical entropy generation within the context of the JE. Additional models of interest would certainly include, though not be limited to, the dynamics of the freely-rotating chain or freely-jointed chains with the possibility of slight excluded volume interaction and the worm-like chain with either bending or bending and stretching potentials.

4.7 Appendix 1

In a previous chapter, we demonstrated that entropy generating processes, in other words processes where phase space density is substantially redistributed, may lead to slow convergence of the work cumulant expansion. In those cases, the slow convergence of the cumulant sum was directly attributed to contributions from important though rare configurations. In light of this, it was argued that large systems undergoing changes of state generating entropy constituted particularly pathological cases. Stiff chains under tension, however, undergo small free energy changes as the tension at one end is varied and the resulting work distribution is expected to be only slightly non-Gaussian[45]. By stiff chain, we simply mean that $\lambda L_o \sim \mathscr{O}(1)$ where λ is the persistence length of the chain and L_o is the chain length [46, 47, 48, 49, 50, 51, 52, 53].

As a pedagogical sidenote, we illustrate asympotically how in the weak bending or "fluctuating rod" limit[49, 50] the free energy changes of state for a pure bending discrete chain under differing tension leads to a tension dependent bending force constant. Since the bare bending force constant, $\kappa \equiv \beta^{-1}/2\lambda$, changes when external tension is added, so does the chain's configurational entropy.

In d dimensions, we begin with a chain of mass points, labeled 1 through N at positions $\{x\}$, interacting via a discrete pure bending potential, U_{bend}[47]

$$U_{bend} = \sum_{j=1}^{N-1} \kappa_o \left(b^2 - (x_j - x_{j-1}) \cdot (x_{j+1} - x_j) \right) \tag{4.29}$$

where κ_o as the uniform bending force constant. The zeroth bead is set at the origin, i.e. this is the tethered end. The magnitude of $(x_j - x_{j-1}) \equiv \Delta x_{j,j-1}$ is fixed, i.e. $|\Delta x_{j,j-1}| \equiv b$ so that $L_o = bN$. Vectorial quantities are decomposed along a longitudinal, subscripted l, direction and multiple transversal, subscripted tr, directions, i.e. $\Delta x_{j,j-1} = b \prod_{tr} \cos \theta_{tr,j-1} \hat{e}_l + b \sum_{tr} \sin \theta_{tr,j-1} \hat{e}_{tr}$ where $\theta_{tr,j-1}$, for any transversal direction, is the angle between $\hat{e}_l$ and the bond vector in the longitudinal-transversal plane of interest. In the weakly bending limit,

any such angle is small.

The potential for an external force acting along the longitudinal direction on the end-to-end polymer distance is $U_f = -\boldsymbol{f} \cdot (\boldsymbol{x}_N - \hat{\boldsymbol{z}} L_o)$ where $\boldsymbol{f} \geq 0$. Linearizing $U_{bend} + U_f$ to leading order in $\mathcal{O}(\theta^2)$ the continuum potential reads

$$U \equiv U_{cont} = \int_0^{L_o} ds \left(\frac{\kappa}{2} (\partial_s \boldsymbol{\theta})^2 + \frac{(\boldsymbol{f}(t) \cdot \hat{e}_l)}{2} \theta^2 \right) \tag{4.30}$$

where we have adopted the continuum analogs[47]: $\sum_j b \rightarrow \int_0^{L_o} ds$, $(\theta_{tr,j} - \theta_{tr,j-1})^2 / b^2 \rightarrow (\partial_s \theta_{tr})^2$ and $\kappa_o b^3 \rightarrow \kappa$.

While the coordinate system employed is not orthogonal, the various transversal angular variables decouple to $\mathcal{O}(\theta^2)$ and the expansion should hold provided the external force is chosen so that U_f remains small compared to U_{bend}.

Since the tangent vector at one end of the polymer is aligned with the force while the other end is tethered, the boundary conditions $\boldsymbol{\theta}(s = L_o) = \boldsymbol{\theta}(s = 0) = 0$ are appropriate [54]. In this case it is possible to expand the angular variables as $\boldsymbol{\theta}(s) = \sum_{k=1}^{\infty} \sin(k\pi s / L_o) \boldsymbol{\theta}_k$. It is clear that to this order, each normal mode now contains bending force constant dependent on the external force.

The free energy change for the external force varied from 0 to $\boldsymbol{f} \cdot \hat{e}_l$ is simply $\Delta F = -\beta^{-1} \Delta S = +\frac{\beta(d-1)}{2} ln(\xi csch \xi)$ where $\xi = \sqrt{\boldsymbol{f} \cdot \hat{e}_l L_o^2 / \kappa}$.

4.8   Bibliography

[1] S. Pressé and R.J. Silbey. *Phys. Rev. E*, 74:061105, 2006.

[2] C. Jarzynski. *Phys. Rev. Lett.*, 78:2690, 1997.

[3] C. Jarzynski. *J. Stat. Mech.: Theor. Exp.*, page P09005, 2004.

[4] J. Liphardt, S. Dumont, S. Smith, I. Tinoco, and C. Bustamante. *Science*, 296:1832, 2002.

[5] F. Douarche, S. Ciliberto, A. Petrosyan, and I. Rabbiosi. *Europhys. Lett.*, 70:593, 2005.

[6] F. Douarche, S. Ciliberto, and A. Petrosyan. *J. Stat. Mech.: Theor. Exp.*, page P09011, 2005.

[7] D. Collin, F. Ritort, C. Jarzynski, *S.B* Smith, I. Tinoco, and C. Bustamante. *Nature*, 437:231, 2005.

[8] S. Park and K. Schulten. *J. Chem. Phys.*, 120:5946, 2004.

[9] I. Bena, C. van den Broeck, and R. Kawai. *Europhys. Lett.*, 71:879, 2005.

[10] R. van Zon and *E.G.D* Cohen. *Phys. Rev. Lett.*, 91:110601, 2003.

[11] O. Narayan and A. Dhar. *J. Phys. Chem. A*, 37:63, 2003.

[12] U. Seifert. *Phys. Rev. Lett.*, 95:040602, 2005.

[13] *G.E* Crooks. *Phys. Rev. E*, 61:2361, 2000.

[14] *W.D* Roeck and C. Maes. *Phys. Rev. E*, 69:R026115, 2004.

[15] V. Chernyak, M. Chertov, and C. Jarzynski. *Phys. Rev. E*, 71:025102, 2005.

[16] F. Ritort. *J. Stat. Mech.: Theor. Exp.*, page P10016, 2004.

[17] S. Mukamel. *Phys. Rev. Lett.*, 90:170604, 2003.

[18] S. Yukawa. *J. Phys. Soc. Japan*, 69:2367, 2000.

[19] T. Monnai. *Phys. Rev. E*, 72:027102, 2005.

[20] G. Hummer and A. Szabo. *Proc. Natl. Acad. Sci. (USA)*, 98:3658, 2001.

[21] D. Wu and *D.A* Kofke. *J. Chem. Phys.*, 123:054103, 2005.

[22] J. Gore, F. Ritort, and C. Bustamante. *Proc. Natl. Acad. Sci. (USA)*, 100:12564, 2003.

[23] J. Kurchan. *J. Phys. A: Math. Gen.*, 31:3719, 1998.

[24] A. Imparato and L. Peliti. *Phys. Rev. E*, 72:046114, 2005.

[25] A. Imparato and L. Peliti. *Europhys. Lett.*, 70:740, 2005.

[26] C. Jarzynski. *Phys. Rev. E*, 73:046105, 2006.

[27] T. Yamada and K. Kawazaki. *Prog. Theor. Phys.*, 38:1031, 1967.

[28] *G.P* Morriss and *D.J* Evans. *Mol. Phys.*, 54:629, 1985.

[29] G. Gallavotti and *E.G.D* Cohen. *J. Stat. Phys.*, 80:931, 1995.

[30] *J.L* Lebowitz and H. Spohn. *J. Stat. Phys.*, 95:333, 1999.

[31] C. Maes. *J. Stat. Phys.*, 95:367, 1999.

[32] *G.M* Wang, *E.M* Sevick, E. Mittag, *D.J* Searles, , and *D.J* Evans. *Phys. Rev. Lett.*, 89:050601, 2002.

[33] T. Hatano. *Phys. Rev. E*, 60:R5017, 1999.

[34] T. Hatano and *S.I* Sasa. *Phys. Rev. Lett.*, 86:3463, 2001.

[35] *E.H* Trepagnier, C. Jarzynski, F. Ritort, *G.E* Crooks, *C.J* Bustamante, and J. Liphardt. *Proc. Natl. Acad. Sci. (USA)*, 101:15038, 2004.

[36] *A.B* Adib. *Phys. Rev. E*, 71:056128, 2005.

[37] S. Pressé and R. Silbey. *J. Chem. Phys.*, 124:054117, 2006.

[38] H. Oberhofer, C. Dellago, and P. Geissler. *J. Phys. Chem. B*, 109:6902, 2005.

[39] A. Dhar. *Phys. Rev. E*, 71:036126, 2005.

[40] *E.G.D* Cohen and David Mauzerall. *J. Stat. Mech: Theor. Exp.*, page P07006, 2004.

[41] *E.G.D* Cohen and D. Mauzerall. *Mol. Phys.*, 103:2923, 2005.

[42] Irwin Oppenheim. *Prog. Theor. Phys. Supp.*, 99:369, 1989.

[43] D. Ronis and I. Oppenheim. *Physica*, 86A:475, 1977.

[44] R. Zwanzig. *Nonequilibrium Statistical Mechanics*, pages 21–24. Oxford University Press, 2001.

[45] S. Blinnikov and R.Moessner. *Astron. Astrophys. Suppl. Ser.*, 130:193, 1998.

[46] A. Aragón and R. Pecora. *Macromolecules*, 18:1868, 1985.

[47] K. Soda. *J. Phys. Soc. Jap.*, 35:866, 1973.

[48] K. Soda. *J. Chem. Phys.*, 95:9337, 1991.

[49] T. Odijk. *Macromolecules*, 28:7016, 1995.

[50] J. Marko. *Phys. Rev. E*, 57:2134, 1998.

[51] N. Saitô, K.Takahashi, and Y. Yunoki. *J. Phys. Soc. Jap.*, 22:219, 1967.

[52] J. Marko and E. Siggia. *Macromolecules*, 28:8759, 1995.

[53] M. Fixman and J. Kovac. *J. Chem. Phys.*, 58:1565, 1973.

[54] Y. Hori, A. Prasad, and J. Kondev. *Phys. Rev. E*, 75:041904, 2007.

Chapter 5

Radiating Dipoles Near Curved Surfaces

5.1 Prologue

The contents of this chapter are already published in the cited reference[1]. Within this chapter, we have only changed minor aspects of our presentation.

The many technical aspects of vector wave scattering are relegated to some specialized texts [2, 3, 4, 5] and we have instead focused on our work related to local electric field enhancement generated by radiating fluorophores near non-planar conducting surfaces resulting in lifetime variations observable at the single molecule level.

The image theory, for dipoles located above flat surfaces, accounts for the results of ensemble experiments and is extensively used to interpret single molecule results. Nonetheless, smooth local surface inhomogeneities give rise to deviations of the single fluorophore properties from the image theory predictions. For this reason, we compute the effects of leading order corrections to the reflected fields of vertical dipoles located above locally curved perfectly conducting surfaces by invoking a small slope approximation.

5.2 Introduction

Local field enhancement effects experienced by molecules adsorbed near a protrusion tip, as in surface enhanced Raman spectroscopy(SERS), have proven crucial in achieving single molecule sensitivity[6, 7, 8, 9, 10]. For small and imperfectly conducting tips, the tip field may be further amplified, beyond the electrostatic "lightning rod" effects attributable to tip geometry, by exciting local dipolar plasmon resonances[11]. In fluorescence experiments, the image contribution to the reflected field of a radiating molecule near a surface may be the only source of local field enhancement. This effect, first studied in the pioneering ensemble atomic fluorescence experiments of Drexhage in $Ag/Eu^{3+}/Air$ mirror systems[12], was quantitatively fit by theoretical work relying on classical image theory[13, 14]. While the interpretation of current experiments relies heavily on the classical image result, observations at the single molecule level call for increasingly detailed microscopic modelling[15, 16, 17].

In what follows, we consider geometric corrections to the image result for the reflected field generated by a point electric dipole, ED, radiating above a smooth non-planar reflecting surface by drawing from the retarded interaction between the dipole and its distorted image. The analysis of wave scattering from rough and periodic surfaces is of wide practical interest and a variety of successful approximate methods exist to tackle such problems[18, 19, 20, 21, 3, 22, 23, 24, 25]. While insisting on a measure of smoothness of the interface, we invoke an analogue of the small slope approximation to perturbatively compute and physically interpret the effects of local surface curvature on the radiating dipole for the first time.

5.3 Unperturbed Interface

One of the solutions to the unperturbed reference problem, the radiating ED above an imperfectly conducting planar medium[26], follows from the scattered dyadic Green's function, DGF, treatment of the radiating ED within an imperfectly conducting cylindrical waveguide[2].

We recall the steady state electric field equation in the presence of an electric source term in medium I, $J_1(R)$, oscillating at frequency ω[2]

$$\left(\nabla \times \nabla \times -k_1^2 \right) E_1(R) = i\omega\mu_o J_1(R) \tag{5.1}$$

with wavenumber $k_1 \equiv \omega\sqrt{\epsilon_1\mu_o}$ where ϵ_1 is the dielectric constant and μ_o the magnetic permeability of the medium containing the source. The wavenumber for medium II, with magnetic permeability μ_o and conductivity σ is $k_2 \equiv \sqrt{\omega^2\epsilon_2\mu_o + i\omega\mu_o\sigma}$. Outside the source region, the electric field in medium I enclosed by volume V_I, is written as

$$E_1(R) = i\omega\mu_o \int_{V_I} J_1\left(R'\right) \cdot \overleftrightarrow{G}^{(11)}\left(R'|R\right) dV' \tag{5.2}$$

in terms of the DGF, $\overleftrightarrow{G}^{(11)}\left(R'|R\right)$, and the known electric source term. The first(second) superscripted index of the DGF denotes the location of the field(source point).

In the presence of a flat interface along the $z = 0$ plane separating media I and II, with the electric source in medium I, the DGF for media I and II satisfy the following equations

$$\left(\nabla \times \nabla \times -k_1^2 \right) \overleftrightarrow{G}^{(11)}\left(R|R'\right) = \overleftrightarrow{I}\delta\left(R - R'\right) ; \tag{5.3}$$

$$\left(\nabla \times \nabla \times -k_2^2 \right) \overleftrightarrow{G}^{(21)}\left(R|R'\right) = 0 \tag{5.4}$$

Similar expressions hold for the DGF when the electric source is located in medium II for the equation above and for what follows. The DGF $\overleftrightarrow{G}^{(11)}$, can be expressed as the

109

sum of a free DGF and scattered(reflected) components, $\overleftrightarrow{G}^{(11)}\left(R|R'\right) = \overleftrightarrow{G}^{(o)}\left(R|R'\right) +$ $\overleftrightarrow{G}_s^{(11)}\left(R|R'\right)$, while $\overleftrightarrow{G}^{(21)}$, is written as a single scattered(refracted) component, $\overleftrightarrow{G}^{(21)}\left(R|R'\right) =$ $\overleftrightarrow{G}_s^{(21)}\left(R|R'\right)$. The free DGF expanded in a cylindrical basis for any point in space, excluding the point source, is

$$\overleftrightarrow{G}^{(o)}\left(R'|R\right) = \frac{i}{4\pi}\int_0^\infty d\lambda \sum_{n=0}^\infty \frac{2-\delta_{n,o}}{\lambda h_1}\overleftrightarrow{A}^{(o)}\left(R'|R\right) \tag{5.5}$$

having defined

$$\overleftrightarrow{A}^{(o)}\left(R'|R\right) \equiv \begin{cases} M'_{\binom{e}{o}n\lambda}(-h_1)M_{\binom{e}{o}n\lambda}(h_1) + N'_{\binom{e}{o}n\lambda}(-h_1)N_{\binom{e}{o}n\lambda}(h_1) & , z > z'; \\ M'_{\binom{e}{o}n\lambda}(h_1)M_{\binom{e}{o}n\lambda}(-h_1) + N'_{\binom{e}{o}n\lambda}(h_1)N_{\binom{e}{o}n\lambda}(-h_1) & , z < z'. \end{cases} \tag{5.6}$$

where $h_1^2 = k_1^2 - \lambda^2$ and $M'_{\binom{e}{o}}M_{\binom{e}{o}}$ $(N'_{\binom{e}{o}}N_{\binom{e}{o}})$ is shorthand for $M'_e M_e + M'_o M_o$ $(N'_e N_e + N'_o N_o)$. The prime superscript on M and N denotes its dependence on the primed coordinate system. In addition, the basis functions used in the expansion are derived from the usual solutions to the scalar Helmholtz equation in cylindrical, (r, ϕ, z), coordinates: $M_{\binom{e}{o}n\lambda}(h) = \nabla \times \left(J_n\left(\lambda r\right)\binom{cos(n\phi)}{sin(n\phi)}e^{ihz}\hat{z}\right)$, where J_n is the integer Bessel function of order n, and $N_{\binom{e}{o}n\lambda}(h) = (1/k)\nabla \times M_{\binom{e}{o}n\lambda}(h)$.

It is possible to assume a spectral expansion for $\overleftrightarrow{G}_s^{(11)}\left(R'|R\right)$ and $\overleftrightarrow{G}_s^{(21)}\left(R'|R\right)$ in a fashion similar to Eqs.(5.5) and (5.6) where $\overleftrightarrow{A}^{(o)}\left(R'|R\right)$ is subsituted by

$$\overleftrightarrow{A}^{(11)}\left(R'|R\right) = aM'_{\binom{e}{o}n\lambda}(h_1)M_{\binom{e}{o}n\lambda}(h_1) + bN'_{\binom{e}{o}n\lambda}(h_1)N_{\binom{e}{o}n\lambda}(h_1) \tag{5.7}$$

$$\overleftrightarrow{A}^{(21)}\left(R'|R\right) = cM'_{\binom{e}{o}n\lambda}(h_1)M_{\binom{e}{o}n\lambda}(-h_2) + dN'_{\binom{e}{o}n\lambda}(h_1)N_{\binom{e}{o}n\lambda}(-h_2) \tag{5.8}$$

for the reflected and refracted fields, respectively, and where we define $h_2^2 = k_2^2 - \lambda^2$[2]. The Fresnel coefficients a, b, c and d, are determined by boundary matching. In the limit of the perfect conductor $b = -a = 1$ and $c = d = 0$.

5.4 Perturbed Interface

We perturb the flat earth interface, originally defined in the $z = 0$ plane, to lie in the $\tilde{z} \equiv z + \zeta(r, \phi) = 0$ plane. The height function $\zeta(r, \phi)$ considered in this section is smooth and vanishes sufficiently far away from the spatially localized electric source, $\boldsymbol{J}_1(\boldsymbol{R})$, in medium I. The normal to the perturbed interface is then $\hat{n} = (\hat{z} + \nabla\zeta) / \sqrt{1 + (\nabla\zeta)^2}$ with $|\nabla\zeta| \ll 1$.

It is well known that boundary matching at the perturbed interface is not possible since $\tilde{z}$ is not a constant coordinate surface of the basis used to spectrally expand the DGF[27]. This motivates the following perturbation analysis.

The coefficients a, b, c and d arising from boundary matching in the $z = -\zeta$ plane, for constant ζ, are known. In the case of the perfect conductor these are $b = -a = e^{2ih_1\zeta}$ and $c = d = 0$. If ζ, appearing in the Fresnel coefficients, is allowed to vary weakly with (r, ϕ) the DGF simultaneously fail to satisfy the boundary conditions across the surface boundary, S_b, and Eqs.(5.3)-(5.4). The equations satisfied by the perturbed DGF, $\overleftrightarrow{G}_p$, instead read

$$\left(\nabla \times \nabla \times -k_1^2\right) \overleftrightarrow{G}_p^{(11)} \left(\boldsymbol{R}|\boldsymbol{R}'\right) = \overleftrightarrow{T} \delta\left(\boldsymbol{R} - \boldsymbol{R}'\right) + \overleftrightarrow{\Gamma}_1, \quad z \geq -\zeta; \tag{5.9}$$

$$\left(\nabla \times \nabla \times -k_2^2\right) \overleftrightarrow{G}_p^{(21)} \left(\boldsymbol{R}|\boldsymbol{R}'\right) = \overleftrightarrow{\Gamma}_2, \quad z < -\zeta \tag{5.10}$$

where the perturbations, $\overleftrightarrow{\Gamma}_1$ and $\overleftrightarrow{\Gamma}_2$, are $\mathscr{O}(\nabla\zeta)$. It is now possible to use the vector Green's theorem to express the electric field in either medium I or II outside the source region, for a source arbitrarily chosen to be located in medium I, as a perturbative series in $\nabla\zeta$. The resulting integro-differential equations obtained, which couple the electric field in media I and II, involve both volume corrections and surface terms which are of $\mathscr{O}(\nabla\zeta)$.

For a perfectly conducting medium II, the electric field generated by a radiating ED

above a perfectly conducting medium takes the form of an inhomogeneous integral equation

$$E_{p,1}\left(\boldsymbol{R}\right) = E_1^{(o)}\left(\boldsymbol{R}\right) - \int_{V_1} E_{p,1}\left(\boldsymbol{R'}\right) \cdot \overleftrightarrow{\Gamma}_1\left(\boldsymbol{R'}|\boldsymbol{R}\right) dV'$$

$$+ \int_{S_b}\left(\nabla \times E_{p,1}\left(\boldsymbol{R'}\right)\right) \cdot \left(\hat{n} \times \overleftrightarrow{G}_p^{(11)}\left(\boldsymbol{R'}|\boldsymbol{R}\right)\right) dS' \qquad (5.11)$$

Outside the source region, we have defined $\boldsymbol{E}_1^{(o)}\left(\boldsymbol{R}\right)$ in Eq.(5.11) as follows

$$\boldsymbol{E}_1^{(o)}\left(\boldsymbol{R}\right) \equiv i\omega\mu_o \int_{V_1} \boldsymbol{J}_1\left(\boldsymbol{R'}\right) \cdot \overleftrightarrow{G}_p^{(11)}\left(\boldsymbol{R'}|\boldsymbol{R}\right) dV' \qquad (5.12)$$

with $\boldsymbol{J}_1\left(\boldsymbol{R}\right) = p\delta(x)\delta(y)\delta(z-d)\hat{e}_i$ where $\hat{e}_i$ is the unit vector in the direction of the dipole. The parameter p is related to the conventional dipole strength d_o, with units of charge $\times$length, by $p = -i\omega d_o$.

Iterating Eq.(5.11) once, we denote the volume and surface corrections by $\boldsymbol{E}_1^{(1)}\left(\boldsymbol{R}\right)$ so that the resulting leading order electric field is expressible as follows

$$E_{p,1}\left(\boldsymbol{R}\right) = \boldsymbol{E}_1^{(o)}\left(\boldsymbol{R}\right) + \boldsymbol{E}_1^{(1)}\left(\boldsymbol{R}\right) + \mathscr{O}\left((\nabla\zeta)^2\right) \qquad (5.13)$$

Both $\boldsymbol{E}_1^{(o)}\left(\boldsymbol{R}\right)$ and $\boldsymbol{E}_1^{(1)}\left(\boldsymbol{R}\right)$ contain scattered and incident field components.

For what follows, we uniquely consider a vertical dipole, $\boldsymbol{J}_1\left(\boldsymbol{R}\right) = p\delta(x)\delta(y)\delta(z-d)\hat{z}$, directly above the radially symmetric surface inhomogeneity, $\zeta = \zeta\left(r\right)$.

From Eq.(5.12) and the definitions of $\boldsymbol{J}_1\left(\boldsymbol{R}\right)$ and the perturbed DGF, we have

$$\boldsymbol{E}_1^{(o)}\left(\boldsymbol{R}\right) = \left(\frac{-\omega\mu_o p}{4\pi}\right) \int_0^\infty d\lambda \frac{\lambda}{h_1 k_1}\left(e^{-ih_1 d} + e^{ih_1 d + 2ih_1\zeta}\right) \boldsymbol{N'}_{eo\lambda}\left(h_1\right) \qquad (5.14)$$

By employing the Sommerfeld integral representation[26], we find the scattered part of

112

Eq.(5.14)

$$\boldsymbol{E}^{(o)}_{1,scatt}\left(\boldsymbol{R}'\right) \cdot \hat{\boldsymbol{z}}' = \left(\frac{i\omega\mu_o p}{4\pi k_1^2}\right)\Psi(r',z') \tag{5.15}$$

having defined $\Psi(r',z') \equiv \left(k_1^2 + \partial^2_{z'}\right)e^{ik_1 R'}/R'$ and $R' \equiv \sqrt{(r')^2 + (z' + d + 2\zeta(r'))^2}$.

The scattered part of $\boldsymbol{E}^{(1)}_1\left(\boldsymbol{R}\right)$, evaluated at the dipole position, $\boldsymbol{R}_{obs} \equiv (0,0,d)$, follows

$$\boldsymbol{E}^{(1)}_{1,scatt}\left(\boldsymbol{R}_{obs}\right) \cdot \hat{\boldsymbol{z}} = -\frac{1}{2}\left(\frac{i\omega\mu_o p}{4\pi k_1^4}\right) \times \int_0^\infty dr'\,r'\left(\frac{\zeta'(r')}{r'} + \zeta''(r')\right)\left[\Psi(r',z')^2\right]_{z'=-\zeta(r')}$$

$$-\frac{1}{2}\left(\frac{i\omega\mu_o p}{2\pi k_1^2}\right) \times \int_0^\infty dr'\,r'\left[\partial_{r'}\left(e^{ik_1 R'}/R'\right)\zeta'(r')\Psi(r',z')\right]_{z'=-\zeta(r')} \tag{5.16}$$

We make note of the fact that the above corrections to the self-field of the dipole above surfaces described by $z = -\zeta\left(r\right)$ are suitable provided $\left(\nabla\zeta\left(r\right)\right)^2 \ll \nabla\zeta\left(r\right)$. In the immediate neighborhood of its image, the real part of the reflected field at the dipole position, with $\boldsymbol{E}^{(o)}_{1,scatt} \propto \Psi$, leads to the usual near field $\Psi \sim D^{-3}$ where $D \equiv \left(k_1\left(d + \zeta\right)\right)$ while the corresponding imaginary part reaches a constant. Asymptotic analysis reveals the small D scalings for $\boldsymbol{E}^{(1)}_{1,scatt}$ given in the penultimate section.

Figure 5.1: The left(right) images depict the possible physical layouts of the dipole above the bumpy surface under consideration.

Figure 5.2: The solid curves in the left(right) images are plots of the $Re\,(F)$ $(Im\,(F))$, versus $k_1 d$ in the presence of a convex surface inhomogeneity. F is defined in the main body. Parameter values used are $\{\omega = 3.77 \times 10^{15} Hz, k_1 = \omega\sqrt{\epsilon_o\mu_o} = \omega/c, \delta = 100nm, h_o = 30nm\}$ where c is the speed of light. The long(short) dashed curves in both images denote the unperturbed reflected E-field with interfaces in the constant plane $z = 0$ $(z = h_o)$.
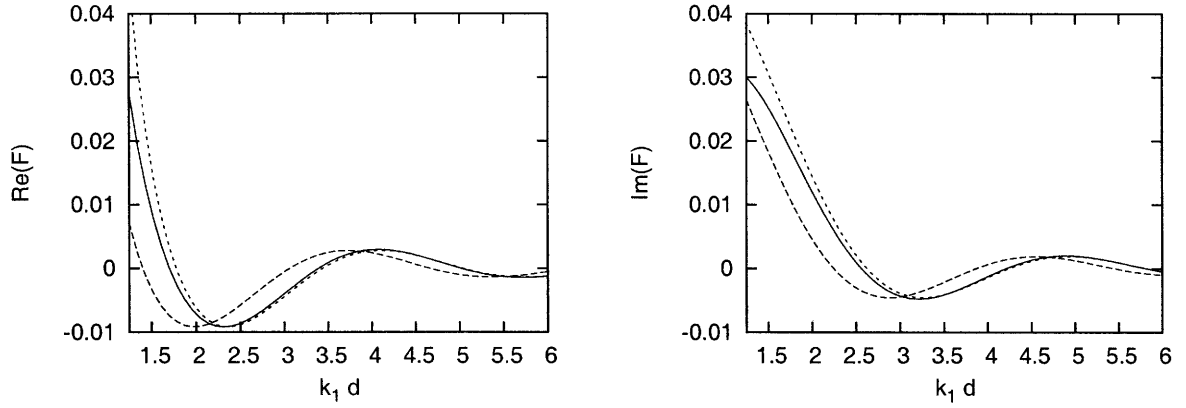
Figure 5.3: The solid curves in the left(right) images are plots of $Re\,(F)$ $(Im\,(F))$, versus $k_1 d$ in the presence of a concave surface inhomogeneity. The parameters are identical to those of Fig.(5.2) with the exception that $h_o \to -h_o$ with $h_o > 0$. The long(short) dashed curves in both images denote the unperturbed reflected E-field with interfaces in the constant plane $z = 0$ $(z = -h_o)$.
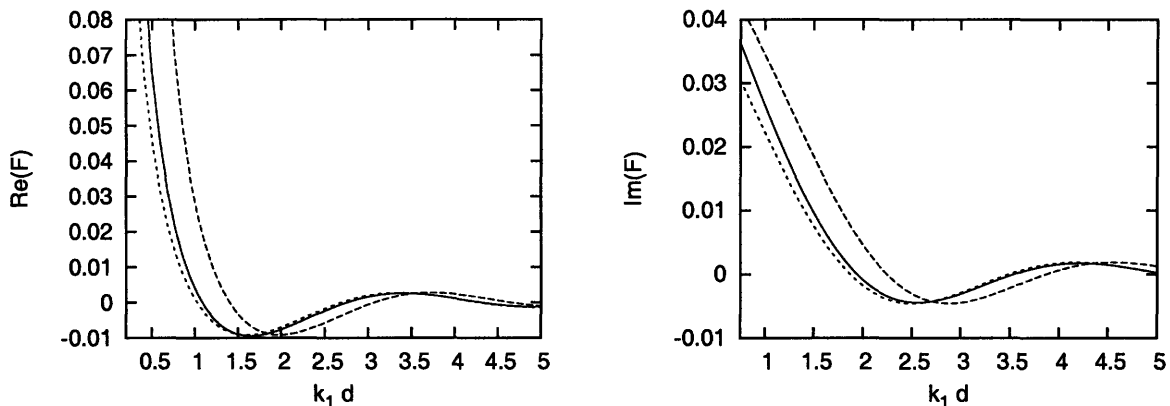
5.5 Application of the Perturbed Boundary Problem

Small surface induced frequency shifts, $\Delta\omega$, and radiation inverse lifetimes, Γ, for radiating EDs are related to the real, in-phase, and imaginary, out-of-phase, scattered fields evaluated at the source position[14, 28]. Following Kuhn, these relations are established by approximating the dipole as a harmonically bound charge externally driven by the scattered field at the position of the dipole[13]. While frequency shifts and radiation inverse lifetimes vary as the dipolar distance from the surface is changed, we study the reflected field variations with distance of the dipole to the surface for both convex and concave Gaussian inhomogeneities as shown in Fig.(5.1).

We recall the three relevant length scales in our problem: 1. k_1^{-1}, which depends on the material properties of medium I and the ED, 2. the distance of the ED from the surface, d, and 3. some length scale characteristic of the surface perturbation.

Both Figs.(5.2)-(5.3) which depict the z-component of the dimensionless reflected leading order field at the dipole position, $F \equiv \left(\boldsymbol{E}^{(o)}_{1,scatt}\,(\boldsymbol{R}_{obs}) + \boldsymbol{E}^{(1)}_{1,scatt}\,(\boldsymbol{R}_{obs})\right) \cdot \hat{z}/(\omega^2 \mu_o d_o k_1)$, versus $k_1 d$ exhibit two qualitative features distinguishing flat from perturbed surfaces. The first is a zeroth order effect: there is a uniform shift of the reflected field, both real and
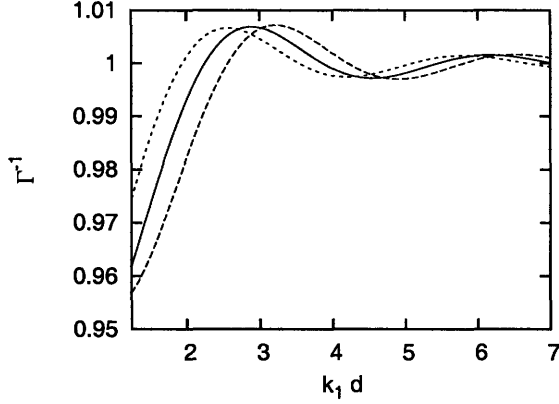
115

Figure 5.4: Plot of the dimenionless fluorescence lifetime Γ^{-1}, normalized with respect to the surface unaffected lifetime, versus $k_1 d$ in the presence of a flat conducting surface(solid curve), a convex surface inhomogeneity(long-dashed curve) and a concave surface inhomogeneity(short-dashed curve). We use the formula $\Gamma = 1 + (3/2)Im\,(F)$ from ref. [14] having assumed a unit quantum yield. The parameter F is defined in the main body.

imaginary parts, with respect to $k_1 d$ because of the effective readjustment of the height of the surface below the dipole in the presence of a perturbation. The second effect is a short-distance, $d \sim \mathcal{O}(k_1^{-1})$, positive or negative enhancement of the reflected field dependent on nature of the surface perturbation. The reflected field is largest at very short distance, $d \leq k_1^{-1}$, when the dipole strongly interacts with its perturbed image. For such distances, asymptotic analysis reveals that $Re[\boldsymbol{E}_{1,scatt}^{(1)}\,(\boldsymbol{R}_{obs}) \cdot \hat{\boldsymbol{z}}]/\,(\omega^2 \mu_o d_o) \sim \mathcal{O}\left((h_o/\delta)\,/\,(D^4\delta)\right)$ and $Im[\boldsymbol{E}_{1,scatt}^{(1)}\,(\boldsymbol{R}_{obs}) \cdot \hat{\boldsymbol{z}}]/\,(\omega^2 \mu_o d_o) \sim \mathcal{O}\left((h_o/\delta)\,/\,(D^3\delta)\right)$ so that the perturbation expansion is poorly behaved while in practice the dipole is often quenched by the imperfectly conducting medium II.

At this point, we briefly discuss how we have obtained these scalings from the radial integral of Eq.(5.16), the dominant contribution at short distances. We first define $I \equiv -\frac{1}{k_1^4}\int_0^\infty dr'r'\left(\frac{\zeta'(r')}{r'} + \zeta''(r')\right)\left[\Psi(r',z')^2\right]_{z'=-\zeta(r')}$ which has units of inverse length. The integral I is related to the radial integral of Eq.(5.16) up to the real constant $8\pi/\omega^2\mu_o d_o$. By

116

defining a dimensionless length $R \equiv k_1 r$ and $X^2 \equiv R^2 + D^2$, we re-write I as follows

$$I = \int_D^\infty dX e^{-\frac{(X - 2k_1^2 \delta^2 i)^2}{2k_1^2 \delta^2}} f(X)$$

where

$$f(X) \equiv \frac{e^{\frac{D^2}{2k_1^2 \delta^2} - 2k_1^2 \delta^2} h_o}{k_1^2 \delta^4 X^9} p(X)$$

and

$$p(X) \equiv \left(X^2(-1 + iX + X^2) - D^2(-3 + 3iX + X^2) \right)^2 (-D^2 + X^2 - 2k_1^2 \delta^2).$$

The form for I motivates the subsitution $X = \xi + 2k_1^2 \delta^2 i$. With the poles of the new integrand along the pure imaginary axis, we deform the contour by writing $I = I_1 + I_2 + I_3$ with ξ in I_1 integrated along $D - 2k_1^2 \delta^2 i$ to D, in I_2 integrated from D to ∞, and in I_3 from $\infty - 2k_1^2 \delta^2 i$ to ∞. It is clear that the contribution to I from I_3 is vanishingly small. Furthermore both real and imaginary parts of I_2 scale as to $O(D^0)$ so that I_2 can be ignored provided I_1 scales faster than $O(D^0)$ for small D.

We have thus narrowed our problem to evaluating the small D scaling of $\int_{D - 2k_1^2 \delta^2 i}^D d\xi F(\xi)$ with $F(\xi)$ defined in context. As D approaches 0, the path of integration gets closer to the ninth order pole of $F(\xi)$ located at $\xi = -2ik_1^2 \delta^2$. For this reason, we are motivated to let $\xi = D + \epsilon$ and rotate our integration path by letting $\epsilon = -i\theta$ so that $I \sim \int_0^{2k_1^2 \delta^2} d\theta i F(D - i\theta)$. Asymptotically for small D, it is the upper boundary, closest to the ninth order pole, which contributes most significantly to I. For this reason, we expand the integrand around the upper boundary. Doing so, we recover the small D scalings previously given.

In Fig.(5.2), curves of F versus $k_1 d$ are presented for an ED in vacuum with $\zeta(r) \equiv -h_o e^{-r^2/2\delta^2}$. In the latter, h_o is intended positive and the small slope approximation requires that $h_o/\delta < 1$.

A few remarks are in order regarding Fig.(5.2). When shifted, the unperturbed reflected

E-field at the dipole position and the zeroth order curves superpose, by definition. For this convex inhomogeneity, the reflected field scatters away from the direction of the original dipole. For this reason, the reflected field amplitude at the dipole position is smaller. For small $k_1 d$, where the differences between the curves on each figure are more pronounced, the perturbed reflected field lies somewhere between the zeroth order curve and the unperturbed reflected field. This is true everywhere except for very small $k_1 d$ where the perturbation fails. In addition, for larger δ it can be shown that the difference between the zeroth order term and the perturbed reflected field is smaller than the corresponding difference in Fig.(5.2). For large $k_1 d$, as compared to the characteristic size of the surface inhomogeneity, the perturbed reflected field collapses into the zeroth order curve.

For the concave perturbation at the surface we define $\zeta(r) \equiv +h_o e^{-r^2/2\delta^2}$ where h_o is once again intended positive. As is shown in Fig.(5.3), the reflected field at the dipole position is greater because the concave surface in general scatters the field towards the ED. The qualitative change in the force experienced by the dipole in the presence of surface curvature, even to leading order in the surface smoothness, is apparent in the fluorescence lifetime plot, Fig.(5.4).

5.6 Concluding Remarks

Experience gained from SERS has shown that geometric field enhancement effects merit serious attention for the case of single molecules. We have shown, for the first time, how single fluorophore properties are expected to deviate from image theory predictions near smooth, locally curved, surfaces. We focused on quantifying, perturbatively, the effects of a locally smooth inhomogeneity on the reflected fields of a radiating dipole near a perfect conductor. The formalism developed lends itself to a physical interpretation, order-by-order, of how surface curvature exerts a measurable differential stress on the neighboring dipole. We computed the leading order force on the dipole by invoking a small slope phase perturbation technique on the DGF. In addition, the powerful technique of superposition of DGF can be generalized with ease to radiation problems involving higher order multipolar sources near multilayered planar surfaces. With the present results at hand, it is possible to analyze molecular lifetime variations and frequency shifts for fluorophores near surfaces with disorder on multiple length scales.

5.7 Bibliography

[1] S. Pressé and R. J. Silbey. *Phys. Rev. A*, 77:043402, 2008.

[2] Chen-To Tai. *Dyadic Green Functions in Electromagnetic Theory*. IEEE Press, 1994.

[3] L. Tsang and J.A. Kong. *Scattering of Electromagnetic Waves: Advanced Topics*. John Wiley and Sons, 2001.

[4] L. Tsang, J.A. Kong, and K.H. Ding. *Scattering of Electromagnetic Waves: Theories and Applications*. John Wiley and Sons, 2000.

[5] A.D. Yaghjian. *Proc. IEEE*, 68:248, 1980.

[6] M. Moskovits. *J. Ram. Spec.*, 36:485, 2005.

[7] J. Gersten and A.Nitzan. *J. Chem. Phys.*, 73:3023, 1980.

[8] A.C. Pineda and D. Ronis. *J. Chem. Phys.*, 83:5330, 1985.

[9] P.F. Liao and A. Wokaun. *J. Chem. Phys.*, 76:751, 1982.

[10] H. Xu and M. Käll. *Phys. Rev. Lett.*, 89:246802, 2002.

[11] L. Novotny and S.J. Stranick. *Ann. Rev. Phys. Chem.*, 57:303, 2006.

[12] K.H. Drexhage. *Prog. Opt.*, XII:165, 1974.

[13] H. Kuhn. *J. Chem. Phys.*, 53:101, 1970.

[14] R.R. Chance, A. Prock, and R. Silbey. *Adv. Chem. Phys.*, 37:1, 1978.

[15] O. Labeau. et al., *Phys. Rev. Lett.*, 98:143003, 2007.

[16] B.C. Buchler. et al., *Phys. Rev. Lett.*, 95:063003, 2005.

[17] M.A. Wilson. et al., *Phys. Rev. Lett.*, 91:213602, 2003.

[18] E. Rodríguez. *Radio Science*, 24:681, 1989.

[19] E. Rodríguez and Y. Kim. *Radio Science*, 27:79, 1992.

[20] S.L. Chuang and J.A. Kong. *Proc. IEEE*, 69:1132, 1981.

[21] C.N. Vazouras. et al., *Radio Science*, 35:1049, 2000.

[22] G.S. Agarwal and C.V. Kunasz. *Phys. Rev. B*, 26:5832, 1982.

[23] A. Voronovich. *Waves in Random Media*, 4:337, 1993.

[24] A. Voronovich. *Waves in Random Media*, 6:151, 1996.

[25] R.E. Collin. *Antennas and Propagation Society International Symposium*, 2:894, 1998.

[26] A. Baños. *Dipole Radiation in the Presence of a Conducting Half-Space*. Pergamon Press, 1966.

[27] P.M. Morse and H. Feshbach. *Methods of theoretical Physics*. McGraw-Hill Book Company, 1953.

[28] W.L. Barnes. *J. Mod. Opt.*, 45:661, 1998.

Curriculum Vitae

Steve Pressé
Department of Chemistry, Room 6-228
Massachusetts Institute of Technology, 77 Massachusetts Ave., Cambridge MA 02139
617-253-1539, spresse@mit.edu

Date of Birth: 05/07/81, Montréal QC

Education

2003 -present	**Massachusetts Institute of Technology, Cambridge MA** Ph.D. in Physical Chemistry Doctoral advisor: Robert J. Silbey Title: Role of Fluctuations and Defects in Select Condensed Matter Problems
2000 -2003	**McGill University, Montréal QC** B.Sc. Honors Chemistry with minor in German Language(GPA: 3.94/4.00) Research advisor: Bryan C. Sanctuary Honors project: Theory of polarization transfer in coupled spin systems

Work

02/2004 -05/2004	**TA [1], General Chemistry(MIT)**
09/2003 -12/2003	**TA, Undergraduate Quantum Mechanics(MIT)**
Summers 2002-2003	**Partly Fellowship Supported Undergraduate Summer Research**
Springs 2002-2003	**TA, Undergraduate Quantum Mech. for Biochem. (McGill University)**
1995 -2002	**Tutor** Active private tutor in mathematics, French and music(violin) at the elementary and secondary levels.

---

[1]Teaching Assistant

Publications

S. Pressé, R.J. Silbey, "Radiating dipoles near curved interfaces", *Phys. Rev. A*, **77**, 043402(2008).

S. Pressé, R.J. Silbey, "Memory effects on the convergence properties of the Jarzynski equality", *Phys. Rev. E*, **74**, 061105(2006).

J.M. Hodgkiss, N.H. Damrauer, S. Pressé, J. Rosenthal, D.G. Nocera, "Electron transfer driven by proton fluctuations in a hydrogen-bonded donor-acceptor assembly", *J. Phys. Chem. B*, **110**, 18853(2006).

S. Pressé, R. Silbey, "Anomalous temperature-isotope dependence in proton-coupled electron transfer", *J. Chem. Phys.*, **124**, 164504(2006).

S. Pressé, R. Silbey, "Ordering of limits in the Jarzynski equality", *J. Chem. Phys.*, **124**, 054117 (2006).

Scholarships and Awards

Academic year 2008-2010	**FQRNT** [2] **postdoctoral fellowship**
Academic year 2007-2008	**FQRNT doctoral scholarship**
Academic years 2005-2006, 2006-2007	**NSERC** [3] **doctoral scholarship**
Academic years 2003-2004, 2004-2005	**NSERC master's scholarship**
2004	**Outstanding Teaching Award, M.I.T. Chemistry Dept.**
2003	**J.W.F. Peacock** [4]**Mem. Scholarship Award** **Society of Chemical Industry Merit Award** **Anachemia Prize in Chemistry** **Lucien Piché Award** **R.F. Robertson Award in Physical Chemistry**

[2]Le Fonds québécois de la recherche sur la nature et les technologies
[3]Natural Sciences and Engineering Research Council of Canada
[4]John Williamson Frederick Peacock

2002	Herbert J. Brennen Scholarship
	Canadian Society for Chemistry, Silver Medal
	Frederic J. LeMaistre Award
Summer 2002	Undergraduate research NSERC scholarship

Conferences, Workshops and Invited Talks

XXIII IUPAP International Conference on Statistical Phyics, Genoa, Italy, Jul. 2007
American Chemical Society Meeting(ACS), Atlanta GA, Mar. 2006
American Conference of Theoretical Chemistry(ACTC), Los Angeles CA, Jul. 2005
Computational Biophysics Workshop, Boston MA, Dec. 2004

Ad Hoc Reviewer

Phys. Rev. E, Phys. Rev. A

Initiatives

2008	**Volunteer TA, Non-equ. stat. mech.(MIT)** (Instr: Prof. J. Cao).
2005-2008	**MIT organizer of the Greater Boston Area Theoretical Chemistry Lecture Series**
2004	**Trainer for new teaching assistants**

Graduate Course Work for Credit

Statistical Mechanics(Chem. Dept., J. Cao), Statistical Physics(Phys. Dept., M. Kardar) Phase Transitions and Renorm. Group(Phys. Dept., N. Berker), Strongly Correlated Systems in CM Physics(Phys. Dept., X.-G. Wen), Quantum Theory I and II(Phys. Dept., J. Negele), Complex Analysis(Math. Dept., D. Benney).

Skills

Languages: French, English and Italian equally fluently, solid working knowledge of German and Spanish.

Computer Programs: Mathematica, C++

Hobbies

Traveling(Italy, Greece, Brazil, Serbia, Egypt, Austria, Canada and U.S.), playing the violin, drawing, painting, reading.